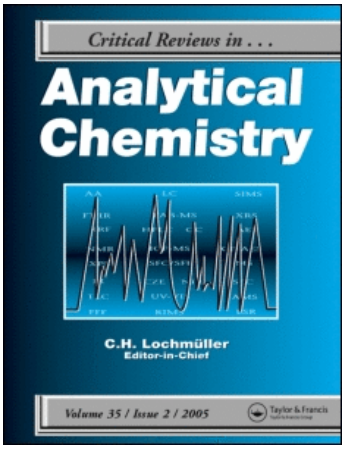

Critical Reviews in Analytical Chemistry
Publication details, including instructions for authors and subscription information:
http://www.informaworld.com/smpp/title~content=t713400837

Thermo-Optical Spectrophotometries in Analytical Chemistry

Norman J. Dovichi; Stephen E. Bialkowski

To cite this Article Dovichi, Norman J. and Bialkowski, Stephen E.(1987) 'Thermo-Optical Spectrophotometries in Analytical Chemistry', Critical Reviews in Analytical Chemistry, 17: 4, 357 — 423
To link to this Article: DOI: 10.1080/10408348708542799
URL: http://dx.doi.org/10.1080/10408348708542799

THERMO-OPTICAL SPECTROPHOTOMETRIES IN ANALYTICAL CHEMISTRY

Author: **Norman J. Dovichi**
Department of Chemistry
University of Alberta
Edmonton, Alberta, Canada

Referee: Stephen E. Bialkowski
Department of Chemistry and Biochemistry
Utah State University
Logan, Utah

I. INTRODUCTION

A. Background

The incorporation of lasers as light sources in analytical spectroscopic instrumentation has resulted in spectacular detection limits. These detection limits arise from several unique properties of laser radiation. As an example, the spectral purity and high power of the laser facilitates detection of individual gas phase atoms with isotopic resolution by both fluorescence and ionization techniques.[1-3] The temporal coherence of the laser has been used to discriminate signals generated by very fast scatter processes from relatively slower luminescence relaxation.[4,5] In addition, the high spatial coherence of the laser allows measurement by thermo-optical techniques of very small absorbance, the subject of this review. A recent review in this journal considered the related technique of photoacoustic spectroscopy, another high-sensitivity absorbance method.[6]

At least in liquids, the performance of thermo-optical spectrophotometries approaches the better-known performance of laser-induced fluorescence. For example, individual immunoglobulin molecules labeled with approximately 100 fluorescein isothiocyanate tags have been detected by laser-induced fluorescence.[7] Similarly, a detection limit corresponding to 120 iron-1,10-phenanthroline molecules has been achieved with a crossed-beam thermal lens measurement.[8] Good liquid phase laser-induced fluorescence detection limits tend to fall around 10^{-13} M for highly fluorescent dye.[5,9] Similar detection limits are expected for a strongly absorbing analyte and time-resolved thermal lens measurements.[10]

B. Thermo-Optics

Thermo-optics is a branch of laser spectroscopy which measures, by optical means, the temperature rise within a sample produced by absorbance of light. Thermo-optical techniques, based upon the interaction of two laser beams within a sample, have produced significant improvements in absorbance measurements compared with conventional transmission methods. The improvements arise from increased sensitivity and precision compared with simple transmission measurements.

In thermo-optical spectrophotometries, absorbance of a pump light beam produces a temperature rise within the sample. Since the refractive index of most materials changes with temperature, the heated sample acts as an optical element to defocus or deflect a second probe beam. Usually, a modulated pump laser is employed to produce a periodic thermo-optical element which modulates the probe beam intensity profile. The profile distortion is

measured with either a position- or power-sensitive detector and demodulated with a lock-in amplifier, signal averager, or box-car averager.

The pump and probe beams may be collinear or crossed; the overlap region of the beams defines the probe volume of the experiment. Collinear designs produce high-concentration sensitivity within microliter volumes, whereas crossed-beam instruments produce excellent mass sensitivity within picoliter probe volumes. Furthermore, surface-sensitive techniques produce localized absorbance measurements at a liquid-solid or gas-solid interface.

The lexicon of thermo-optical techniques is surprisingly rich. These techniques are often classified by analogy with conventional optical elements: a lens in thermal lens calorimetry,[11-13] a cylindrical lens in the crossed-beam thermal lens,[14] a prism in thermal deflection spectroscopy,[15] a grating in thermal diffraction,[16] a curved mirror in thermally induced deformation,[17] or a simple change in optical path length in interferometry.[18,19] Of course, the interpretation of thermally induced beam perturbation in terms of the action of conventional optical elements is only an approximation; the thermo-optical element often is aberrant. If nothing else, the temporal behavior of thermo-optical elements differs significantly from conventional optical elements.

Thermo-optical spectrophotometries produce improved sensitivity and precision compared with conventional transmission measurements. The high sensitivity of thermo-optical techniques is a direct result of the linear property of heat flow: an increase in pump laser power produces a proportional increase in temperature within the sample. Since the sensitivity of most thermo-optical measurements increases linearly with a temperature rise, a very small absorbance may be transformed, in principle, into an arbitrarily large thermo-optical signal by utilization of a high-power pump laser. Ultimately, noise proportional to the solvent absorbance will determine the smallest detectable signal.

The high precision of thermo-optical techniques is a direct result of the time-varying nature of the temperature rise induced by a modulated pump beam. Powerful electronic demodulation techniques, such as lock-in amplification, box-car averaging, or signal averaging with regression analysis, are used to enhance the precision of the measurement. The combination of a stable probe laser with these demodulation techniques results in absorbance detection limits corresponding to a few parts-per-thousand of the solvent background absorbance.[10]

Proportional noise in the background signal, generated by very weak solvent absorbance, limits the precision of both thermo-optical and fluorescence techniques for liquid phase analysis. In thermo-optical techniques, the background signal is generated by very weak overtones of infrared transitions.[20-23] In fluorescence, the background signal is generated primarily by Raman scatter from the solvent.[9,24,25] Solvent absorbance is quite weak in the visible portion of the spectrum for many liquids: the molar absorptivity of water is about 2×10^{-6} LM^{-1} cm^{-1},[26] and of carbon tetrachloride is about 5×10^{-7} LM^{-1} cm^{-1},[10] both measured near 515 nm. The Raman cross section for water, 3×10^{-8} LM^{-1} S^{-1},[27] is about two orders of magnitude smaller than the absorbance cross section. It is interesting to note that both thermo-optical and fluorescence measurements are limited ultimately by a background signal arising from vibrational transitions within the solvent.

C. An Example

As an example of a thermo-optical technique, consider the crossed-beam thermal lens.[14,28] In this experiment, a modulated pump laser beam illuminates a weakly absorbing sample, Figure 1. Absorbance of the pump beam, followed by nonradiative relaxation of the excited states, produces a cylindrically symmetric temperature rise within the sample. This heated region is probed at right angles with a coplanar beam. The thermo-optical element acts as a cylindrical lens to defocus the probe beam symmetrically about the plane containing the two beams. Since the temperature change within the sample is governed by thermal diffusion, the strength of the thermo-optical element will change with time and will

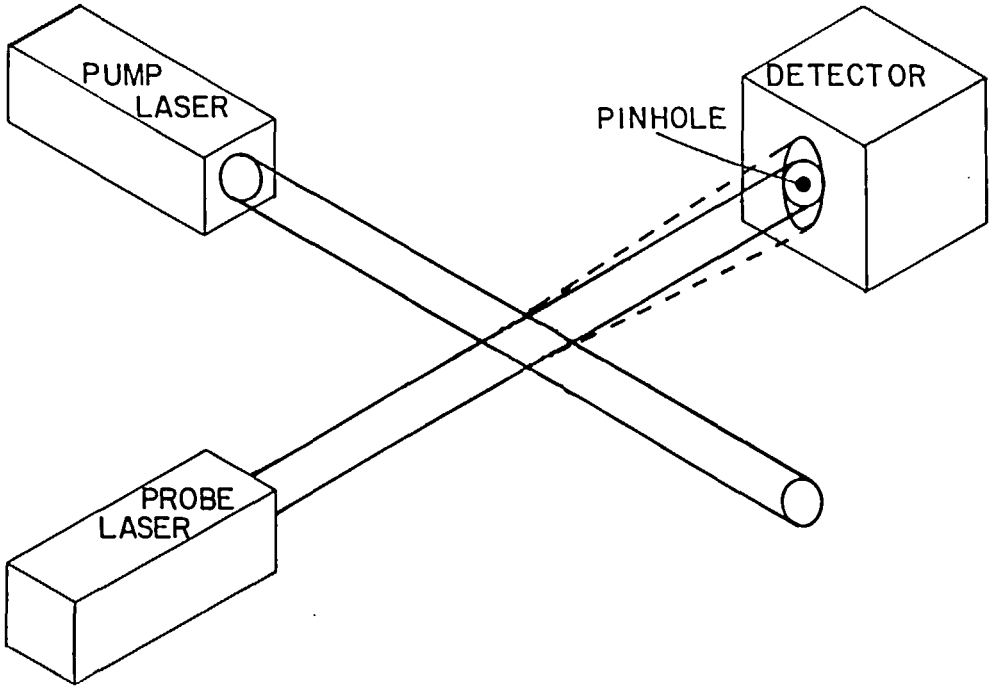

FIGURE 1. Crossed-beam thermal lens. A modulated pump laser beam produces a cylinder of heated material within the weakly absorbing sample. This heated region acts as a thermal cylindrical lens whose focal length varies in phase with the pump beam modulation function. The heated region acts to defocus a second, coplanar probe laser beam about the plane containing the two beams. A detector located behind a small pinhole measures a periodic change in the probe beam center intensity.

mimic the modulation function of the pump laser. The strength of the thermal cylindrical lens, and hence the absorbance of the sample, is measured as a change in the probe beam center intensity with a simple photodiode.

A typical experimental diagram is shown in Figure 2. Here, a chopped pump beam is focused into the weakly absorbing sample. A second cw laser beam is focused into the sample to probe the heated region. After transmission through the sample, the probe beam is centered on a pinhole and small photodetector. Any defocusing produced by the heated sample will spread out the probe beam and decrease the beam-center intensity. The signal from the photodetector is demodulated with a box-car averager, a lock-in amplifier, or a signal averager phase-referenced to the pump laser chopper. In the insert of Figure 2, the pump power and probe beam-center intensities are considered as functions of time. When the pump beam is turned on, the sample heats and acts to defocus the probe beam, decreasing the intensity transmitted through the pinhole. When the pump beam is turned off, the temperature within the sample relaxes and the probe beam intensity returns to an unperturbed value.

As an example of the unperturbed profile of a laser beam, Figure 3a presents a photograph of a probe laser beam profile after passing through a cuvette containing a small amount of iodine dissolved in carbon tetrachloride. The beam demonstrates circular symmetry and a Gaussian intensity profile. If a pump laser beam is focused into the absorbing sample at right angles to the probe laser beam, then the probe beam profile is changed, Figure 3b. The temperature rise formed by the absorbance of the pump beam produces a cylindrically symmetric refractive index perturbation which defocuses the probe beam. Clearly, a photodetector centered on the probe beam profile will measure a large change intensity as the

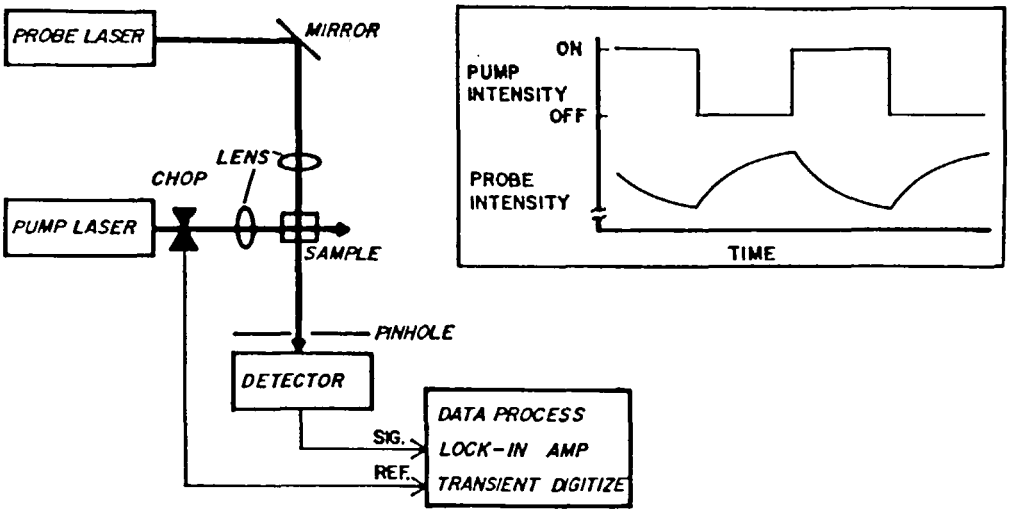

FIGURE 2. Experimental diagram for the crossed-beam thermal lens. A cw pump laser beam is modulated with a mechanical chopper and focused into the sample with a short focal length lens. The probe beam is focused at right angles to the coplanar pump beam within the weakly absorbing sample. The periodic defocusing of the probe beam is detected as a change in beam center intensity with a photodetector located behind a small area pinhole. The beam-center intensity change is demodulated by a phase-sensitive amplifier, referenced to the pump beam modulation function. The insert shows a typical waveform recorded by the data-processing electronics. The upper trace shows the pump beam intensity and the lower trace shows the probe beam center intensity as a function of time. As the pump beam illuminates the sample, thermally induced defocusing produces a decrease in the probe beam center intensity. When the pump beam is blocked, the probe beam intensity returns to an unperturbed value. Typically, the probe beam intensity is modulated by a small amount, less than a few percent, and detected with a phase-sensitive amplifier. The rise and fall times of the signal are governed primarily by thermal diffusion.

pump beam is blocked and unblocked. This experiment demonstrates the aberrant nature of the thermo-optical element; an unaberrant cylindrical lens would produce a Gaussian beam with an elliptical profile.

In this review, a description of a generic thermo-optical technique, including a discussion of some theoretical aspects, will be presented. In general, the theory is quite complicated; useful results arise from clever approximations and tedious numerical methods. The remainder of the manuscript presents a description of several thermo-optical experiments. The experimental arrangements are classified with respect to utility for bulk samples, small volume samples, and surface absorbance measurements. In each case, a number of analytical applications are presented.

II. PROPERTIES OF A GENERIC THERMO-OPTICAL EXPERIMENT

A. Introduction

A description of a generic thermo-optical experiment may be divided into four parts: absorbance of light from the pump beam generating heat within the sample, thermal diffusion of the heat, production of a refractive index profile within the sample, and diffraction of the probe beam by the refractive index profile. Some very challenging photo-physics and mathematics are encountered in the description of thermo-optical experiments. For example, both thermal diffusion and optical diffraction are intimately connected to thermo-optical phenomena and are notoriously difficult mathematical problems. In general, useful theories of thermo-optical phenomena arise from appropriate approximations and numerical methods.

Lasers are generally used to produce (and probe) the heated region within the sample.

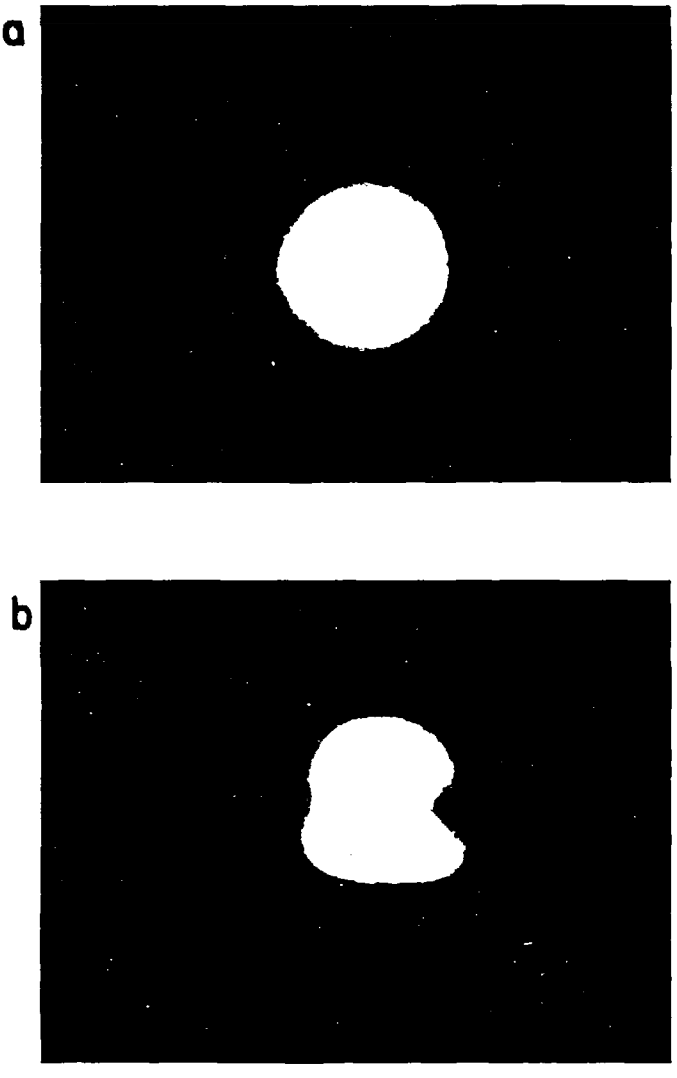

FIGURE 3. The probe beam profile in the crossed-beam thermal lens. (a) Unperturbed Gaussian profile obtained with the pump beam blocked; (b) defocused profile obtained with the pump beam illuminating the sample. (Photos courtesy of Dr. Thomas G. Nolan and Mr. H. Hogan.)

Therefore, propagation of laser beams is of fundamental importance in thermo-optics. A number of reviews and descriptions of laser beams have been presented.[11,29,30] A laser beam may be described in terms of either its electric field, U, or intensity, I. The electric field is a complex valued function containing information on both the amplitude and phase of the light beam. The electric field is important in the diffraction theory of optical propagation and is considered briefly in Section II.E of this paper. The intensity of the laser beam is measured directly by most optical detectors and is given by the square of the amplitude of the electric field:

$$I(x,y,z) = |U(x,y,z)|^2 \quad (1)$$

Of greatest interest are lasers operating in the fundamental Gaussian mode, TEM_{∞}. The simple mathematical description of these laser beams facilitates the description of thermo-

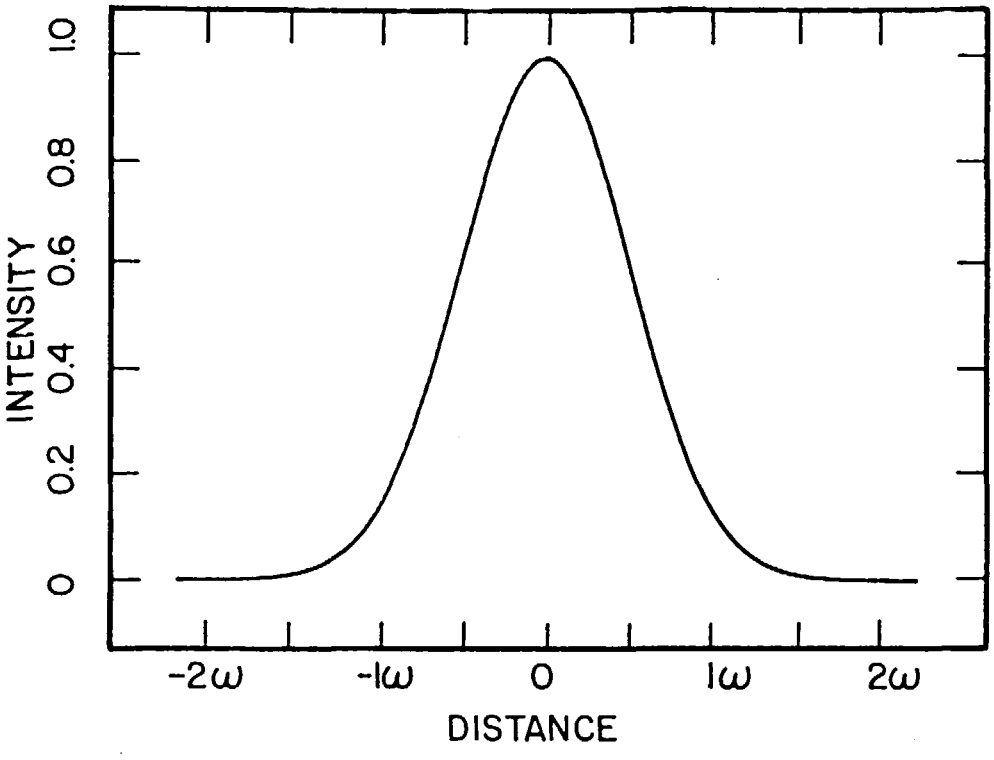

FIGURE 4. Radial intensity profile produced by a Gaussian laser beam. The ω is the beam spot-size.

optical experiments. Furthermore, relatively inexpensive low-power cw lasers typically operate in this spatial mode. For a laser operating in the TEM_{∞} mode, the beam intensity profile is given by Figure 4,

$$I(x,y,z) = \frac{2P}{\pi\,\omega^2(z)}\, e^{\{-2(x^2+y^2)/\omega^2(z)\}} \tag{2}$$

where P is the total power of the beam, z is the direction of beam propagation, x and y are perpendicular to the beam axis, and ω(z) is the beam spot-size and provides a measure of the radius of the beam. The spot-size of the beam varies with distance along the beam axis, and the spot-size of the beam at the waist or focus is denoted ω_o. The spot-size of the beam increases with distance from the beam waist, Figure 5, and depends upon the waist spot-size and the wavelength of light, λ;

$$\omega^2(z) = \omega_0^2\,[1 + (z/z_c)^2] \tag{3}$$

where the confocal (sometimes called Rayleigh) distance, $Z_c = \pi\,\omega_o^2/\lambda$.

B. Absorbance of Light

The temperature rise within the sample is a result of nonradiative relaxation of excited states produced by absorbance of the pump beam. For molecules which relax nonradiatively, the entire energy of the absorbed photon is converted to heat. On the other hand, fluorescence removes energy from the system in the form of a photon and some bookkeeping is required to compute the heat deposited within the sample for highly fluorescent molecules.[24] Neglected

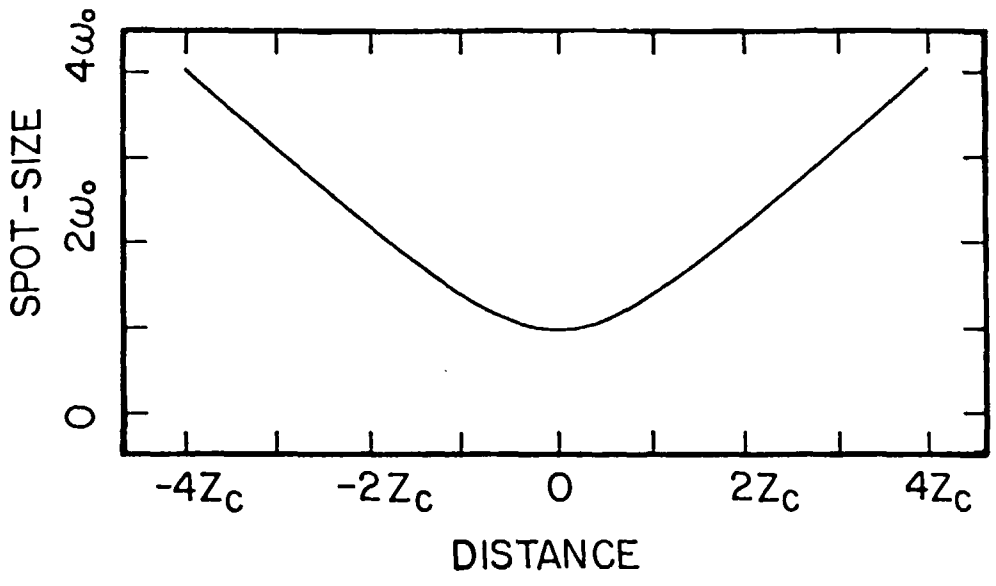

FIGURE 5. Variation in Gaussian beam profile along beam axis. Z_c is the confocal distance.

are intersystem crossing to the triplet state, Raman scatter, anti-Stokes fluorescence,[31] and photochemical reaction.[32]

The average amount of energy lost by fluorescence per photon absorbed is given by the product of the quantum yield of fluorescence, Φ_f, with the average energy of an emitted photon, $<\nu>$. The remaining energy is converted to heat. If A is the sample absorbance and N is the number of photons per laser pulse, then the heat deposited within the sample is given by[33]

$$E_{thermal} = [N(1 - 10^{-A})]\,[h(\nu_{pump} - \Phi_{fluor} <\nu>)] \quad (4)$$

where the first term after the equal sign corresponds to the number of photons absorbed and the second term corresponds to the average thermal energy produced per absorbed photon. Note that the thermal energy deposited in the sample can be quite large even for highly fluorescent molecules if the excitation wavelength is significantly shorter than the average emission wavelength. For a weakly fluorescent standard and very dilute analyte, the thermal energy deposited within the sample is given by:

$$E_{thermal} = 2.303\,\epsilon bCE_{pump} \quad (5)$$

where ϵ is the decadic molar absorptivity, b is path length, C is analyte concentration in moles per liter and E_{pump} is the energy per pump laser pulse.

Thermo-optical methods have been employed to measure quantum yields of both fluorescence and photochemical reaction.[32-35] In general, relative measurements may be made against a weakly fluorescent standard with high precision. Knowing the absorptivity of the standard and the pump laser energy, the magnitude of the thermo-optical signal can be calibrated with the power deposited within the sample[33]

$$\Phi_{fluor} = \frac{\nu_{pump}}{<\nu>}\left[1 - \frac{\theta_{analyte}/A_{analyte}}{\theta_{standard}/A_{standard}}\right] \quad (6)$$

where $\Theta_{analyte}$ is the thermo-optical signal produced by the analyte, $A_{analyte}$ is the absorbance of the analyte, $\Theta_{standard}$ is the thermo-optical signal produced by a weakly fluorescent standard, and $A_{standard}$ is the absorbance of the standard.

C. Temperature Rise

The temperature rise within the sample will depend upon the spatial and temporal nature of the pump beam and the homogeneity, thermal diffusivity, and heat capacity of the sample. Flow also perturbs the temperature profile within the sample and is important for chromatographic applications. A number of good references are available for the thermal diffusion problem, including several books by Carslaw and Jaeger.[36-38] Papers by Whinnery and colleagues,[12,39-41] Stone,[18] Twarowski and Kliger,[42] Weimer and Dovichi,[43-46] Swofford and Morrell,[47] and Fang and Swofford[48] have all considered variations of thermal lens measurements; Eichler[49] considered thermal diffraction; Aamodt and Murphy[50] and Jackson et al.[15] have considered the heating of surfaces.

The temperature rise in gases is a much more complicated phenomenon than in liquids.[51-55] At low pressures, an excited analyte can diffuse from the pump laser vicinity before thermally relaxing. Competition between mass and thermal diffusion is particularly important at low pressures. Furthermore, acoustic waves can also remove energy from the system. Consideration of gas phase thermo-optical phenomena is beyond the scope of this review. The interested reader is urged to consult the references listed.

In general, the thermal diffusion problem is difficult, particularly for inhomogeneous and composite materials; heat flow in static, homogeneous samples is comparatively straightforward. This section first considers the temperature rise produced by a pulsed, Gaussian pump beam within a homogeneous and stationary sample. Inhomogeneous and flowing samples are considered briefly at the end of the section.

Let us first construct an impulse response model. This impulse response function not only models pulsed excitation but also may be convoluted with the excitation function to model the signal produced by an arbitrary pump waveform. Furthermore, a weakly absorbing, optically thin sample is considered. Then, a relatively simple model may be constructed based upon the temperature rise due to an instantaneous line source using a Green's function, ΔT_G. Physically, the Green's function describes the spatial and temporal profile of the temperature rise produced by an impulse of heat along a long, thin path. Mathematically, this function may be integrated over the spatial (and temporal) profile of the pump beam to describe a temperature rise within the sample.[36]

$$\Delta T_{Green}(x,y,x',y',t) = \frac{q}{4\pi kt} e^{-[(x-x')^2 + (y-y')^2]/4Dt} \quad (7)$$

where the thin, heated path is aligned along the Z axis at position (x′,y′), the temperature rise is measured at (x,y), t is time in seconds, q is the heat per unit length deposited in the line in J cm^{-1}, k is the thermal conductivity of the sample in J S^{-1} cm^{-1} $°C^{-1}$, and the thermal diffusivity, $D = k/\rho C_p$ where ρ is density in g cm^{-3} and C_p is the specific heat at constant pressure in J g^{-1} $°C^{-1}$. The equation $(x - x')^2 + (y - y')^2$ measures the squared distance between the heating and measuring points. A pulsed, thin line of heated material is converted into a Gaussian temperature distribution by thermal diffusion.

The Green's function for the temperature rise, integrated over the spatial profile of the pump beam, E(x,y), yields the impulse response spatial profile of the temperature rise within the sample.

$$\Delta T_{Sample}(x,y,t) = \int_{-\infty}^{\infty}\int_{0}^{t} 2.303\,\epsilon C I_{pump}(x',y',t-t') \times \Delta T_{Green}(x,y,x',y',t')dt'dx'dy' \quad (8)$$

where $2.303\epsilon C$ accounts for the absorption per unit length. Consider the case when a pulsed pump laser is operating in the TEM_{∞} mode. Then, the pump laser energy flux is given by:

$$E_{pump}(x',y') = \frac{2E_0}{\pi\omega^2} e^{[-2(x'^2+y'^2)/\omega^2]} \quad (9)$$

where E_o is the total energy of the laser pulse. This example is interesting for both the relatively simple mathematical treatment and the substantial analytical utility. The resulting temperature rise is the basis of four important thermo-optical spectrophotometries: coaxial thermal lens, crossed-beam thermal lens, coaxial thermal prism, and crossed-beam thermal prism. Substitution of both the pulse profile and the Green's function into Equation 8 will produce the temperature rise within the sample.

$$\Delta T_{impulse}(x,y,t) = \frac{4.606\,E_0\epsilon C}{\pi^2\,4kt\omega^2} e^{[-(x^2+y^2)/4Dt]} \times \int_{-\infty}^{\infty} e^{[-(x'^2+y'^2)(1/4Dt+2/\omega^2)+x'x/2Dt+y'y/2Dt]}\,dx'dy' \quad (10)$$

The following integral is useful in simplifying Equation 10:

$$\int_{-\infty}^{\infty} e^{-ax^2+bx}\,dx = (\pi/a)^{1/2}e^{[b^2/4a]} \quad (11)$$

to produce

$$\Delta T_{Impulse}(x,y,t) = \frac{2.303\,E_o\epsilon C}{2\pi k\omega^2/4D(1+8Dt/\omega^2)} e^{\left[\frac{-2(x^2+y^2)/\omega^2}{1+8Dt/\omega^2}\right]} \quad (12)$$

The temperature distribution produced by absorption of a pulsed Gaussian pump laser in a homogeneous sample is also Gaussian. The distribution remains Gaussian with time, but increases in area and decreases in peak temperature rise. A thermal time constant is defined

$$t_C = \frac{\omega^2\rho C_p}{4k} = \frac{\omega^2}{4D} \quad (13)$$

so that the temperature rise may be simplified

$$\Delta T_{Impulse}(x,y,t) = \frac{2.303\,E_o\epsilon C}{2\pi kt_C(1+2t/t_C)} e^{\left[\frac{-2(x^2+y^2)/\omega^2}{(1+2t/t_C)}\right]} \quad (14)$$

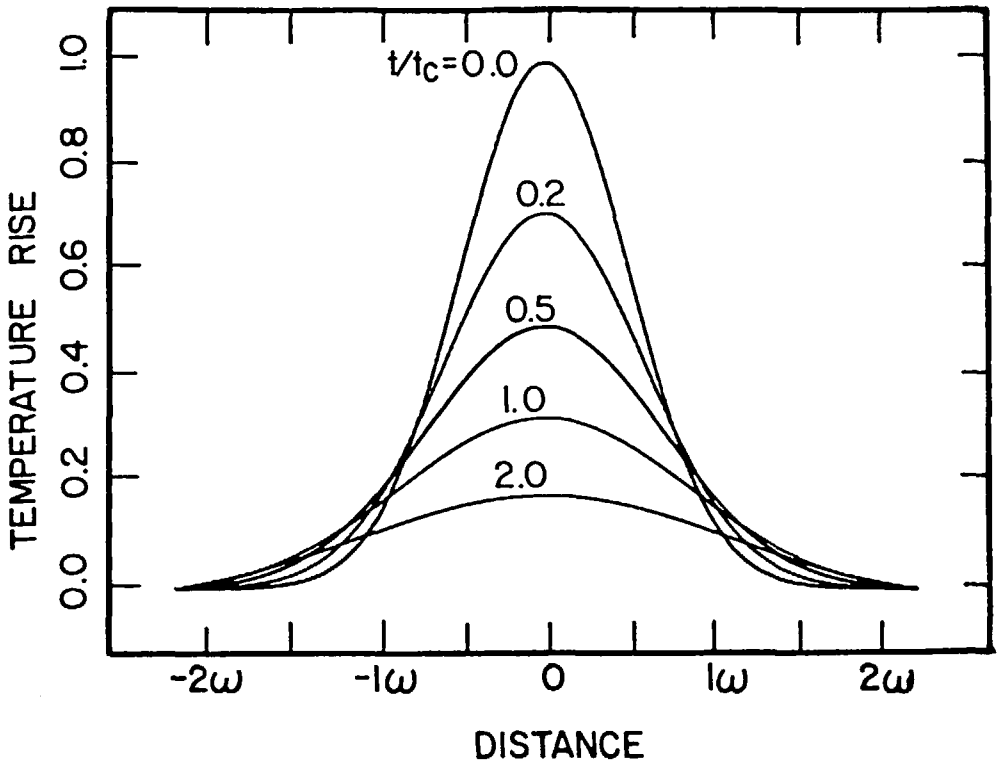

FIGURE 6. Radial temperature change produced by absorbance of a Gaussian pump beam within a stationary, homogeneous sample — impulse response.

Figure 6 presents the temperature rise within the sample as a function of the radial distance for several values of time. Note that this impulse response consists of a set of Gaussian temperature profiles. The temperature rise expands radially with time as heat diffuses throughout the sample. The temperature rise for a pulsed Gaussian pump beam heating a homogeneous sample, along with most other thermo-optical experiments, is characterized by the time constant given in Equation 13. For liquids, the time constant produced by a 1-mm spot-size pump beam falls in the range of 2 to 3 sec. Since the time constant is proportional to the square of the pump laser spot-size, very small spot-size lasers will produce very short time constants. For example, a thermal time constant of 2 μsec is predicted for a 1-μm spot-size pump beam in water. Much shorter time constants are expected for gas phase samples.

The temporal behavior of the temperature rise will depend upon the temporal behavior of the excitation pulse. The impulse response presented above is appropriate for pulsed pump lasers. However, it is often convenient to utilize chopped cw lasers in thermo-optical experiments. The response for a particular excitation function is given by the convolution of the impulse response with the excitation waveform.[56]

$$\Delta T_{Arbitrary}(t) = \int_0^t \Delta T_{Impulse}(x,y,t')P(t - t')dt' \quad (15)$$

where P(t) is a time-dependent function which describes the pump beam power. A number of examples of excitation functions may be found in the literature, including a step function, square pulse, periodic square wave, and periodic trapezoid wave.

As an example of the convolution integral, consider the temperature rise produced by a cw pump laser beam. If the pump beam is turned on at t = 0, the temperature rise is that produced by step excitation of average power P:

$$\Delta T_{Step}(x,y,t) = \frac{2.303P\epsilon C}{2\pi k t_c} \int_0^t \frac{1}{1 + 2t'/t_c} e^{\left[\frac{-2(x^2+y^2)/\omega^2}{1+2t'/t_c}\right]} dt' \tag{16}$$

This integral is solved by first substituting

$$T = \frac{2(x^2 + y^2)/\omega^2}{1 + 2t'/t_c} \tag{17}$$

using Abromowitz and Stegun's first definition of the exponential integral[57]

$$E_1(Z) = \int_Z^\infty 1/x\, e^{-x} dx \tag{18}$$

so that

$$\Delta T_{Step}(x,y,t) = \frac{2.303P\epsilon C}{4\pi k} \left\{ E_1\left[\frac{2(x^2 + y^2)/\omega^2}{1 + 2t/t_c}\right] - E_1[2(x^2 + y^2)/\omega^2] \right\} \tag{19}$$

The temperature rise produced by a cw pump beam is the time integral of the impulse temperature rise, Figure 7. Several differences between the step and impulse temperature profile may be noted. The first, and most obvious difference, is that the temperature rise increases with time for cw excitation and decreases with time for pulsed excitation; a longer exposure time deposits more energy within the sample for cw excitation. The second difference — a longer time is necessary to approach steady state for cw excitation compared with pulsed excitation. Finally, the temperature rise extends for a much greater distance from the beam axis for cw compared with pulsed excitation.

The analysis of the temperature rise produced in this thermo-optical experiment suggests one advantage of lasers as pump light sources in thermo-optical measurements. The temperature rise, and hence the sensitivity of the thermo-optical measurement, increases linearly with pump laser energy per unit area ($E/\pi\ \omega^2$). To increase the temperature rise within the sample, either a higher power pump laser or a more tightly focused pump beam may be used. However, the use of very tightly focused, high-power lasers is inappropriate for most thermo-optical experiments. The high intensity produced may result in sample damage and unexpected nonlinear optical phenomena. On the other hand, the low energy per unit area produced by conventional light sources is inappropriate as a pump beam in most thermo-optical experiments; the laser is the only practical pump beam source for most thermo-optical experiments.

The temperature rise produced in most thermo-optical experiments is quite small, much less than a degree Kelvin. At the detection limit, the temperature rise is as small as a few microdegrees Kelvin. Larger temperature rises are undesirable for several reasons, the most important being convection and boiling in liquid samples. Convection acts to distort the temperature profile by translating heated material throughout the cuvette. Hu and Whinnery[41] present a limit upon the energy absorbed per unit length to ensure negligible convection, assuming cw excitation:

$$2.303E\epsilon C << \frac{32\mu k^2}{agC_p\omega^3} \tag{20}$$

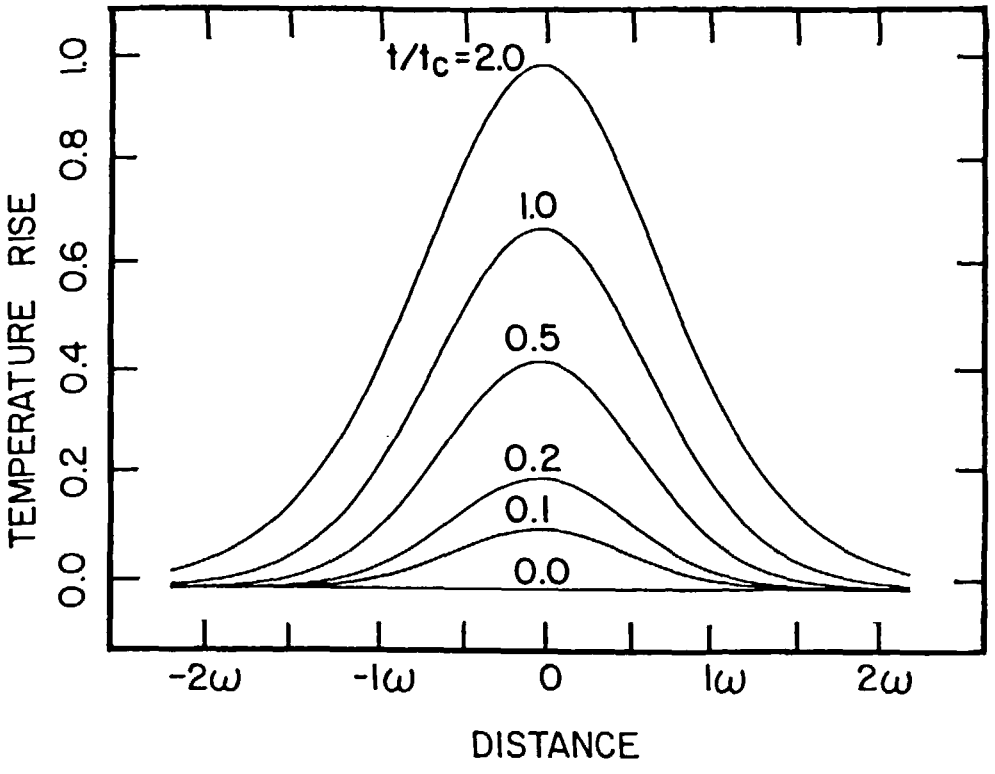

FIGURE 7. Radial temperature change produced by absorbance of a Gaussian pump beam within a stationary, homogeneous sample — step response.

where μ is viscosity, k is thermal conductivity, a is thermal expansion coefficient, and g is acceleration due to gravity. The inverse third power dependence in Equation 7 suggests that large pump beams are more likely to produce convection than small beams. For most liquids, the power absorbed per unit length below which convection is negligible ranges from 100 μW/cm for a 1-mm spot size pump beam to 100 W/cm for a 10-μm spot-size pump beam. It appears that boiling of the solvent presents a greater problem than convection for very small spot-size pump beams.

Flowing or moving samples are often of interest in thermo-optical spectrophotometries. Examples include detection in flowing liquid or gas streams, as in liquid chromatography, flow injection analysis, and convectively distorted beams.[44-46,58-63] Flow usually is assumed to translate the heated material downstream at a constant rate, given by the localized flow velocity. Thermal gradients induced by flow are ignored; the theory is only valid for small flow velocities. Consider the temperature rise produced by the absorbance of a Gaussian beam within a homogeneous sample. If the flow is directed along the y direction, then the translated temperature rise produced by impulse excitation is given by

$$\Delta T_{Flow}(x,y,t) = \frac{2.303E_o\epsilon C}{2\pi k\omega^2/4D(1 + 2t/t_c)} e^{\left\{\frac{-2[x^2+(y+Vt)^2]/\omega^2}{(1+2t/t_c)}\right\}} \quad (21)$$

where V is flow velocity. Under conditions of steady laminar flow, the flow velocity is known and may be substituted into Equation 21. As in static samples, the temperature rise produced by an arbitrary excitation function is given by the convolution integral of the impulse response with the excitation function.

Finally, this discussion has ignored the inhomogeneous nature of the sample; if nothing else, heat flow along the beam axis to the cuvette windows can be important, particularly for very thin cuvettes employed in chromatography. Here, the problem of heat flow between a thick window and a transparent solvent is considered; the problem of subsequent heat flow into the surrounding atmosphere is too difficult to be presented. If the pump beam is perpendicular to the cuvette window, the problem may be simplified into radial and longitudinal components.[38] Then, the radial temperature rise of Equation 14 is multiplied by the result of the one-dimensional heat flow problem along the beam axis. The temperature rise along the beam axis, for impulse excitation, is given by[38]

$$\Delta T_{Impulse}(x,y,z,t) = \Delta T_{Impulse}(x,y,t) \frac{k_1\sqrt{D_1}}{k_1\sqrt{D_1} + k_2\sqrt{D_2}} \times \left\{1 + \frac{k_2\sqrt{D_2}}{k_1\sqrt{D_1}} \operatorname{erf}\left(\frac{z}{2\sqrt{D_1 t}}\right)\right\} \qquad z > 0$$

$$= \Delta T_{Impulse}(x,y,t) \frac{k_1\sqrt{D_1}}{k_1\sqrt{D_1} + k_2\sqrt{D_2}} \left\{1 - \operatorname{erf}\left(\frac{|z|}{2\sqrt{D_2 t}}\right)\right\} \qquad z < 0 \quad (22)$$

where erf is the error function, the subscript 1 corresponds to the physical properties of the absorbing sample, and the subscript 2 corresponds to the transparent window.

Figure 8 presents a plot of the axial temperature rise near a transparent (quartz) window and an absorbing (aqueous) sample; the transparent window is on the left and the absorbing solution is on the right. This plot only considers axial heat flow. Radial heat flow will simultaneously act to decrease the temperature rise. The high thermal conductivity and diffusivity of the quartz compared to water results in a rapid transfer of heat away from the interface into the quartz. An individual would expect heat flow along the beam axis to be significant when the cuvette length is small compared to the pump beam spot-size. Note that the temperature change, but not the derivative of temperature with the axial distance, is continuous across the interface. Heat flow along the beam axis acts to decrease the maximum temperature rise within the sample but not to distort the radial shape of the temperature rise.

D. Refractive Index Profile

The derivative of refractive index with temperature, dn/dT, relates the temperature rise produced by absorption of the pump beam, ΔT, with the refractive index change within the sample, Δn. Unfortunately, dn/dT for any particular solvent varies with temperature (and wavelength and pressure). For the small temperature change typically produced in thermo-optical spectrophotometries and the narrow bandwidth of the probe laser, dn/dT may be considered a constant; the refractive index profile within the sample, Δn, is given by the product of dn/dT with the temperature rise, ΔT:

$$\Delta n = dn/dT \Delta T \quad (23)$$

If dn/dT varies appreciably over the temperature rise, then dn/dT must be integrated over the temperature change.

$$\Delta n = \int_{T_0}^{T_0 + \Delta T} (dn/dT)\, dT \quad (24)$$

where T_0 is the initial temperature.

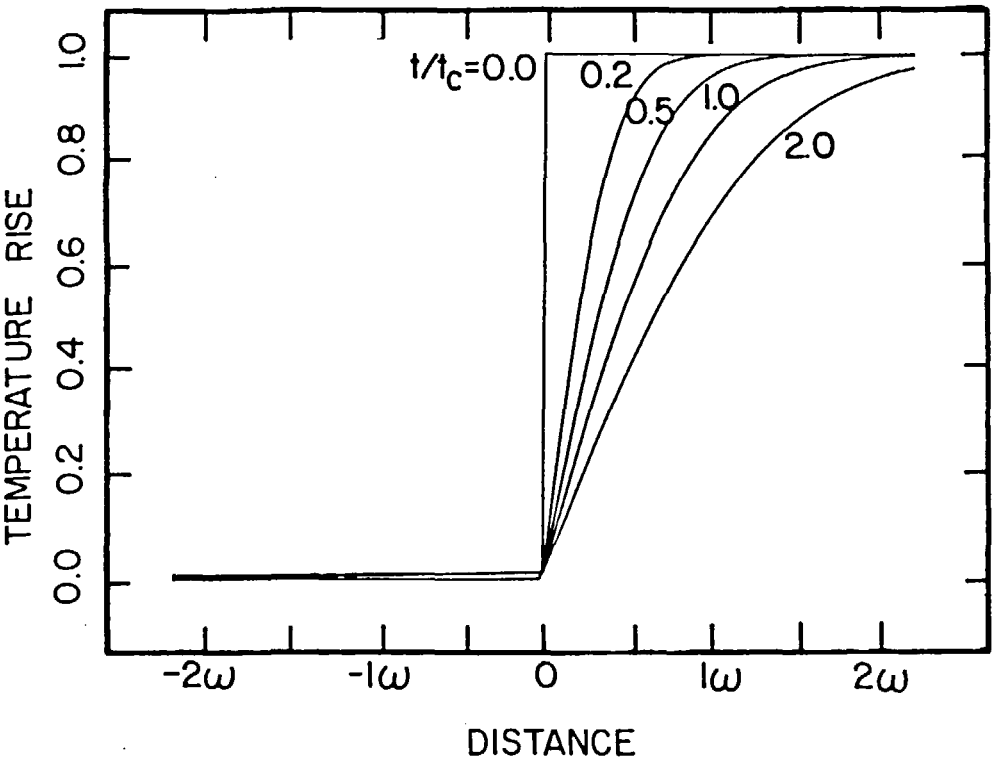

FIGURE 8. Axial temperature change produced by absorbance of a Gaussian pump beam within a stationary, inhomogeneous sample. The region on the left corresponds to transparent quartz and the region on the right corresponds to weakly absorbing water — impulse response. Time constant calculated for the aqueous sample.

E. Diffraction of Probe Beam

1. Introduction

In thermo-optical experiments, the probe beam interacts with a thermally induced, time-varying refractive index variation within the sample. This variation induces a perturbation upon the phase of the probe beam electric field. The phase distortion induced at the sample is transformed into an intensity distortion at the detector plane.[64,65] The intensity distortion is measured as a change in the beam center intensity with a simple photodiode, a deflection of the entire beam with a position-sensitive detector, or the entire profile is studied with a photodiode array.

The refractive index perturbation may be considered as an optical element, somewhat analogous to a lens, prism, grating, or curved mirror. However, a thermo-optical element is unusual in several respects. Initially, and most importantly, the properties of the optical element will change with time. For an unheated sample, no thermo-optical element will be formed so that the transmitted probe beam is undistorted. When the pump laser illuminates the sample, a thermo-optical element is formed along the pump beam path. For pulsed excitation, the element is formed rapidly and decays slowly, whereas cw excitation produces a gradual formation of the element. Next, the strength of the element is continuously adjustable by varying the pump laser power; although the element may be well behaved for low pump power, distortions often result at high pump laser power. Finally, the element is often highly aberrant; a description based upon conventional optical elements is limited to low power, weak effects. The perturbation induced upon the probe beam by the refractive index profile is considered in this section.

Change in the probe beam intensity at the detector produced by the thermally induced refractive index perturbation is usually taken as the analytical signal. This change has been modeled using several techniques of optical propagation. This section considers two: Fraunhofer diffraction, a rigorous method which requires numerical integration, and the paraxial approximation, which yields particularly simple results.

2. Fraunhofer Diffraction

There have been three examples of diffraction theory applied to the thermal lens which have appeared in the literature.[66-68] The general conclusion of these diffraction theories is that the behavior of the thermal lens is quite similar to the temporal and alignment behavior predicted by the paraxial approximation when the pump beam spot-size is the same size or larger than the probe beam spot-size. However, the magnitude of the signal and time constant predicted by the diffraction theory differs significantly from that predicted by the paraxial theory. Solution of the diffraction integral is particularly important when the pump beam is small compared to the probe beam, while the paraxial approximation is accurate when the pump beam is much larger than the probe beam.

This section presents a relatively simple example of diffraction theory. In diffraction, the probe beam intensity profile at the detector plane is determined by applying the diffraction integral to the phase and amplitude of the beam at the exit face of the sample. This diffraction integral simplifies to a Fourier transform under conditions of Fraunhofer diffraction. This diffraction approach is valid under two conditions: either the detector plane is located far from the sample or the detector plane is located at the focus of a lens.

In diffraction, the heated sample induces a phase shift in the probe beam. The phase shift is transformed by diffraction into an intensity change at the detector.[64,65] Therefore, it is necessary to begin with a description of the electric field, U(x,y,t), of the probe beam, a complex valued function which may be expressed in terms of amplitude and phase.

$$U = \text{Amplitude } e^{(i\ \text{phase})} \tag{25}$$

where i is the square root of -1. The amplitude has units of watt$^{1/2}$/cm. The amplitude or magnitude of the electric field is a real valued function given, for a probe beam operating in the TEM_∞ spatial mode,[30] by

$$\text{Amplitude} = \frac{(2/\pi)^{1/2}U_0}{\omega} e^{[-(x^2+y^2)/\omega^2]} \tag{26}$$

where U_0 is the average probe beam electric field amplitude, ω is the probe beam spot-size, and ω_0 is the probe beam waist spot-size. The radial component of the amplitude is Gaussian and centered at the beam axis, whereas the variation of amplitude with distance from the beam waist, z, scales with the probe beam spot-size, Equation 3.

The phase of the beam is real valued and given by

$$\text{Phase} = \frac{-2\pi z}{\lambda} + \pi\frac{(x^2 + y^2)}{R} \tag{27}$$

where z is distance to the probe beam waist, λ is the wavelength of the probe laser, and R is the radius of curvature of the probe beam wave-fronts

$$R = z[1 + (Z_c/z)^2] \tag{28}$$

Z_c is the confocal distance, and x and y are perpendicular distance from the beam axis.[30]

The phase increases with distance from the beam waist when far from the waist and inversely with distance when close to the beam waist. The radial component of phase increases quadratically with distance from the beam axis; surfaces of constant phase are parabolae of revolution centered on the beam axis. The phase surfaces are quite broad and usually may be approximated with spherical wave-fronts.

Upon propagation through the heated region produced by absorbance of the pump beam, a perturbation is introduced in the probe beam by the refractive index perturbation. The sample acts as a phase filter with complex transmission

$$T(x,y) = e^{i\phi} = e^{\left[\frac{i2\pi}{\lambda}\int \Delta n(x,y,z)\, d\,\mathrm{Path}\right]} \tag{29}$$

where the phase shift, ϕ, is given by the integral of the thermally induced refractive index change over the path of the probe beam.[65] This approximation is valid for thin samples such that the probe beam spot-size remains constant over the sample length. If the probe beam spot-size varies over the sample length, then the sample may be considered as a set of thin transparencies and the effect of each integrated over the probe beam path. The theory becomes more complicated if the refractive index change is sufficiently large to perturb the pump beam path within the sample.[69] Under certain conditions, thermally induced focusing may lead to a runaway situation wherein the thermally focused pump beam produces increased intensity and temperature rise, leading to greater thermally induced focusing. This self-focusing or self-action of powerful pump beams often destroys the sample.

The electric field of the probe beam at the exit of the sample, U_+, is given by the electric field incident upon the sample, U_-, times the complex transmission of the sample, T,[65]

$$U_+ = T\,U_- \tag{30}$$

After exiting the sample, the probe beam will propagate to the detector plane. Variation in phase at the sample is transformed into a variation in intensity at the detector plane. The electric field at the detector plane is governed by diffraction. Under Fraunhofer diffraction, the shape of the intensity profile does not change with distance from the sample, although the area of the profile scales with the square of distance. In this far-field approximation, the electric field of the probe beam at the sample exit is related by a Fourier transform to the electric field at the detector plane[65]

$$U_{\mathrm{Detector}} = B_{12}\, e^{\left\{\frac{i\pi(x^2+y^2)}{\lambda z_{12}}\right\}}\, \mathcal{FF}\{U+\} \tag{31}$$

where B_{12} is a complex constant with unit magnitude, z_{12} is the distance from the sample to the detector, and $\mathcal{FF}$ denotes the two-dimensional Fourier transform.

Usually, the electric field may be separated into the product of two components, one dependent upon the x dimension and the other dependent upon the y dimension. In this case, the two-dimensional transform may be written as the product of the transforms of the two component functions. In general, explicit evaluation of the Fourier transform, and hence the intensity, is very difficult. However, the discrete Fourier transform may be applied advantageously in the numerical evaluation of the probe beam electric field and intensity at the detector. The fast Fourier transform is an efficient method for the evaluation of the intensity profile of the probe beam, whereas numerical integration of the electric field is an efficient method for calculating the beam center intensity at the detector plane.

Photodetectors respond to the intensity and not the electric field of the probe beam, where intensity is given by the square of the electric field

$$I(x,y,t) = |U_{Detector}|^2 = |\mathcal{FF}(U_+)|^2 \tag{32}$$

If only the probe beam center intensity is monitored at the detector plane, then the central value theorem of Fourier transforms may be applied[65]

$$I(0,0,t) = \left| \int_{-\infty}^{\infty}\int U_+(x,y,t)dx\, dy \right|^2 \tag{33}$$

To compute the expected far-field probe beam center intensity, the electric field is integrated over all space and then squared. A transform is not necessary.

As the only example of diffraction theory, consider the crossed-beam thermal lens where the probe beam crosses the pump beam at right angles within a homogeneous sample. This model will be compared with Figure 3, the photographs of the beam profiles produced by a strong crossed-beam thermal lens. No phase shift is induced in the direction of the pump beam, only perpendicular to the plane containing the two beams. Under pulsed excitation, the phase shift is given by the integral of Equations 14 and 23 over the probe beam path, the Y direction.

$$\phi_{Impulse}(x,t) = \frac{2\pi}{\lambda}\int_{-\infty}^{\infty} \Delta N_{Impulse}(x,y,t)dy$$

$$= \frac{2.303E_0\epsilon C}{\lambda(2\pi)^{1/2}k(t_c/\omega)(1 + 2t/t_c)^{1/2}}\, e^{\left[\frac{-2x^2/\omega^2}{(1+2t/t_c)}\right]} \tag{34}$$

Instead of modeling the impulse response, consider the step response, given by the integral of Equation 34 over time

$$\phi_{Step}(x,t) = \int_0^t \phi_{Impulse}(x,t')\, dt' \tag{35}$$

which is simplified using the change of variables

$$T = \frac{-2\, x^2/\omega^2}{1 + 2t/t_c} \tag{36}$$

and the integral

$$\int x^{-3/2}e^{-x}dx = -2\sqrt{\pi}[(\pi x)^{-1/2}e^{-x} + \text{erf}(\sqrt{x})] \tag{37}$$

to yield

$$\phi_{step}(x,t) = \frac{2.303E\epsilon C\, dn/dT}{(2\pi)^{1/2}k\,\lambda} \times$$

$$(\omega\{(1 + 2t/t_c)^{1/2}\, e^{\left[\frac{-2(x^2)/\omega^2}{(1+2t/t_c)}\right]} - e^{[-2(x^2)/\omega^2]}\}$$

$$+ (\pi/2)^{1/2}\{\text{erf}\left[\frac{x}{\omega}\left(\frac{2}{1 + 2t/t_c}\right)^{1/2}\right] - \text{erf}\,[x(2)^{1/2}/\omega]\}) \tag{38}$$

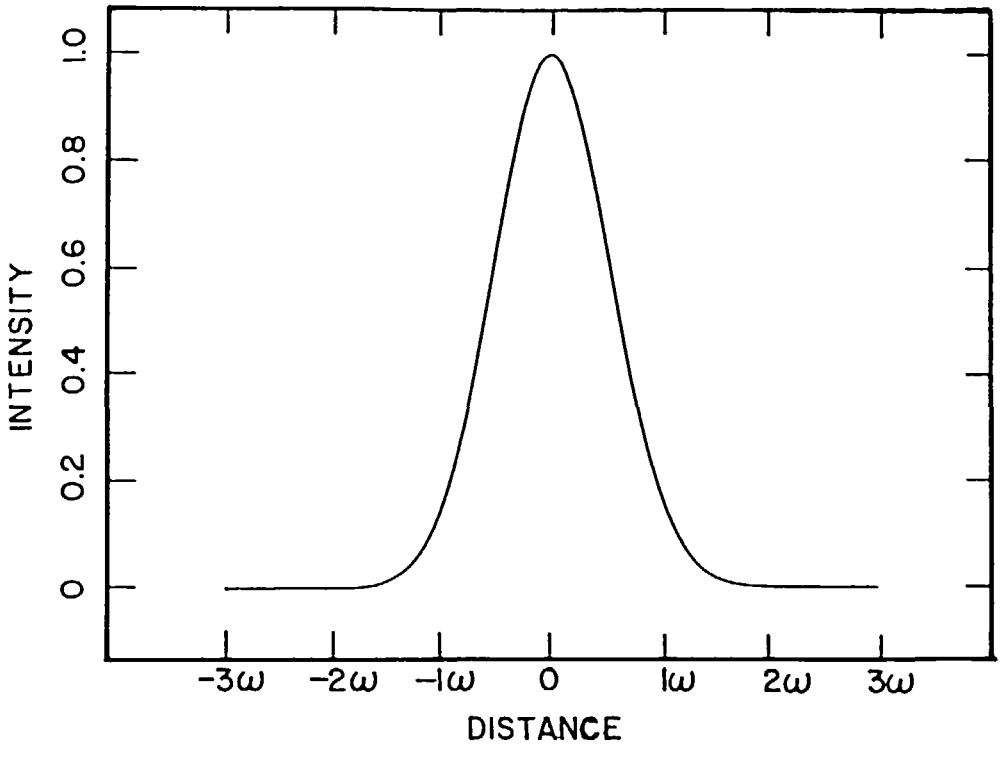

FIGURE 9. Diffraction theory prediction of intensity profile for crossed-beam thermal lens in direction perpendicular to plane containing the two beams. (A) Pump beam off; (B) pump beam on.

Numerical evaluation of the diffraction integral in the absence of the thermally induced phase shift yields a Gaussian beam profile, as expected, at the detector plane, Figure 9A. In the presence of a fairly strong crossed-beam thermal lens, the diffraction theory predicts a beam profile shown in Figure 9B. Here, the pump beam spot-size is one tenth the probe beam spot-size. If the beams are similar in size, the probe beam profile is not severely distorted and instead appears as a defocused Gaussian beam. Note the decrease in intensity predicted for the beam center and the redistribution of energy into the wings of the beam. Also note that the width at half-height of the unperturbed and perturbed profiles are similar in magnitude. When compared with the photographs of Figure 3 in the beginning of this article, the agreement between the observed profile and the result of the diffraction integral is quite good. Unfortunately, the high contrast of the photographic paper used in Figure 3 does not allow a more quantitative comparison between the beam profile and diffraction theory; a more detailed study will be published elsewhere.

3. Paraxial Approximation

Particularly simple results are produced by the paraxial approximation for optical propagation. The approximation is based upon the refractive index profile and its derivatives evaluated at the probe beam axis; off axis contributions are ignored. This approximation is valid when (1) the sine of the angle of divergence of the probe beam is sufficiently small so that it may be replaced by the angle itself and (2) the Taylor's series expansion of the refractive index profile with respect to radius may be truncated at the second derivative. The latter assumption equates the refractive index perturbation within the heated sample with a conventional optical element such as a change in optical path detected interferometrically, a lens to defocus the probe beam, or a prism to deflect the probe beam.

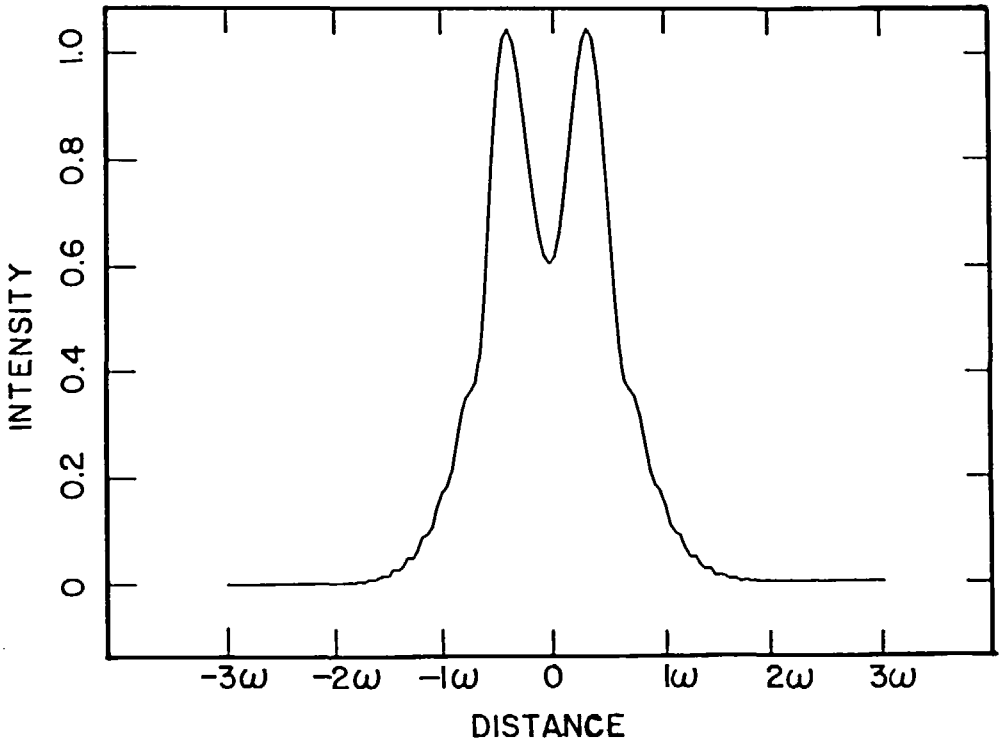

FIGURE 9B.

The change in refractive index, integrated over the probe beam path, is equal to the thermally induced change in optical path, $\Delta\mathcal{L}$, evaluated at the probe beam axis. This change in optical length is detected as a phase shift in an interferometer and often is much less than the wavelength of the probe beam. If the nondiverging pump beam is coaxial with the probe beam, the phase shift, ϕ, is simply given by

$$\phi = \frac{2\pi}{\lambda}\Delta n\mathcal{L} \tag{39}$$

where $\mathcal{L}$ is the path length; the coaxial optical path change measurement increases in sensitivity with path length.

For a crossed-beam measurement, the optical path is integrated over the probe beam path and maximizes when the two beams are coplanar.

$$\phi = \frac{2\pi}{\lambda}\int \Delta n \, \mathrm{dpath} \tag{40}$$

The phase shift produced by the crossed-beam instrument is independent of path length and better suited to small volume samples.

The first derivative of the refractive index with distance perpendicular to the probe beam axis produces a deflection of the beam and is modeled as a thin prism, Figure 10. The heated region acts to deflect the probe beam away from its original path. The deflection

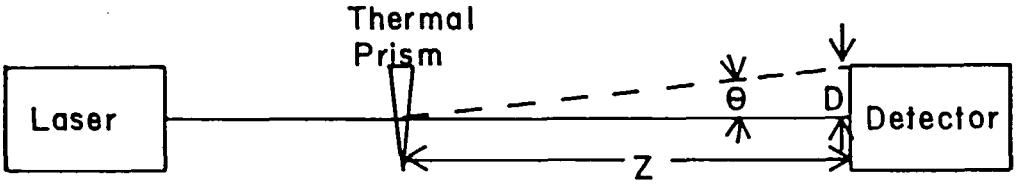

FIGURE 10. Deflection of the probe laser beam by a thermal prism. The θ is the deflection angle, Z is the distance from the thermal prism to the detector, and D is the offset of the probe beam.

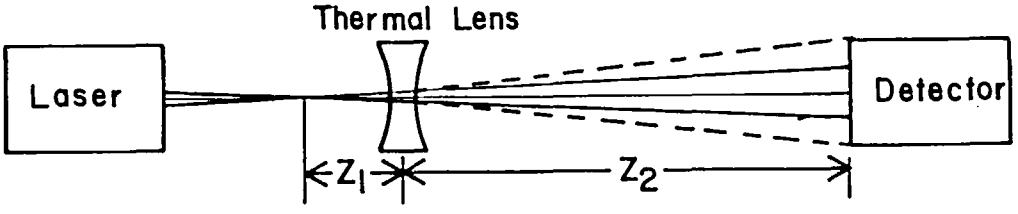

FIGURE 11. Defocusing of the probe beam by a thermal lens. Z1 is the distance from the beam waist to the thermal lens and Z2 is the distance from the thermal lens to the detector.

angle, θ, is given by the integral over the optical path of the first derivative of refractive index change with distance[15]

$$\theta = \int dn(x,y,t)/dy \; dpath \tag{41}$$

For the paraxial approximation to be valid, the deflection angle must be sufficiently small so that $\sin\theta = \theta$, or $\theta < 0.3$ radians. Furthermore, the pump beam must be larger than the probe beam so that dn/dy does not change across the probe beam radius.

If the probe beam is aligned parallel to the Gaussian refractive index profile produced by absorption of a pulsed Gaussian beam within a homogeneous sample, then the deflection angle equals zero when the pump and probe beams are coaxial since the first derivative of the refractive index equals zero at the center of the distribution. The deflection angle maximizes when the probe beam passes through the inflection point of the Gaussian refractive index profile.

The deflection angle is converted into an offset of the probe beam at the detector. The offset distance is given by

$$\text{Offset} = \theta Z \tag{42}$$

where Z is the distance from the sample to the detector. This displacement is measured by a number of photodetector methods described below in the thermal prism section. At first glance, it would appear that very long distances between the sample and detector are desirable since the displacement increases proportionally with this distance. However, the probe beam spot-size and beam pointing instabilities increase with the distance. A compact instrument should produce a better signal-to-noise ratio than a long path instrument.

The second derivative of refractive index with distance perpendicular to the probe beam axis results in defocusing (or focusing) of the probe beam and is often modeled as a lens, Figure 11.[15] In most liquids, thermal expansion produces a decrease in optical path at the probe beam center, resulting in an action analogous to a negative focal length lens. The

inverse focal length of the thermal lens is given by the integral of the second derivative of the refractive index with distance, integrated over the optical path. If the probe beam is coaxial with the pulsed Gaussian beam, then the inverse focal length is given by

$$1/f_{Impulse} = \int \frac{d^2\Delta n(r)}{dr^2} \, dpath\Big|_{r=o} = \frac{-4.606E\epsilon C\mathcal{L} \, dn/dT}{\pi k\omega^2 t_c(1 + t/t_c)^2} \tag{43}$$

where $\mathcal{L}$ is path length.

The effect of a thermal lens upon the probe beam is usually measured as a change in the probe beam center intensity. The intensity, in turn, is inversely proportional to the square of the probe beam spot-size at the detector

$$I = \frac{2P}{\pi\omega_x\omega_y} \tag{44}$$

where P is the total power of the probe beam and ω_x and ω_y are the probe beam spot-sizes aligned along the x and y direction. In the case of a radially symmetric probe beam in the coaxial thermal lens measurements, $\omega_x = \omega_y = \omega^2$. In the crossed-beam thermal lens, the probe beam is defocused in only one direction and Equation 44 must be used. However, for this discussion, let us consider the coaxial thermal lens.

The probe beam spot-size is often described using the ABCD law. In this algorithm, the propagation of the probe beam is described in terms of a 2 × 2 system matrix equal to the product of individual 2 × 2 matrices, each associated with a specific optical element through which the probe beam passes.[11,29,30]

The effect of a lens upon the probe beam is considered in Figure 11. The lens is located a distance Z1 from the probe beam waist of spot-size ω_0 and the beam traverses a distance Z2 to the detector plane. Of course, before formation of the thermal lens, the probe beam spot-size at the detector plane, ω_{off}, is given by Equation 3 for a propagation distance Z = Z1 + Z2

$$\omega_{off}^2 = \omega_0^2\left[1 + \frac{(z_1 + z_2)^2}{z_c}\right] \tag{45}$$

The probe beam spot-size at the detector plane with a finite thermal lens is given by[11]

$$\omega_{on}^2 = \omega_0^2\left[(1 - z_2/f)^2 + \frac{(z_1 + z_2 - z_1z_2/f)^2}{z_c^2}\right] \tag{46}$$

The relative change in probe beam center intensity due to the thermal lens is found

$$\Delta I = \frac{I_0 - I(t)}{I(t)} = \frac{\omega_{on}^2 - \omega_{off}^2}{\omega_{off}^2}$$

$$= \frac{(1 - z_2/f)^2 + (z_1 + z_2 - z_1z_2/f)^2}{[1 + (z_1 + z_2)^2/z_c^2]} - 1 \tag{47}$$

where I_0 is the unperturbed probe beam intensity and I(t) is the time-dependent thermal lens signal. The small signal limit is found by assuming $1/f \to 0$; terms containing $1/f^2$ are not retained:

$$\Delta I = \frac{\frac{-2z_2}{f}[1 + z_1(z_1 + z_2)/z_c^2]}{1 + (z_1 + z_2)^2/z_c^2} \tag{48}$$

Optimization of the thermal lens signal is important to produce high sensitivity. In particular, optimization of the thermal lens instrument with respect to Z1 and Z2, the distance from the probe beam waist to the sample and the distance from the sample to the detector, respectively, is important. The derivative of ΔI with respect to Z2 may be equated with zero to find the optimum spacing between the sample and detector. Four extrema are found: $Z2 = -\infty; -(Z1^2+Z_c)/(Z1+Z_c); -(Z1^2+Z_c)/(Z1-Z_c); \infty$. The first extremum is rejected since it implies that the detector should be placed before the sample. The middle two extrema are associated with saddle points and are not absolute extrema. The last extremum is the far-field approximation, analogous to that employed in Fraunhofer diffraction.

In the far-field approximation, ΔI is evaluated in the limit $Z2 \rightarrow \infty$; only terms second order in Z2 are retained:

$$\Delta I = -z_1/f \tag{49}$$

The relative far-field change in intensity increases with Z1. In the small signal limit, the relative change in the probe beam intensity increases linearly with both the inverse focal length of the thermal lens and the distance between the probe beam waist and the sample. The optimum value of Z1 is ∞ or $-\infty$; that is, the sample should be located far from the probe beam waist.

It should be noted that this far-field approximation is somewhat imprecise. The two limits employed, $Z2 \rightarrow \infty$ and $1/f \rightarrow 0$, produce two undefined terms, $(Z2/f)^2$ and $(Z1Z2/fZ_c)^2$ in the numerator of ΔI. Instead, the following two limits should be taken: $Z2/f \rightarrow 0$ and $Z2 \rightarrow \infty$. The first limit is valid if the focal length of the thermal lens is greater than the spacing between the sample and detector, while the second limit is valid if $Z2 >> Z1, Z_c$.

To obtain maximum thermal lens signal, one would use a negative focal length lens to locate the (virtual) probe beam waist far from the sample. One the other hand, an unfocused probe beam could be employed so that the beam waist is located in the probe laser cavity.

Care must be employed in the application of the far-field approximation for dual beam thermal lens instrumentation. The signal is maximized by locating the probe beam waist far from the sample. However, this alignment produces an arbitrarily large probe beam spot-size within the sample. Simultaneous optimization of the thermal lens signal by minimizing the pump beam spot-size results in the probe beam spot-size being much larger than the pump beam spot-size. Unfortunately, this experimental configuration invalidates the paraxial assumption since higher order terms cannot be ignored in the Taylor's series expansion of refractive index with distance.

Another difficulty with the far-field approximation is the unwieldy experimental configuration; optical paths of several meters are commonly employed to ensure the validity of the far-field limit. The use of an unfocused probe beam would necessitate *very* long path lengths to ensure the far-field limit.

A much more compact experimental configuration arises from consideration of the near-field performance, albeit with a decrease in sensitivity.[70] Furthermore, it is desirable to locate the sample near the probe beam waist to decrease the probe beam size and hence decrease thermal lens aberration. Inspection of Equation 48 reveals that placement of the sample at the probe beam waist, $Z1 = 0$, produces a thermal lens signal of $\Delta I = -Z_c/f$ when the detector is placed one confocal distance past the beam waist, $Z2 = Z_c$.

A slight increase in probe beam spot-size is produced when the sample is located one confocal distance before the beam waist, $Z1 = -Z_c$ compared with the beam waist spot-size. A local maximum in the thermal lens signal is observed when the detector is placed at the probe beam waist, $Z2 = Z_c$, $\Delta I = -2Z_c/f$. This signal is twice the magnitude of the signal observed when the sample is located at the beam waist within a more compact instrument.

These near-field alignment configurations would appear to offer several advantages compared to the far-field configuration. The probe beam spot-size is minimized so that aberration effects in the thermal lens will be minimized. Then, a much more compact instrument should be produced compared to the far-field instrument; optical paths of centimeters compared to meters would be required. As a disadvantage, some decrease in sensitivity is expected with the near-field alignment, although a complete diffraction theory would be required to compare the sensitivity of the near- and far-field configurations. Since the detector is not located in the far field of the probe laser, the less restrictive and more complicated Fresnel diffraction integral will be required to model the experiment.

The sensitivity of thermal lens measurements increases with path length. However, the theory presented above implicitly assumes the sample is equivalent to a thin lens. If the sample is larger than the confocal distance of either the pump or probe laser beam, the beam spot-size will change over the sample length, violating the thin-lens assumption. For thick samples, it is necessary to recalculate the focal length of the heated sample across the path length, taking care to consider weak self-defocusing or -focusing of the pump beam. This problem has been considered by Fang and Swofford[48] for the dual beam thermal lens instrument and by Carter and Harris[71] for the single beam instrument. Essentially, the problem is iterative whereby the pump beam propagates through a thin slice of the sample, a new spot-size is calculated, the beam is propagated through another slice, a new spot-size is computed, etc.

The result of these calculations shows that the thermal lens signal does not increase linearly with path length. However, the use of a very loosely focused pump beam with a confocal parameter much larger than the sample length generates a signal which increases nearly linearly with path length for weakly absorbing samples. Unfortunately, a weakly focused pump beam yields decreased sensitivity for the dual beam instrument and long thermal time constants for both the single and dual beam instruments. On the other hand, the high sensitivity of the thermal lens measurements suggests that moderate power pump lasers will produce a background limited absorbance measurement for liquid phase samples more than a few millimeters in length.

Finally, and most importantly, Carter and Harris[67] have compared the results of the diffraction theory with the paraxial result for the single-beam thermal lens. Their work showed that the shape of the temporal and Z1 dependence are very similar for the two models. The paraxial results are quite simple but are not in good quantitative relation with experimental results, whereas the diffraction theory is more complicated but in good agreement with the experiment. Carter and Harris suggested the following modifications to the paraxial formulas to produce good agreement between theory and data:[67]

$$1/f = 0.52 \int \frac{d^2\Delta n(r)}{dr^2} \, dpath$$

$$t_c = \frac{\omega^2}{8D} \tag{50}$$

where the amplitude of the thermal lens signal is a factor of 0.52 decreased from the paraxial result and where the temporal response is a factor of two slower. The experiment is configured to operate with the detector in the far field and the maximum sensitivity occurring when the sample is located $\sqrt{3}\ Z_c$ past the beam waist.

F. Thermo-Optical Constants

Tables 1 to 3 present several useful thermo-optical constants for a number of liquids, gases, and solids.[72-83] The values should be taken as approximate since differences of several percent are frequently found for values published by different laboratories. Furthermore, the parameters change with temperature by several percent for a few degrees of temperature

Table 1
THERMO-OPTICAL CONSTANTS FOR GASES

Compound	$10^3 \times$ Density (Gcm^{-3})	Specific heat (J/g/C)	$10^4 \times$ Thermal conductivity (W/cm/C)	$10 \times$ Thermal diffusivity ($sec^{-1}cm^{+2}$)	$10^6 \times$ dn/dT ($°C^{-1}$)	C (μsec)	$10^4 \times \Delta n_{impulse}$	$10^{10} \times \Delta n_{Step}$
Air	1.17	1.01	2.61	2.21	−0.88	1.13	4.74	2.95
N_2	1.14	1.04	2.60	2.19	−0.90	1.14	4.83	3.03
O_2	1.30	0.92	2.67	2.23	−0.82	1.12	4.36	2.68
Ar	1.62	0.52	1.77	2.10	−0.86	1.19	6.49	4.25
He	0.16	5.32	15.00	17.62	−0.11	0.14	0.83	0.06
H_2	0.08	14.4	18.15	15.75	−0.42	0.16	2.30	0.20
CO_2	1.79	0.84	1.66	1.10	−1.38	2.27	5.82	7.27
CH_4	0.65	2.24	3.43	2.36	−1.35	1.06	5.90	3.44
C_2H_6	1.22	1.76	2.18	1.02	−2.35	2.45	7.00	9.42

change. Therefore, the data of Tables 1 to 3 are primarily intended as estimates of relative sensitivities in thermo-optical experiments.

The time constant is computed for $\omega_{pump} = 10$ μm. $\Delta n_{impulse}$ is computed for the initial beam center refractive index change under impulse excitation and a semi-infinite, homogeneous sample, $2.30E\epsilon C = 1.0 \times 10^{-6}$ J/cm and $\omega_{pump} = 10$ μm. The Δn_{step} is the beam center refractive index change for step excitation of a homogeneous sample evaluated for $2.303P\epsilon C = 1.0 \times 10^{-6}$ W/cm, $\omega_{pump} = 10$ μm, and $t = t_c$. In general, liquids produce a larger refractive index change and longer time constants than solids or gases. The Δn varies by about a factor of four between different organic solvents. Small chain hydrocarbons, like pentane, produce greater sensitivity than long chain hydrocarbons, such as decane. Nonpolar solvents such as carbon tetrachloride and carbon disulfide produce the highest sensitivity, and polar solvents such as methanol produce smaller sensitivity. Water is a particularly poor solvent for thermo-optical spectrophotometries, having a refractive index change, and hence a sensitivity, almost an order of magnitude smaller than methanol.

Usually, thermo-optical properties are reasonably well behaved. Water is an important exception; dn/dT changes exponentially from −3 to 80°C, Figure 12.[75] For temperatures less than 4°C, dn/dT is positive. At higher temperatures, dn/dT is negative and rapidly increases in absolute value. Since the other thermo-optical parameters of water are relatively insensitive to temperature, the sensitivity of thermo-optical analysis of aqueous samples should increase by nearly a factor of four from 20 to 80°C.

The poor thermo-optical constants of water result in low sensitivity for thermo-optical absorption determination of aqueous samples. It is fairly common practice to utilize mixed water-acetone and water-methanol solvents to increase the thermo-optical sensitivity.[43,76] In general, the sensitivity of the mixed solvent is equal to the average of the thermo-optical sensitivity of the individual solvents, weighted by the mole fraction of each liquid. It also appears that mixtures of water and nonvolatile solutes produce enhanced sensitivity compared with pure water. An aqueous maltose hydrate solution[77] is one example. The dn/dT for dilute solutions is similar to that measured for pure water, 1×10^{-4} $°C^{-1}$. However, more concentrated solutions, greater than 25% by weight, demonstrate a factor of two greater dn/dT than pure water.

A rather obscure effect is observed for partially miscible solvent mixtures near their critical concentration and temperature.[84] Thermally induced concentration gradients can be formed which produce enhanced thermo-optical sensitivity. Unfortunately, the response time of the thermally induced concentration gradient is very slow, tens of minutes, which will limit analytical applicability.

Table 2
THERMO-OPTICAL CONSTANTS FOR LIQUIDS

Compound	Density (g/mℓ)	Specific heat (J/g/C)	Thermal conductivity (mW/cm/C)	$10^3 \times$ Thermal diffusivity ($sec^{-1}cm^{+2}$)	Refractive index	$10^4 \times$ dn/dT ($°C^{-1}$)	t_c (msec)	$10^4 \times \Delta n_{Impulse}$	$10^4 \times \Delta n_{Step}$
n-Pentane	0.63	2.29	1.18	0.82	1.360	−5.5	0.31	−2.4	−4.1
n-Hexane	0.66	2.23	1.23	0.84	1.377	−5.2	0.30	−2.2	−3.7
n-Heptane	0.67	2.21	1.27	0.86	1.390	−4.9	0.29	−2.1	−3.4
n-Octane	0.71	2.19	1.32	0.85	1.400	−4.7	0.29	−1.9	−3.1
n-Nonane	0.72	2.18	1.36	0.87	1.407	−4.5	0.29	−1.8	−2.9
n-Decane	0.73	2.21	1.40	0.87	1.414	−4.2	0.29	−1.7	−2.6
cyclo-Hexane	0.78	1.81	1.23	0.87	1.43	−5.56	0.29	−2.5	−4.0
CS_2	1.26	1.02	1.50	1.17	1.63	−8.09	0.21	−4.1	−4.7
CCl_4	1.60	0.85	1.03	0.75	1.46	−6.12	0.33	−2.9	−5.2
Chloroform	1.52	0.95	1.17	0.81	1.446	−6.03	0.31	−2.6	−4.5
CH_2Cl_2	1.33	1.08	1.22	0.85	1.425	−5.5	0.29	−2.5	−3.9
Benzene	0.88	1.71	1.37	0.90	1.504	−6.52	0.28	−2.7	−4.2
Toluene	0.87	1.69	1.35	0.92	1.500	−5.68	0.27	−2.5	−3.7
Ortho-xylene	0.88	1.77	1.43	0.92	1.511	−5.0	0.27	−2.1	−3.1
Ethyl ether	0.72	2.31	1.37	0.82	1.35	−6.06	0.30	−2.3	−3.9
Acetone	0.80	2.18	1.90	1.09	1.362	−5.42	0.23	−2.0	−2.5
Ethyl acetate	0.91	1.96	1.49	0.84	1.372	−4.9	0.30	−1.7	−2.9
Methanol	0.79	2.46	2.02	1.04	1.311	−3.94	0.24	−1.3	−1.7
Ethanol	0.80	2.36	1.67	0.89	1.361	−4.0	0.28	−1.4	−2.1
n-Propanol	0.80	2.22	1.56	0.88	1.385	−3.7	0.28	−1.3	−2.1
Acetic acid	1.04	2.05	1.72	0.81	1.372	−3.9	0.31	−1.2	−2.0
Water (0°C)	1.00	4.21	5.80	1.38	1.334	+0.28	0.18	+0.04	+0.04
Water (20°C)	1.00	4.18	5.95	1.42	1.334	−0.81	0.18	−0.12	−0.12
Water (80°C)	0.97	4.20	6.70	1.64	1.333	−2.10	0.15	−0.33	−0.27

Table 3
THERMO-OPTICAL CONSTANTS FOR SOLIDS

Compound	Volume specific heat ($Jcm^{-3}C^{-1}$)	Thermal conductivity (mW/cm/C)	$10^3 \times$ Thermal diffusivity ($sec^{-1}cm^{+2}$)	Refractive index	$10^5 \times$ dn/dT ($°C^{-1}$)	t_c (μsec)	$10^6 \times \Delta n_{Impulse}$	$10^{12} \times \Delta n_{Step}$
LiF	4.12	113	27.4	1.39	−1.27	9.1	−2.0	−9.8
NaF	3.04	100	32.9	1.32	−1.6	7.6	−3.35	−14
NaCl	1.845	65	35.2	1.54	−3.65	7.1	−12.6	−49
KCl	1.347	65	48.3	1.49	−3.4	5.2	−16.0	−46
KBr	1.197	48	40.1	1.52	−4.0	6.2	−21.4	−73
CsBr	1.171	09.6	08.2	1.66	−6.3	30.5	−34.2	−574
Csl	0.9094	11.3	12.4	1.79	−10.0	20.2	−69.7	−773
AgCl	1.984	11.5	05.8	2.06	−6.1	43.1	−19.6	−464
CaF_2	2.715	97	37.5	1.43	−0.77	6.7	−1.9	−6.9
MgO	3.129	250	79.9	1.66	1.89	3.1	+4.0	+6.6
Al_2O_3	2.999	250	83.4	1.78	1.41	3.0	+3.0	+4.9
Quartz	2.084	85	40.8	1.54	−0.539	6.1	−1.7	−5.5
ZeSe	2.646	130	49.1	2.43	4.8	5.1	+11.5	+32
CdTe	1.224	70	57.2	2.67	11.75	4.4	+60.7	+147
GeAs	1.420	370	261	3.30	18.7	1.0	+80.4	+44
Diamond	1.561	1510	967	2.42	0.98	0.3	+3.4	+0.6
Si	1.58	1200	760	3.41	16.2	0.3	+72.6	+12
Ge	1.652	590	357	4.0	26.8	0.4	+180.6	+40

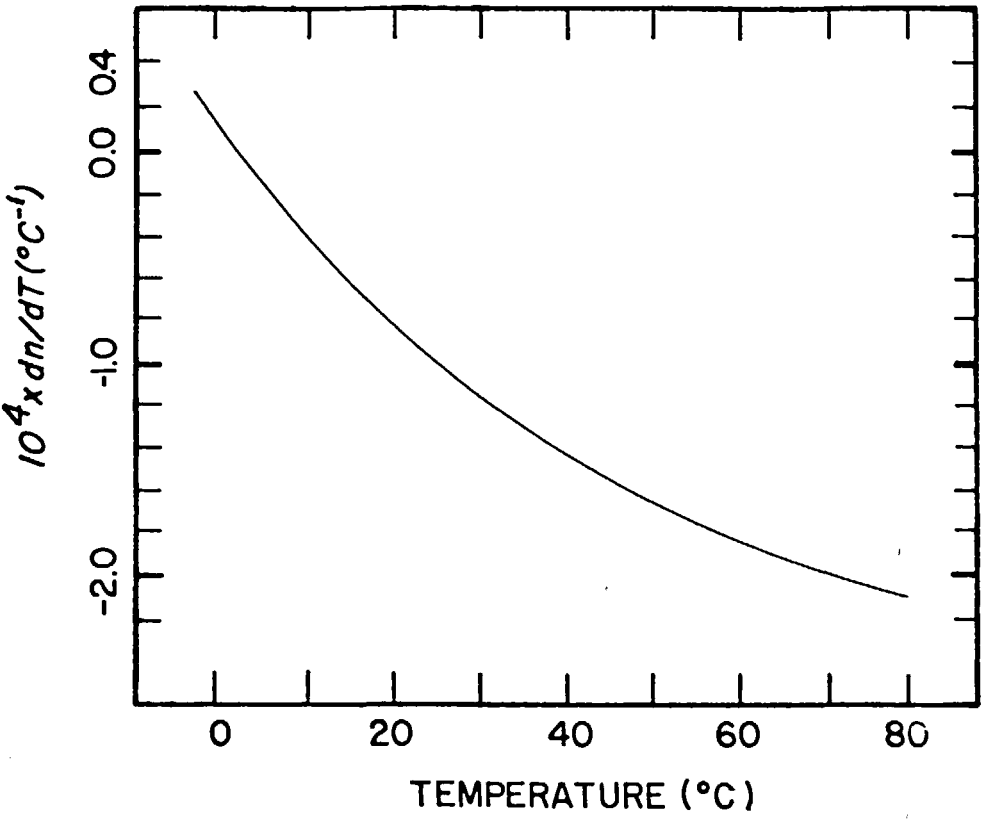

FIGURE 12. dn/dT for water as a function of temperature.

Tables of dn/dT for liquids are limited to common organic solvents. However, supercritical fluids have also been employed as solvents for thermo-optical spectroscopy.[78] Since dn/dT is expected to change drastically with both temperature and pressure near the critical point, the study of dn/dT and other thermo-optical properties is appropriate for supercritical fluids. The Lorentz-Lorenz formula relates the refractive index and density of a substance[64] which has been applied to the calculation of dn/dT for gases and liquids[72,75] and supercritical fluids.[78] This formula may be written as

$$dn/dT = 3L/2(1 + 2L\rho/M)^{-1/2}(1 - L\rho)^{-3/2}d\rho/dT \quad (51)$$

where M, the molar mass, and L, the molar refraction, are independent of temperature. Since extensive tables of density as a function of temperature may be found in the literature, dn/dT may be computed indirectly using the Lorentz-Lorenz formula. The formula is an approximation and small deviations are relatively common.[72]

The change in the refractive index with temperature is a much more complicated phenomenon for solids. Both negative and positive values of dn/dT are observed for different materials.[74] The physical mechanism for the change in refractive index with temperature does not appear to be well understood.

III. THERMO-OPTICS FOR LONG PATH LENGTH SAMPLES

A. Introduction

A number of thermo-optical instruments have been designed for the high-sensitivity measurement of absorbance in long path length samples. These measurements are based upon a

change in optical path length, measured interferometrically; a thermal lens, measured as a change in probe beam center intensity; and a thermal prism, measured as a deflection of the probe beam. Although a number of advantages have been claimed for each technique, the difference between their performance is slight and usually dominated by background solvent absorbance,[10,85-88] two photon absorbance generated by pulsed pump laser excitation,[89] the reagent blank,[90,91] and cuvette window absorbance.[92]

Certainly, the single-beam thermal lens has the simplest optical design; one laser beam both produces and probes the thermo-optical element. The only optical components required are a lens, chopper, cuvette, and photodetector. The highest precision is produced by digitization of the transient waveform with regression analysis to a deterministic model. A dual channel box-car averager can be constructed at little cost and produces fairly good results. Recently, a simple single-beam thermal lens instrument has been reported which utilizes a lock-in amplifier to demodulate the signal and produces good precision. For routine, single wavelength measurements, lock-in demodulation is quite attractive.

The pump-probe thermal lens instrument offers one significant advantage over the single beam, albeit at the price of greater instrumental complexity: tunable pulsed lasers may be employed to produce the pump beam, which facilitate access to a wide spectral region. Unfortunately, signal-to-noise often suffers from pulse-to-pulse irreproducibility in the pump beam intensity profile and nonlinear background signals. Regression analysis of the transient signal appears to be required for greatest precision.[93] Higher sensitivity is possible with the dual-beam design compared to the single-beam instrument by use of a tightly focused pump beam; however, the background limit observed with modest power pump beams suggests that this advantage is not particularly valuable for high background samples. Unfortunately, the dual-beam instrument is inherently more complicated than the single-beam instrument. At a minimum, two laser beams, a chopper, a lens, beam splitter, cuvette, spectral filter, and photodetector are required. Optical alignment for all double-beam designs is more difficult than the single-beam thermal lens. Potentially problematic is the background signal generated within all optical components through which both beams pass: the beam splitter, cuvette windows, and spectral filter.

The thermal prism instrument offers an interesting advantage compared with the thermal lens instruments: intensity noise is traded for pointing noise in the probe beam. The thermal prism signal is given by a deflection of the probe beam which is measured using a position-sensitive detector. Position detectors are insensitive to probe beam intensity fluctuations. Unfortunately, the deflection experiment is dominated by pointing noise in the probe beam. Of course, thermal lens measurements record the probe beam center intensity and are insensitive to probe beam pointing noise.

The interferometric instruments have employed Jamin, Mach-Zehnder, and Fabry-Perot interferometers. The first two designs provide a reference beam for removal of some proportional noise, whereas the latter design provides very high sensitivity. Unfortunately, the interferometric instruments are optically and electronically the most complicated thermo-optical designs.

Each of these techniques produces a signal which increases with path length. However, the divergence of the pump beam evidently results in a limitation on sensitivity improvement produced by path length increase. Furthermore, the background signals generated over long paths will limit the precision of the measurement.

The sensitivity of these thermo-optical techniques goes to zero for small path length samples. However, another set of thermo-optical techniques have been developed for short path length, small volume samples; these thermo-optical techniques are not dependent upon path length. The tradeoff between the long path length techniques and the small volume techniques is somewhat fuzzy but appears to fall in the 100-μm to 1-mm path length range.

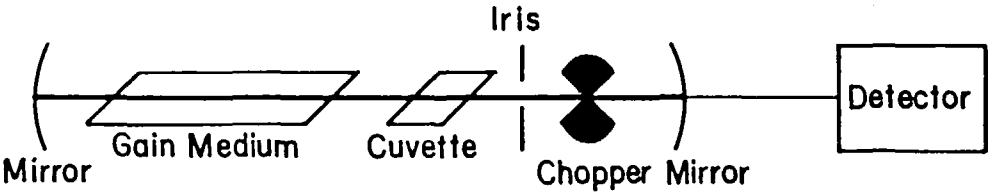

FIGURE 13. An intercavity thermal lens. The cuvette is tilted at Brewster's angle to minimize reflective loss. Defocusing of the beam produces diffraction loss at the intercavity iris. A chopper is used to modulate the laser beam. The transmitted intensity through the output coupler of the laser is measured with a photodetector.

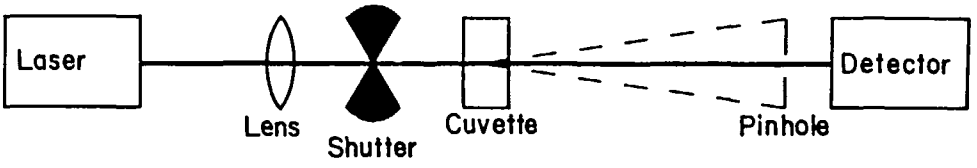

FIGURE 14. Conventional single-beam thermal lens. The laser beam is focused with a lens into the sample. Thermally induced defocusing is detected as a change in the beam center intensity by a photodetector located behind a small area pinhole. The shutter is positioned after the focusing lens to avoid thermally induced intensity modulation generated within the lens itself.

B. Coaxial Thermal Lens

Historically, the first thermal lens measurements employed an intercavity design where a weakly absorbing sample was placed within the laser cavity, Figure 13.[39] Defocusing produced by the heated sample results in increased diffraction losses on the intercavity iris, yielding a decreased laser output power upon formation of the thermal lens. The high circulating power within the laser, combined with the extreme sensitivity to optical configuration of a laser operating slightly above threshold, results in very high sensitivity. The early instrument was used to generate absorbance data for a number of organic solvents.[94,95] It is interesting that the first reference to the thermal lens effect was also the first analytical study; the thermal lens signal was calibrated by dilutions of a strongly absorbing sample. However, the tedious and irreproducible alignment of the intercavity system discouraged most applications. Recently, Grishko et al.[96] utilized a coupled cavity to measure very weak absorbances with a relatively low-power laser. Under certain conditions, the intercavity thermal lens produces a pulsed output from a normally cw laser.[97] The pulse width is related to sample absorbance. Two intercavity detectors have been reported that were based upon a thermal deflection signal in a pump-probe configuration.[98,99]

An improved thermal lens instrument was produced when the sample was placed outside the laser cavity.[41] Early studies considered the divergence and convection effects produced by the absorbance of unfocused cw lasers.[100,101] An early study of the extracavity thermal lens is interesting for the number of parameters studied,[58] including flow, convection, cell length, analyte concentration, and laser power.

The first detailed study of the extracavity thermal lens utilized a far-field detector and a sample located one confocal distance past the beam waist, Figure 14.[41] After transmission through the sample, the beam is centered on a small area photodetector and the time-dependent formation of the thermal lens is recorded as a time-dependent change in the beam center intensity. In their important thermal lens paper, Hu and Whinnery[41] presented a paraxial theory for the extracavity thermal lens. The theory considered quantum yield of fluorescence, laser power, sample absorbance, thermal properties of the solvent, temporal properties of the signal, and dependence of the signal upon focusing conditions of the laser. This theory forms much of the basis for the thermal lens theory presented above.

Dovichi and Harris[76] published the first thermal lens paper to appear in the analytical

literature. In that paper, the small absorbance form of Beer's law was considered as a relative change in transmitted and incident intensity:

$$\frac{(I_0 - I)}{I_0} = 2.303A \tag{52}$$

where I_0 is the incident intensity and I is the transmitted intensity of light upon the sample. The thermal lens signal consists of an analogous change in intensity, the initial and steady state beam-center intensities:

$$\frac{I(0) - I(\infty)}{I(\infty)} = 2.303EA \tag{53}$$

where I(0) is the initial far-field beam center intensity produced when the laser beam is unblocked, I(∞) is the steady-state intensity produced by the thermal lens, and E is the enhancement of the thermal lens signal compared with Beer's law response. For optimum alignment, the enhancement is given by

$$E = \frac{0.52P(dn/dT)}{\lambda k} \tag{54}$$

where P is the laser power, dn/dT is the change in refractive index with temperature, λ is the laser wavelength, and k is the thermal conductivity of the sample; the correction due to diffraction effects suggested by Carter and Harris is included in the expression. The enhancement of the thermal lens signal is a function of two parameters related to the laser, power and wavelength, and two parameters related to the solvent, dn/dT and k. To improve the enhancement, mixed solvents are employed. A 3:1 acetone-to-water solvent produced nearly an order of magnitude greater sensitivity than an aqueous solvent.

Values of enhancement utilized in this initial analytical paper were near unity, reflecting the low laser power employed. However, the periodic formation of the thermal lens produced with a modulated laser beam allows demodulation techniques to be employed which greatly reduce low-frequency noise in the measurement. In this instrument, a dual channel box-car averager was constructed and a small laboratory computer was employed to calculate ΔI. The detection limit, $A = 1.0 \times 10^{-3}$, primarily reflects the noise reduction capabilities of the thermal lens and not the increased sensitivity produced by high-power lasers.

The single-beam thermal lens instrument is unique among the thermo-optical techniques; the same laser beam produces and probes the thermo-optical element. The thermal lens signal is a function of the distance of the sample to the laser beam waist formed by the focusing lens, Figure 15, given by

$$\Delta I = 2.303E\epsilon C[z/(z_c + z)^2] \tag{55}$$

where E is the enhancement, given in Equation 54. The signal extrema occur when the sample is located one confocal distance past the beam waist, $Z = \pm Z_c$ for the detector located in the far field. A near-field extremum also exists which produces a signal of identical amplitude when the sample is located $(\sqrt{2} - 1)Z_c$ before the beam waist and the detector is located $(\sqrt{2} - 1)Z_c$ after the beam waist. The near-field configuration should produce a very compact thermal lens instrument with no loss in sensitivity.

Many advances in analytical instrumentation have been described. A single-beam differential thermal lens instrument has been developed which automatically subtracts the ab-

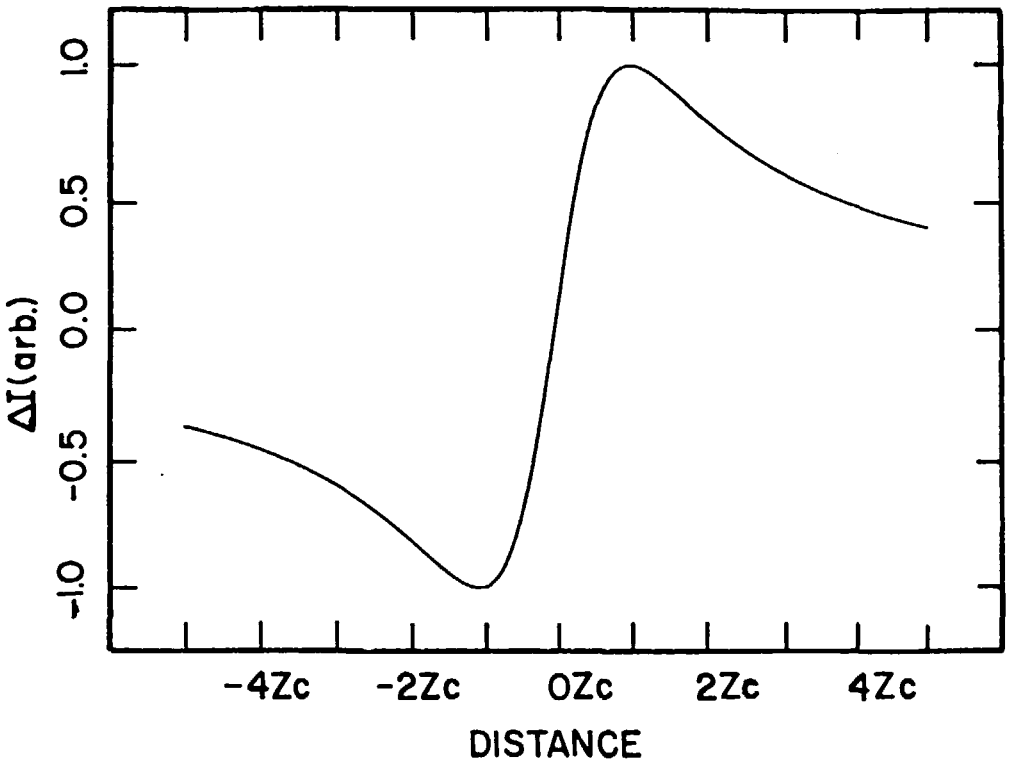

FIGURE 15. Variation in the single-beam thermal lens signal about the beam waist, far-field detector. The thermal lens signal maximizes when the sample is located ±1 confocal distance from the beam waist.

sorbance of the solvent blank and the sample.[102] This differential response is a result of a clever observation made by J. M. Harris: a thermal lens placed before the beam waist collimates the beam and the same lens placed after the beam waist diverges the beam, so that two identical lenses placed symmetrically about the beam waist should have no effect upon the beam propagation. This alignment automatically cancels the background signal generated by solvent absorbance; any change in the absorbance of the sample will produce a thermal lens signal on a near-zero background.

The differential system locates a reference sample one confocal distance before the beam waist and a sample at a confocal distance after the waist. Neglecting laser power loss at the first sample, the thermal lens signal is found to be proportional to the difference in absorbance of the two samples

$$\Delta I = 2.303E(A_2 - A_1) \tag{56}$$

where A_2 is the absorbance of the second sample, A_1 is the absorbance of the first sample, and E is the enhancement of the solvent system employed, assumed to be the same for both samples. Of course, reflective and light scatter losses will decrease the laser power at the second sample compared to the first. However, a small displacement of the position of the first sample will bring the system into null.

The differential thermal lens instrument automatically subtracts up to 99% of the background signal generated by identical samples. Detection limits of $A = 6.3 \times 10^{-7}$ were obtained for iodine in CCl_4, utilizing the dual channel box-car averaging signal processing technique.[102] Similar detection limits were reported for aqueous iron-1,10-phenanthroline, $A = 4 \times 10^{-7}$, corresponding to 5.5×10^{-11} *M* iron.[11,103] The differential instrument has

been applied to chromatographic detection both to remove the solvent blank signal and also to compensate partially for noise produced by flow fluctuations.[88]

Usually, the thermal lens signal is recorded as the relative change in probe beam center intensity, a particularly simple measurement. However, the beam center intensity is particularly sensitive to fluctuations in the spatial profile of the beam generated by light scatter from particles and refractive index gradients along the beam path. For example, the heated air blown across the beam path by a cooling fan on an oscilloscope was found to be the major noise source in a thermal lens experiment in this author's laboratory.

Although filtration of solvents helps minimize light scatter, minute refractive index gradients nevertheless act to distort the laser beam profile at the detector plane. Minimization of spatial noise improves detection limits and is based upon the averaging of the beam profile. For example, early intercavity thermal lens techniques recorded the beam profile generated by a scanned photodiode; the beam spot-size was computed from a measurement of the entire profile.[94] Recently, a diode array has been used to record rapidly the beam profile.[104-106] The spot-size may be computed efficiently from the second moment of the profile

$$\omega^2 = \frac{4\sum^{m}(n - n_0)^2 f(n)}{\sum f(n)} \tag{57}$$

where f(n) is the signal from the nth diode, m is the number of diodes, and n_0 is the center of the beam profile estimated from the centroid

$$n_0 = \frac{\sum nf(n)}{\sum f(n)} \tag{58}$$

Although measurement of the spot-size of the beam does produce improved precision, digitizing and data analysis are relatively slow. Only a few profiles may be digitized per thermal lens time constant. Better detection limits are produced by measuring the beam center intensity at many points in time and using a more efficient demodulation technique.[106]

A simple approach to the reduction of spatial noise utilizes a relatively large area detector;[102] averaging the spatial profile over a larger area acts to reduce beam profile fluctuations as a noise source. However, the detector cross section cannot be a large fraction of the beam radius; the thermal lens signal goes to zero as the detector integrates all of the beam profile.

Jansen and Harris[106] have recently reported a very clever averaging method for spatial noise. A partially transmitting mask was constructed with a radial transmission variation which closely approximated a quadratic function. When centered upon the beam profile, the transmitted power was proportional to the spot-size of the laser beam. A large radius lens collected the transmitted intensity, integrating it upon a photodiode to produce the measurement of beam spot-size. The mask has radial symmetry and integrates the beam intensity over its entire area, not along a single line as a linear photodiode array. Very good averaging of spatial noise is produced. Since the computation of spot-size was based upon optical and not electronic processes, the data-processing rate is limited only by the speed of light. Utilization of rapid signal demodulation techniques is possible with this spatial mask, producing high-precision thermal lens measurements.

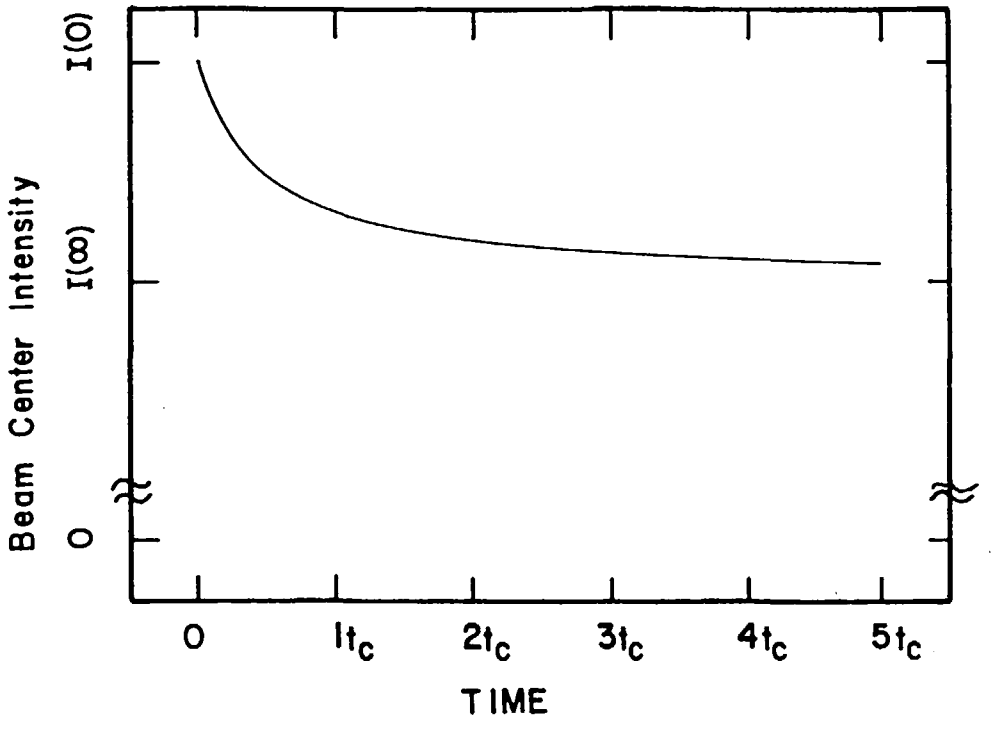

FIGURE 16. Time dependence of the thermally induced beam intensity change. The time axis origin corresponds to the unblocking of the laser beam. I(0) is the original beam intensity and I(∞) is the steady-state value.

A major effort in thermal lens design deals with demodulation of the time-dependent signal, Figure 16.

$$I(t) = \frac{I(0)}{1 + \frac{2.303EA}{(1 + tc/t)} + {}^{1/2}\left[\frac{2.303EA}{(1 + tc/t)}\right]^2} \quad (59)$$

The simplest demodulation technique utilizes a dual channel box-car measurement of the initial and final beam center intensity. This two-point measurement offers a simple, low-cost method to extract the thermal lens signal.[16,76] Despite its simplicity, the two channel box-car measurement has produced good detection limits, $A = 2.2 \times 10^{-6}$, in carbon tetrachloride.[102]

However, the dual channel box-car approach to signal processing suffers from a low rate of data collection; only two data points are taken per thermal lens transient. Instead, a burst of data may be taken when the laser beam is first unblocked. The initial slope of the thermal lens transient, dI(t)/dt, is linearly related to sample absorbance[10,33]

$$\frac{d\,I(t)}{dt}\Big|_{t<<t_c} = -4.606I(0)EA/t_c \quad (60)$$

This initial slope measurement requires rapid data collection since the signal rapidly departs from linearity. One could envision using a Savitsky-Golay initial slope estimation procedure in extracting the thermal lens absorbance signal.[107] Also, the initial slope is inversely proportional to the time constant of the signal and should be particularly useful for short time

constant materials such as gases and certain solids. Unfortunately, initial slope measurements are not well suited to precise thermal lens measurements. The rapid deviation in signal from linearity limits the number of data points collected. Then, the finite time required to unblock the laser beam prohibits measurements at very short times. Next, the diffraction pattern generated by the straight edge of the chopper crossing the laser beam acts to distort initial intensity. Finally, the finite time required to unblock the beam produces rounding in the initial data.[43]

A complete regression analysis of the transient signal has been shown to produce superior precision compared with either the dual channel or the initial slope data-analysis method.[10] Collection and analysis of 512 data points produced about a factor of 30 improvement in the detection limit compared with a two-channel box-car measurement. Detection limits of $A = 7 \times 10^{-8}$, based upon the variance-covariance matrix of the fitting algorithm, were obtained using regression analysis of 512 data points. Iodine in carbon tetrachloride was employed as the sample.

Although the regression analysis of the time-resolved thermal lens data has produced spectacular results, the length of time required for the regression analysis is impractical for real-time applications, such as chromatography or flow injection analysis detection. Unfortunately, it is not possible to linearize the fitting function; nonlinear regression analysis is employed. In this case, two approaches have been employed to speed analysis of the time-resolved data. If the time constant is estimated from a standard data set and if I(0) does not change significantly with time, then the fitting function may be written[108,109]

$$2.303EA = \frac{\sum(1 + t_c/t)\{[2I(0)/I(t) - 1]^{1/2} - 1\}}{\sum 1/s^2(t)} \quad (61)$$

where $s^2(t)$ is a weighting function given by

$$s^2(t) = 2(1 + t_c/2)^2\sigma^2(t)/I^2(t) \quad (62)$$

where σ is the standard deviation of each time-resolved measurement. With this simplified regression analysis, detection limits of $A = 8.5 \times 10^{-7}$ were obtained in carbon tetrachloride and a flow injection analysis system. Less than about 250 msec was required for the regression analysis. A potential difficulty in this linearization technique is the implicit assumption that the time constant does not change as dilute solutions are eluted from the flow injection analysis instrument. However, only very high concentration solutes will perturb the thermal time constant.[43]

A clever approach to rapid regression analysis of thermo-optical data has recently been reported by Nickolaisen and Bialkowski for pulsed photothermal deflection and thermal lens instrumentation.[93,110] The technique constructs a digital filter based upon a well-averaged, low-noise data set. The technique is valid if the time constant does not change with time and if the signal is linear with concentration. The averaged transient is generated and normalized to zero area. Assuming white noise, the signal amplitude may be estimated

$$2.303EA = \frac{\sum h(t)x(t)}{\sum h^2(t)} \quad (63)$$

where h(t) is the averaged thermo-optical signal, normalized to zero area, and x(t) is the time-resolved thermo-optical signal. Note that this approach does not utilize a deterministic model but instead is self-modeling in that a well-averaged data set is used to filter the data.

The requirement of a transient digitizer, laboratory computer, and necessary programing

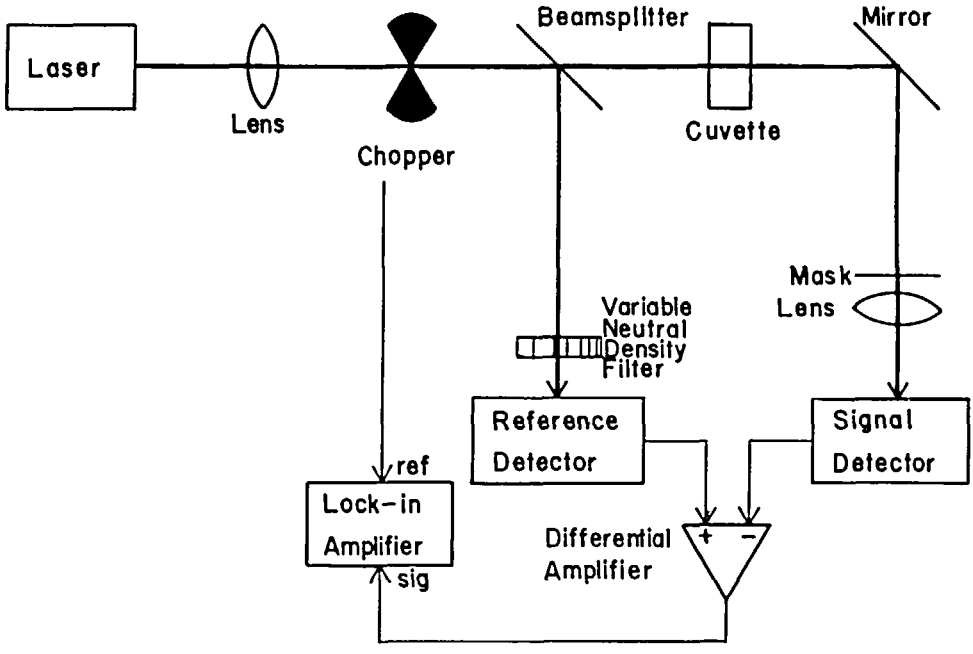

FIGURE 17. A reference beam thermal lens instrument. A portion of the laser beam after the chopper, but before the sample, is split to a reference detector. A spatial filter mask with a quadratically varying radial transmission function is used to compute directly the second moment of the laser beam after transmission through the sample. The reference beam intensity is matched to the signal beam intensity with a variable neutral density filter. The signals from the reference and signal detectors are combined with a differential amplifier. The thermal lens signal is demodulated with a lock-in amplifier.

of either regression analysis or digital filtering has discouraged many investigators from using the otherwise simple single-beam thermal lens instrument. Data collection is simplified by using a lock-in amplifier to demodulate the thermal lens signal. In this case, two approaches have been reported for the single-beam thermal lens. The first application of lock-in detection utilizes demodulation at the second harmonic of the modulation frequency.[111] A symmetric chopping function may be decomposed into a Fourier series containing only odd harmonic terms. However, the monotonic nature of the thermal lens signal ensures that the beam center intensity is not symmetric with time, generating a signal at even harmonics of the chopping frequency. Unfortunately, the second harmonic detection scheme requires outstanding harmonic rejection capabilities of the lock-in amplifier.

An interesting technique has recently been developed for lock-in detection with the single-beam thermal lens.[112] In this reference beam technique, Figure 17, a portion of the laser beam is split between the chopper and sample and sent to a reference detector. If the intensity of the laser beam at the reference detector is matched to the intensity of the laser beam at the sample detector, a simple differential circuit may be constructed to automatically null the signal with the laser beam both blocked and unblocked. The thermal lens signal will ride upon the nulled output, generating a signal at the modulation frequency. Detection limits of $A = 5 \times 10^{-7}$ have been reported with a 60-mW pump beam and carbon tetrachloride solvent. The relative simplicity and performance of the reference beam instrument suggests application for a number of high-sensitivity absorbance determinations.

C. Pump-Probe Thermal Lens

Pump-probe thermal lens instruments fall into two classes, one utilizing pulsed pump lasers and the second utilizing chopped cw laser beams, Figure 18. The thermal lens formed

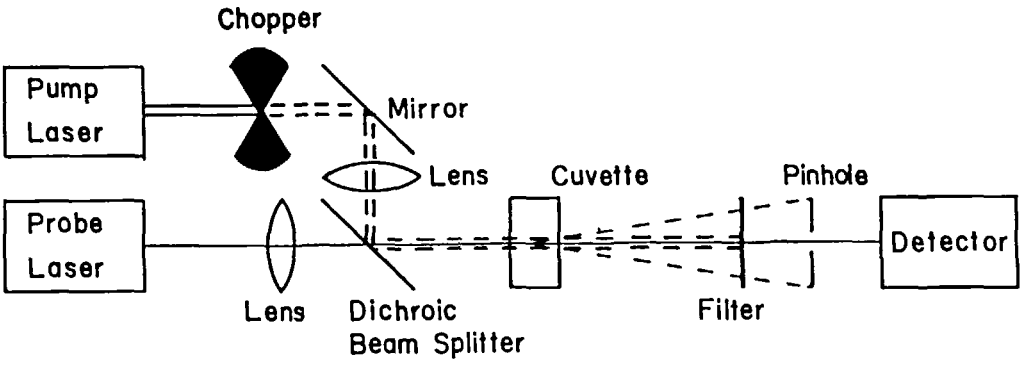

FIGURE 18. A pump-probe thermal lens. A pump laser beam is chopped mechanically and focused into the weakly absorbing sample. Alternately, a pulsed pump laser may be employed. The thermal lens defocuses a coaxial probe beam. The pump beam is blocked with a filter. The probe beam center is isolated with a pinhole and the transmitted intensity is sensed with a photodetector. A lens is included in each optical path to optimize the focusing conditions of each beam.

by the modulated pump beam is probed with a second cw laser beam. Defocusing of the probe beam is detected in phase with the pump beam modulation function.

The first pump-probe thermal lens instrument was reported by Grabiner et al.[113] in 1972 to monitor vibration relaxation in gas phase samples excited by a pulsed CO_2 laser and probed by a cw helium-neon laser. Early in 1977, Twarowski and Kliger published two papers, one modeling and the other applying the pump-probe thermal lens instrument for multiple photon absorbance spectroscopy in liquids.[42,114] The high intensity produced by a focused, pulsed nitrogen-pumped dye laser generates significant two-photon absorbance in aromatic solvents. It is interesting that the focused nitrogen-pumped dye laser produced sufficient intensity at the cuvette windows to decompose liquid benzene, forming a carbon deposit on the window. This artifact was eliminated by locating the pump beam waist in the center of the sample, thereby decreasing the intensity at the window.

The first analytical application of the pulsed-pump laser thermal lens was reported by Mori et al.[89] in 1982 for determination of copper-porphyrin complexes. A nitrogen laser-pumped dye laser produced a tunable pump beam around 417 nm at 20 μJ/pulse energy. The tunability of the pulsed dye laser facilitated excitation of the relatively narrow and intense porphyrin absorption band. Absorbance detection limits for the instrument were not spectacular, $A = 4.7 \times 10^{-4}$, although the large molar absorptivity of the porphyrin complex did result in good concentration detection limit for copper, 1×10^{-9} *M*.

The modest absorbance detection limit arises from several sources in this pulsed laser-excited thermal lens instrument. A two-channel box-car averager was used to quantitate the analyte. As in the single-beam thermal lens, transient averaging and regression analysis should produce superior detection limits. Next, the pulse energy of the pump laser was not very high. Higher energy lasers would produce greater sensitivity. Unfortunately, the pulsed laser peak-power was sufficiently high to generate a large two-photon absorbance signal within the aromatic solvent. This multiphoton absorbance background signal is distressing; defocusing of the pump beam to reduce the peak intensity of the pump beam to reduce the background signal will also reduce the thermal lens signal. Finally, and more generally, pulsed pump lasers have relatively high intensity and spatial noise characteristics.[115] Variations in the pump beam profile can translate to variations in the thermal lens signal. Unfortunately, beam profile quality is difficult to measure or correct. Long and Bialkowski[70] employed an intercavity iris within a pulsed CO_2 laser to improve the pump beam spatial profile. High-energy pulses, 100 mJ, but only weakly focused, allowed detection limits of

10 ppb of dichlorodifluoromethane at 13.3 kPa argon. Absorbance detection limits were about $A = 3 \times 10^{-7}$, comparable to the best single-beam thermal lens measurements. Large background signals were observed, presumably due to window absorbance.

The first gas phase analysis employing pulsed pump lasers was the analysis of nitrogen dioxide in air.[73] Detection limits of 0.8 ppm were reported with 20- to 40-μJ excitation energy.

Long and Bialkowski[70] also discussed the pressure dependence of the thermal lens signal. The signal is predicted to be constant with respect to pressure for pressures higher than about 20-torr buffer gas. However, saturation effects gave rise to a constant increase in the observed thermal lens signal with pressure.

An advantage of pulsed, compared with cw, excitation in thermal lens measurements is found in flowing systems. The relative change in probe beam intensity produced by pulsed pump laser excitation is independent of flow,[116,117] whereas the relative change in intensity for cw-excited systems is strongly influenced by flow.[45,46,118] In pulsed excitation, the entire temperature rise induced by absorbance is formed before flow can act to displace the distribution. However, in cw excitation, thermal diffusion must compete with flow to form the temperature rise; flow decreases the maximum temperature rise for cw excitation but not pulsed excitation. On the other hand, signal amplitudes and precision similar to the static sample case may be obtained by offsetting the probe beam downstream from the pump beam.[46] In a background-limited system, the better noise characteristics of most cw lasers should result in better detection limits than relatively noisy pulsed lasers.

The first report of the cw-excited pump-probe thermal lens instrument appeared in 1976;[20] overtone spectra were obtained corresponding to the fifth overtone of the C–H stretch in liquid benzene. In the pump-probe instrument designed for liquid phase analysis, a tunable dye laser was employed as the pump beam. This pump beam was chopped mechanically, combined coaxially with a cw helium-neon probe beam at a beam splitter, and focused with a lens into the sample cuvette. The pump beam was blocked with a spectral filter and the transmitted probe beam center intensity was observed with a photodetector placed behind a pinhole. This pump-probe design utilizing a chopped cw pump beam allowed demodulation with a lock-in amplifier; the lock-in amplifier provided the first rapid and simple signal processing technique for thermal lens measurements and greatly stimulated applications in the chemical physics and analytical chemistry communities.

Early analytical applications of the cw pump-probe thermal lens instrument were reported by Imasaka et al.[119] for the determination of iron utilizing an argon ion pump laser and a helium-neon probe laser and Haushalter and Morris[120] for the determination of dopamine with an enzymatic analysis, also utilizing an argon ion pump laser and a helium-neon probe beam.

Independently and coincidently, two groups recently described a thermal lens instrument which utilizes the same laser to generate polarization-encoded pump and probe beams, Figure 19.[121-123] The beam produced by an argon ion or helium-neon laser is split into a weak probe and a strong pump beam. The polarization of one laser beam is rotated 90° with a polarization rotator, such as a Fresnel rhomb prism or a 1/2 wave retardation plate. The chopped pump beam and cw probe beam are recombined with a beam splitter and focused into the sample cuvette with a lens. The pump beam is blocked and the probe beam is transmitted with a polarizing filter. A photodiode monitors the transmitted probe beam center and the signal is demodulated with a lock-in amplifier. This single laser approach to pump-probe thermal lens measurements offers two advantages. The design tends to compensate for beam pointing instabilities; the two beams will track each other as the original laser beam moves. Also, the cost of a probe laser is eliminated; unfortunately, the cost of a probe laser is comparable to the cost of the polarization components required by the design.

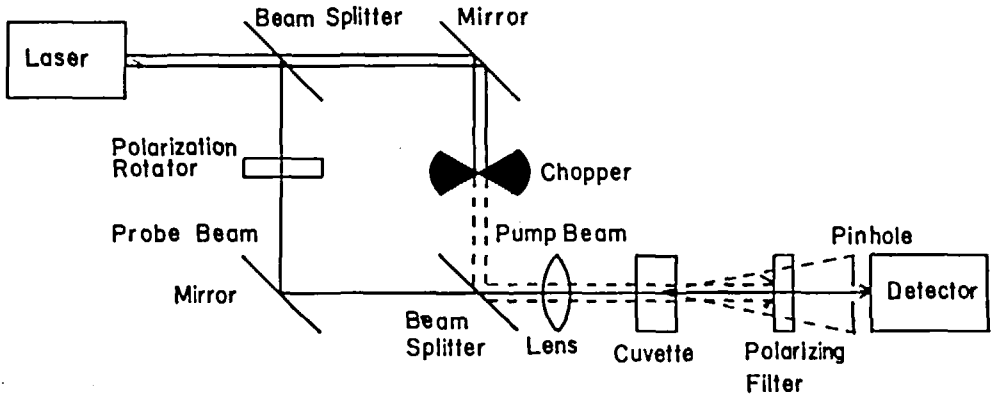

FIGURE 19. A single-laser pump-probe thermal lens. A small portion of the laser beam is split to form a reference beam while the pump portion of the beam is chopped and focused into the sample. The polarization of the probe beam is rotated 90° to the pump beam. A polarizing filter located after the sample blocks the pump beam and transmits the probe beam. A pinhole isolates the center of the probe beam profile.

An important criterion of the cw-excited pump-probe thermal lens instrument is the frequency response of the system. At very low modulation frequencies, $v << 1/t_c$, the thermal lens approaches a steady state and the maximum magnitude signal is obtained. At very high modulation frequencies, $v >> 1/t_c$, the thermal lens does not have a chance to form and the signal magnitude approaches zero. Since the time dependence of the thermal lens signal is given by the convolution of the impulse response with the time domain excitation function, the frequency response of the thermal lens is given by the product of the impulse frequency response with the frequency domain excitation function. The Fourier transform of the impulse response function is tabulated and may be written as[124,125]

$$\Delta I(\nu) = \Delta I(0)\{1 + 2\nu_0[\cos(\nu_0)\mathrm{si}(\nu_0) - \sin(\nu_0)\mathrm{Ci}(\nu_0)] + \nu_0^2[\mathrm{Ci}^2(\nu_0) + \mathrm{si}^2(\nu_0)]\}^{1/2} \quad (64)$$

where $\Delta I(0)$ is the dc component of the frequency response, si and Ci are the sine and cosine integrals, respectively, $\nu_0 = \pi\nu t_c$ is the reduced frequency, and ν is the modulation frequency. Figure 20 presents a plot of signal magnitude as a function of frequency taken from Reference 125. The signal achieves near maximum response at reduced frequencies less than about 0.01 and demonstrates a 20 dB/decade decrease in amplitude at reduced frequencies greater than about 1.

There has been much discussion of the optimum focusing conditions for the dual-beam thermal lens.[42,70,89,126] Unfortunately, much of the literature is confusing and contradictory. Consider the fundamental equation describing the far-field defocusing of a probe beam by a thermal lens

$$\Delta I = . -2z_1/f \quad (65)$$

The focal length of the thermal lens formed by a cw pump laser is proportional to the square of the pump beam spot-size while the focal length of the thermal lens formed by pulsed excitation is proportional to the fourth power of the pump beam spot-size. In both cases, the strongest thermal lens is formed when the pump beam waist is located in the sample. Focusing the pump beam into the sample is advantageous for another reason. All lasers produce some beam wander or pointing instabilities. Beam wander is undesirable in two

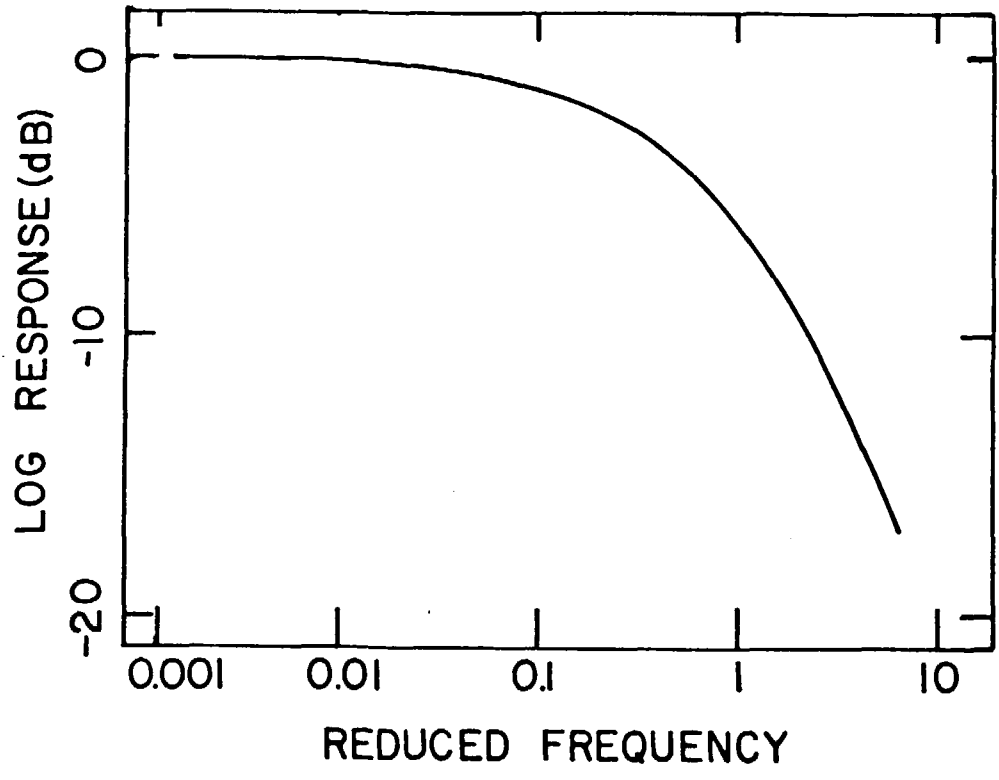

FIGURE 20. The frequency response of the thermal lens. The signal approaches steady state at low frequencies and demonstrates a 20-dB/decade roll-off at high frequencies.

beam thermo-optical measurements since stable overlap between the beams is necessary to maximize the signal. Fortunately, a lens acts to focus a beam to the same location independent of spatial offset.[115] By focusing the pump beam within the sample, pointing instabilities in the pump beam are minimized as a source of noise in pump-probe thermal lens measurements.

The signal is predicted to increase linearly with Z1, the distance from the probe beam waist to the sample. Thus, the paraxial model leads to the following optimum focusing conditions: (1) the pump beam should be focused to a tight waist within the sample, and (2) the probe beam should not be focused in order to locate the probe beam waist as far as possible from the sample. It is interesting to note that very good detection limits have been produced with this design.[87,127]

Unfortunately, these optimum focusing conditions lead to a violation of the fundamental assumption in the paraxial approximation; the dimensions of the thermal lens are much smaller than the probe beam spot-size. Higher order terms in the power series expansion lead to a strongly aberrant thermal lens. Clearly, the diffraction integral is required to model the position dependence of the pump-probe thermal lens. There appears to have been only one published position study of the dual-beam thermal lens.[126] In this work, a tightly focused pump beam and weakly focused probe beam were employed. As predicted by the paraxial approximation, the signal maximized when the pump beam waist was located within the sample. However, the relationship between the signal amplitude and Z1 was linear only over a range of about ± 1 confocal distance. When the sample was located further from the probe beam waist, the signal amplitude rapidly decreased toward zero. A study of the diffraction integral suggests that the thermal lens signal should maximize with Z1 in the range of one to five times the probe beam confocal distance.

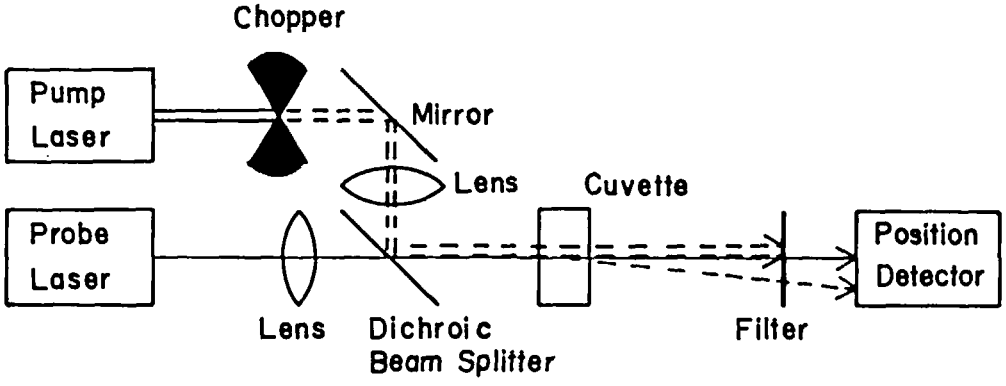

FIGURE 21. The thermal prism. The experimental configuration is similar to the pump-probe thermal lens. The pump and probe beam axes are offset so that the probe beam traverses the inflection point of the temperature distribution. A position-sensitive detector is used to sense the beam deflection.

The symmetric response of the pump-probe thermal lens with respect to the distance from the sample to the probe beam waist suggests that a differential instrument could be constructed by analogy to the single-beam thermal lens; placement of the sample and reference cuvettes at equal distances from the probe beam waist should result in subtraction of the absorbance of the two cuvettes.

D. Thermal Prism

If the refractive index perturbation induced by the absorbance of a pump laser beam is probed off-axis, then the probe beam will be deflected in the direction of the increasing refractive index, Figure 21. A dichroic filter is often used to combine the two beams. The probe beam is deflected in phase with the pump beam modulation function. This thermally induced deflection may be modeled by analogy with a prism, hence the term thermal prism. A more common name for the thermal prism effect is photothermal deflection. Unfortunately, the term photothermal deflection is also applied to the mirage-like phenomenon which occurs near a heated surface. In this paper, the term "thermal prism" is used for beam deflection in a homogeneous sample while the term "mirage effect" is used for deflection associated with a heated interface, Section V.B.

The thermal prism, along with the mirage effect, was described by Jackson et al.[15] in 1981 using the paraxial approximation. A number of important parameters were studied and optimized. The thermal prism signal maximizes when the probe beam axis is located along the inflection point of the temperature profile. Since the radial extent of the temperature rise changes with time or modulation frequency, the optimum location of the probe beam will change with these parameters. As in thermal lens measurements, the signal amplitude is a function of modulation frequency, decreasing at high modulation frequency with a 20 dB/decade roll-off.

Experimental data for pulsed laser-excited thermal prism spectroscopy of liquids are rather meager. However, detection limits of $A = 1 \times 10^{-7}$ in a 100-μm path have been reported with carbon tetrachloride as solvent, with a 1-mJ pump laser.[15] Peck and Morris[91] have applied the thermal prism to the detection of stained proteins in polyacrylamide gels used in electrophoresis. Detection limits of 0.95 ng albumin were reported.

Long and Bialkowski[128] considered the thermal prism for analytical applications of gas phase analyte. Detection limits of 1.3 ppbv for $CHClF_2$, 2 ppbv for CCl_2F_2, and 3 ppbv for SO_2 have been obtained with pulsed CO_2 laser-excited thermal prism measurements at a pressure of 13.3 kPa.

Noise sources in the thermal prism are predominately pointing noise in the probe beam and intensity fluctuations in the pump beam coupled with the finite background signal generated within the solvent and optical components.[15,115] Pointing instabilities and variations in the mode quality of the pump laser are minimized by spatial filtering of the beam, particularly with an intercavity iris, and locating the sample near the focus of the beam. Similarly, beam overlap may be stabilized by locating the probe beam focus near the sample.[115]

Noise in the system often shows a 1/f dependence. If the thermal prism signal possesses reasonably strong high-frequency components, electronic filtering with pulsed excitation or modulation at high frequencies with cw excitation can help reduce low-frequency noise.[115]

Improved precision and sensitivity are produced by high-power pump lasers which saturate the absorbance transition.[128] Precision is improved because the signal is only weakly dependent upon changes in pump laser intensity; both variations in the mode structure of the laser and pulse-to-pulse energy fluctuations are minimized as noise sources. The sensitivity is increased because saturation, along with other nonlinear phenomena, acts to flatten the temperature distribution formed at the pump beam axis; however, the gradient of the refractive index profile increases in the wings of the beam.

Several photodetectors have been developed which can measure the probe beam deflection induced by the thermal prism. The simplest detector consists of a small area photodiode which measures the change in probe beam intensity due to deflection. The sensitivity of the detector will depend upon the location of the detector. For an infinitesimal offset, the change in intensity observed due to deflection is simply given by the derivative of intensity with radius times the displacement, Δr

$$\Delta I = \frac{dI}{dr}\Delta r = \frac{-4rP}{\pi\omega^4}\Delta r\ e^{-2r^2/\omega^2} \tag{66}$$

for a Gaussian probe beam whose spot-size at the detector equals ω and total power equals P. The maximum change in intensity is observed when $r = \omega/2$, so that the detector is located at an inflection point of the probe beam

$$\Delta I_{max} = \frac{-2P\Delta r}{\pi\omega^4} e^{-1/2} \tag{67}$$

Unfortunately, this simple photodiode detector suffers from two difficulties. First, the dynamic range of the measurement is limited. A nonlinear intensity change is observed when the displacement is a few percent of the probe beam spot-size. Second, this detector is sensitive to both power and position fluctuations in the probe beam.

Several position-sensitive detectors have been designed with good linearity and immunity to intensity fluctuations. The simplest consists of a bicell, two photodiodes located adjacent to each other, wired in a differential configuration. The probe beam is centered on the diode pair to achieve null. Any displacement of the beam across the diodes will generate a voltage proportional to the offset. The differential configuration used with the bicell automatically subtracts small fluctuations in the probe beam intensity. Unfortunately, the signal produced by the bicell is nonlinear with position.

A pair of bicells have been employed in a two-probe beam experiment to reduce sensitivity to probe laser pointing noise.[129] The beams travel in close proximity through the experimental apparatus. Small deflections induced by vibrations or refractive index perturbations will produce similar displacements of both beams at the detector. A high-precision measurement of the deflection signal may be produced if it is induced on one of the probe beams.

Another position-sensitive detector is the lateral cell, a photosensitive device which pro-

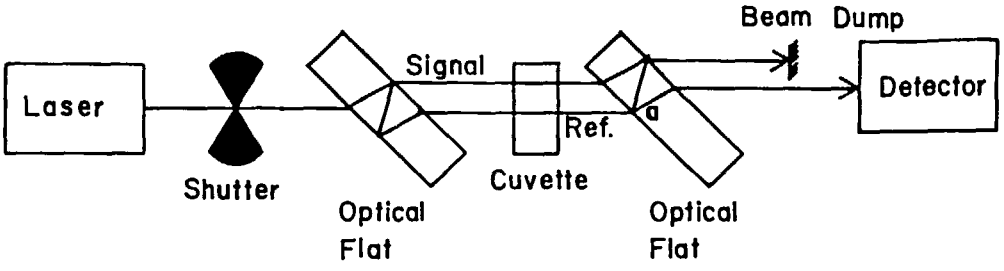

FIGURE 22. The interferometric measurement of thermally induced optical path change: Jamin interferometer. The laser beam is split into a strong signal and weak reference beam by an uncoated optical flat. The signal beam produces relatively greater heating of the sample than the reference beam. The thermally induced refractive index change within the sample induces a difference in optical path between the two beams. The beams are recombined with a second optical flat at point "a". The recombined beams interfere and produce an intensity change at the detector proportional to the optical path difference generated within the sample. The transmitted signal beam may be monitored to measure the intensity of the laser beam.

duces an accurate analog position measurement over a relatively large region. Furthermore, an analog division circuit produces a signal which is independent of intensity fluctuations of the probe beam.

A more complicated position-sensitive device uses a photodiode array.[130] The array read-out is smoothed with a low-pass electronic filter and differentiated with a high-pass filter. The zero crossing of the derivative occurs when the beam center has been read from the diode array. Differences in the time between the beginning of the diode array read-out and the zero crossing correspond to displacement of the laser beam.

E. Interferometry

Thermally induced changes in optical path length may be measured directly using an interferometer. Although the intercavity thermal lens experiments may be considered as interferometric measurements, the signal is dominated by thermal lens induced loss-terms, not phase shifts due to change in path length. An early report by Stone[18] utilized a Jamin interferometer to produce a signal and reference beam within the sample, Figure 22. The two-beam design facilitates compensation for both intensity fluctuations of the laser beam and thermal drift within the interferometer. Transmission through and reflection from the first uncoated optical flat produces two parallel beams which pass through the sample. The transmitted, or signal, beam is relatively high power and acts as both the heating and probe beam. The beam produced by reflections is much weaker and acts as a reference beam. Since the thermally induced optical path difference is proportional to pump laser power, the signal beam will experience a much larger optical path difference than the reference beam. After transmission through the sample, the two beams are recombined with a second uncoated optical flat. The transmitted reference beam and the reflected heating beam undergo interference at the detector which measures the thermally induced phase shift as an intensity change. The transmitted heating beam does not undergo interference effects and acts as a reference beam to correct for intensity fluctuations in the laser.

This design used an unfocused helium-neon laser. The relatively large beam spot-size, $w = 0.95$ mm, resulted in a long thermal time constant. By recording the change in intensity as the laser beam is unblocked, the initial slope of the transient waveform was used to compute sample absorbance. Detection limits of $A = 10^{-6}$ were reported for a 5-cm cuvette. The author noted a large background signal when a cuvette with Pyrex® windows was employed. The signal was generated from absorbance by the windows and subsequent heating of the solvent. Quartz windows eliminated this source of background. Thermal drift in the

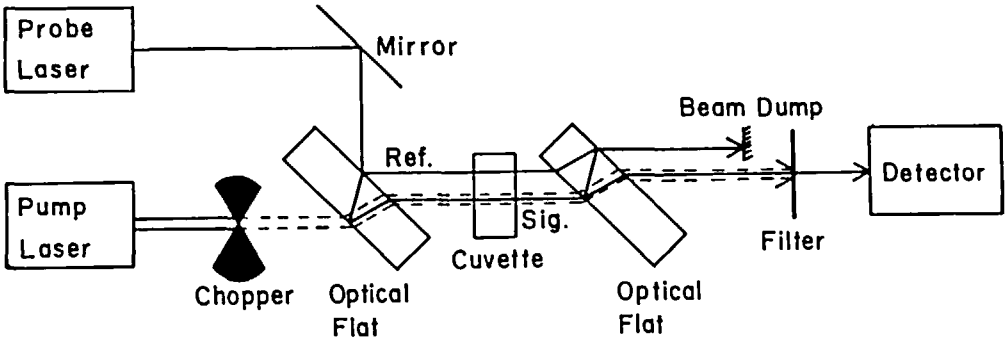

FIGURE 23. A pump-probe interferometric design. Here, a pump laser beam is aligned coaxial with the signal beam, thereby generating a modulated path length perturbation on that beam.

interferometer which was not corrected by the double-beam instrument ultimately limited the smallest detectable absorbance.

In addition to the single-beam Jamin interferometer, a pump-probe design has been investigated, Figure 23.[131] Here, a pump light beam is aligned coaxially with the weak probe laser beam within the interferometer. After passing through the sample, a portion of the strong probe laser beam is combined with the weak beam at a photodetector. Instead of using a laser, light from a high brightness incoherent light source is collimated and filtered to provide the pump beam. Unfortunately, the relatively large size of the incoherent pump beam produced rather weak and noisy signals.

A much more sophisticated pump-probe interferometric instrument has been constructed which provides differential response to subtract the background solvent absorbance signal.[132] Again, a Jamin interferometer is used, although with two heating beams, two probe beams, and two reference beams. The instrument has a slow response time due to the relatively large beam spot-size employed. The pump beam is produced by an argon ion laser of about 100-mW power. Absorbance detection limits in CCl_4 are about 10^{-6} for a 1-cm long cuvette.

In addition to the Jamin interferometer, a Fabry-Perot interferometer has been applied to long path length thermo-optical measurements.[19] The multipass nature of the Fabry-Perot interferometer provides significantly increased sensitivity compared to the single-pass Jamin interferometer, although without the advantage of a reference beam to cancel background drift. In this instrument, a polarization-encoded helium-neon probe beam is directed into the interferometer, Figure 24. Within the cavity, a flow cuvette is positioned. Brewster angle windows minimize loss for the probe beam. An argon ion laser pump beam, with polarization orthogonal to the probe beam, is introduced into the cavity by reflection from the Brewster angle window. The pump beam is attenuated after a few round trips through the cavity by reflections from the windows.

The cavity length is ramped with a piezoelectric drive. A computer records the transmitted probe beam and determines the fringe location as a function of cavity length. The thermo-optical signal is the difference in cavity length with the pump beam on vs. the pump beam blocked. Unfortunately, the pump beam also produces heating of the sample cuvette. Time gating helps minimize the contribution of cell heating from the signal. A crossed-beam instrument has been proposed to minimize heating of the cuvette by stray pump laser radiation.

A Mach-Zehnder interferometer has been used sucessfully to detect thermally induced refractive index changes within the sample, Figure 25.[133-139] This technique, called phase fluctuation optical heterodyne interferometry, appears to have been applied primarily to gas phase samples, including aerosols.[139] Here, a chopped cw CO_2 laser is used as the pump

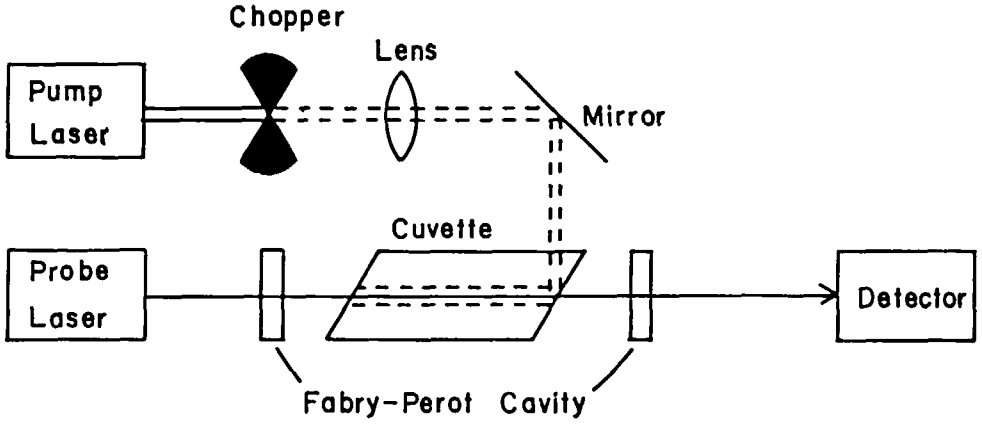

FIGURE 24. The Fabry-Perot interferometric measurement of thermally induced optical path change. A pump beam is reflected from the Brewster's angle cuvette windows into the path of the probe beam within the interferometer. The polarization of the pump and probe beams are orthogonal so that the probe beam undergoes no reflective loss at the cuvette windows, whereas the pump beam undergoes large reflective loss at the windows.

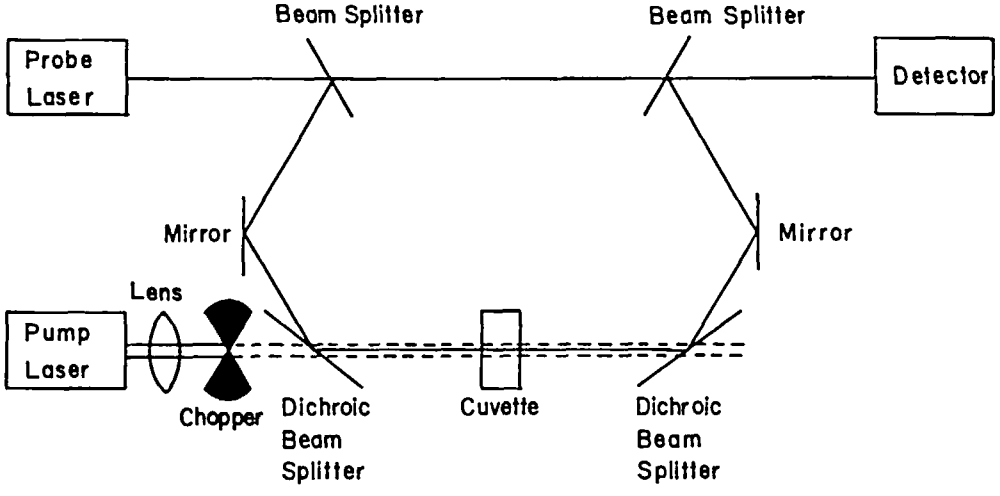

FIGURE 25. Mach-Zehnder interferometric measurement of thermally induced optical path change. The modulated pump beam produces a periodic change in optical path within one arm of the interferometer. A servo system is sometimes used to move one mirror within the interferometer to produce a constant DC intensity at the photodetector.

source, and a single-frequency, low-noise, helium-neon laser produces the probe beam. A thermally induced path change within one arm of the interferometer generates a fringe shift and intensity change at the output of the interferometer. This intensity change is demodulated with a lock-in amplifier phase referenced to the pump beam chopper. Low-frequency drift in the interferometer is corrected by a servo system to maintain a stable DC intensity at the detector. The servo system moves a mirror in one arm of the interferometer with a piezoelectric translator.

Instead of modulating the pump beam, it is possible to use a cw pump laser and instead modulate the absorbance of the sample. For example, a modulated electric field may be placed across the sample cuvette. For Stark active molecules, the electric field acts to modulate the absorptivity at the pump laser wavelength, generating a modulated temperature rise within the sample. Phase-sensitive detection referenced to the electric field modulation

function may be used to demodulate the signal.[135] Dilute analyte may be discriminated from a huge excess of absorbing but non-Stark active contaminant.

The Mach-Zehnder interferometer has produced very good gas-phase detection limits. Detection limits of $A = 1.5 \times 10^{-7}$ have been produced within a 20-cm windowless cuvette for both ammonia and ethylene in nitrogen.[135,137,139] The pump laser intensity was 250 W/cm^2. Concentration detection limits below 1 ppb were obtained for both ammonia and ethylene, and a few parts per trillion for SF_6. The windowless curvette was necessary to eliminate background signals generated in the window. The primary background signals were produced from absorbance by both the Ge beam splitters and trace levels of H_2O and CO_2.

F. Applications

Thermo-optical techniques have produced spectacular absorbance detection limits, Table 4. This list is not comprehensive; instead the data presented are intended to be representative of results produced by different techniques through early 1986. Furthermore, these detection limits are based upon different criteria and different time constants not always reported in the reference; no effort has been made to utilize a consistant definition of detection limit.

The best absorbance detection limits for liquids fall near $A = 10^{-7}$ and utilize carbon tetrachloride as the solvent. Detection limits in other solvents are higher. The data strongly suggest that the detection limits are determined by background absorbance generated within the solvent. The excellent detection limits produced in carbon tetrachloride probably are due to the extremely low background absorbance produced within this solvent. The background absorbance of the solvent appears to be generated by high overtones of vibrational active modes within the molecule. Considering the low energy of the C-Cl vibrational mode, about 750 cm^{-1} for the fundamental, transitions in the visible portion of the spectrum correspond to the 25th harmonic of the fundamental vibrational mode; it is not surprising that CCl_4 is a highly transparent material! The good thermo-optical constants of CCl_4 also are advantageous in producing high-sensitivity measurements.

There appears to be no large advantage of one thermo-optical technique compared to another. As an example, three thermal lens instruments were compared by the same investigators with similar optical and electronic configurations: single beam with regression analysis, double beam with regression analysis, and double beam with lock-in detection.[85] Detection limits were virtually identical for the three instruments. This author personally is attracted by the optical and electronic simplicity of the reference beam thermal lens instrument.[112] Although the detection limits reported are slightly higher than some other instruments, the instrument appears to be well suited for routine application.

There are two results included in Table 4 that differ from the others. Both utilize relatively short path length measurements to produce improved detection limits. In one case, a thermal prism instrument was used to determine absorbance within a 1-mm path length cuvette.[142] The decreased background absorbance produced with the shorter path length allows a proportional improvement in detection limit, $A = 2 \times 10^{-8}$. However, the absorbance per unit length at the detection limit was identical to other thermo-optical techniques.

The last detection limit included in Table 4 utilized a crossed-beam thermal lens design.[8] Here, the interaction length is defined by the diameter of the pump laser beam. The use of very tightly focused pump beams produces very short interaction lengths, 3 μm. Since the sensitivity of the technique is fairly high, excellent absorbance detection limits are produced. $A = 3 \times 10^{-9}$. This technique is optimized for small path length and small volume samples and is considered in the next section of this manuscript.

Table 5 considers concentration detection limits reported for a number of thermo-optical techniques; the same caveats concerning the absorbance detection limits also apply to these results. The best detection limits for liquids fall in the 10^{-10}- to 10^{-11}-*M* range. Typical laser powers of 0.1 to 1 W are required to produce these good detection limits. Compounds

Table 4
ABSORBANCE DETECTION LIMITS

Technique	Pump laser	Matrix	Absorbance detection limit	Path length (cm)	Absorbance per unit length (cm^{-1})	Ref.
SBTL	4 mW	3:1	1×10^{-3}	1	1×10^{-3}	76
Box-car	632.8 nm	Acetone:water				
SBTL	200 mW	CCl_4	6.3×10^{-7}	1	6.3×10^{-7}	102
Box-car	514.5 nm					
SBTL	80 mW	CCl_4	1.1×10^{-7}	1	1.1×10^{-7}	106
Regression	514.5 nm					
SBTL	160 mW	CCl_4	7×10^{-8}	1	7×10^{-8}	10
Regression	514.5 nm					
SBTL	60 mW	CCl_4	5×10^{-7}	1	5×10^{-7}	112
Lock-in	514.5 nm					
SBTL	225 mW	H_2O	2.6×10^{-5}	1	2.6×10^{-5}	85
Regression	514.5 nm					
SBTL	225 mW	H_2O	2.2×10^{-5}	1	2.2×10^{-5}	85
Lock-in	514.5 nm					
SBTL	225 mW	H_2O	1.8×10^{-5}	1	2.2×10^{-5}	85
Regression	514.5 nm					
SBTL	50 mW	Supercritical	2×10^{-7}	1	2×10^{-7}	140
Regression	647.1 nm	CO_2				
PPTL	100 mW	7:3	1×10^{-6}	1	1×10^{-6}	141
Lock-in	488 nm	MeOH:Water				
PPTL	20 μJ	Chloroform	4.7×10^{-4}	1	4.7×10^{-4}	89
Box-car	417 nm					
PPTL	700 mW	Air	1.3×10^{-6}	100	1.3×10^{-8}	127
Box-car	488 nm					
TP	1 mJ	CCl_4	2×10^{-8}	0.1	2×10^{-7}	15
Box-car?	606 nm					
TP	60 mW	CCl_4	1×10^{-6}	0.5	2×10^{-6}	142
Lock-in	605 nm					
IN	100 mW	CCl_4	1×10^{-6}	1	1×10^{-6}	132
Lock-in	514.5 nm					
IN	60 mW	Acetonitrile	2.6×10^{-6}	1	2.6×10^{-6}	19
Computer	514.5 nm					
IN	250 W/cm	N_2	1.5×10^{-7}	20	7.5×10^{-9}	135
Lock-in	10 μm					
XBTL	100 mW	1:1	3×10^{-9}	2.6×10^{-4}	1.1×10^{-5}	8
Lock-in	514.5 nm	Water:MeOH				

Note: SBTL = Single beam thermal lens; PPTL = Pump-probe thermal lens; TP = Thermal prism; IN = Interferometric measurements; and XBTL = Crossed-beam thermal lens measurements.

with relatively high molar absorptivities, 10^4 to 10^5 $M^{-1}cm^{-1}$, and nonpolar solvents are used to produce the best detection limits. In general, the determinations performed with modest power lasers are background limited; laser stability ultimately determines the detection limit. There seems to be no systematic difference in the results produced by any particular instrumental design. For example, the phosphorus analysis reported by Nakanishi et al.[87] showed identical detection limits for single-beam and pump-probe thermal lens instruments.

The best gas-phase detection limits fall in the low-to-sub parts per billion range for a number of analytes. Again, detection limits are determined by noise in the background signal generated by trace impurities in the system or by optical components such as mirrors, beam splitters, or windows. The interferometric results for gas phase analysis are particularly good, primarily because a windowless cuvette was used.[139] Very low background signals could be generated, allowing high-sensitivity measurements with high power pump lasers.

Table 5
LONG PATH LENGTH TECHNIQUES

Liquid Phase Determination

Analyte	Solvent	Type	Laser	Detection limit (*M*)	Ref.
Copper-EDTA	3:1 H_2O/Acetone	SBTL	4 mW 633 nm	1.6×10^{-5}	71
Iron-1,10-phenanthroline	1:1 H_2O/MeOH	SBTL	175 514.5 nm	5×10^{-11}	143
Iron-bathophenantholine	Water	PPTL	100 mW 514.5 nm	3×10^{-7}	119
Iron-bathophenanthroline	Chloroform	PPTL	800 mW 514.5 nm	2×10^{-10}	144
Iron-bathophenanthroline	Chloroform	PPTL	600 mW 514.5 nm	3×10^{-11}	105
NO_2^-	1:1 *n*-Butanol/benzyl alcohol	SBTL	300 mW 514.5 nm	2×10^{-9}	86
Phosphorus	Water	SBTL	150 mW 660 nm	1.6×10^{-10}	145
2,2,4-Trimethylpentane	CCl_4	SBTL	6.2 mW 3.39 μm	1.5×10^{-6}	146
Tetraphenylporphorine	Chloroform	PPTL	20 μJ 417 nm	1×10^{-9}	89
Cobalt-PAN	$CHCl_3$	SBTL	1.2 mW 633 nm	2×10^{-7}	147
Arsenic/molybdenum blue	Isobutanol	IC	8 mW	1×10^{-8}	96
Phosphorus/molybdenum blue	Isobutanol	IC	632.8 nm	2.3×10^{-9}	
Copper-EDTA	H_2O	PPTL	4 mW 632.8 nm	6×10^{-5}	122
Phosphorus/heteropolyblue	2-Butanol	PPTL & SBTL	10 mW 824 nm	6.5×10^{-8}	87
Formaldehyde	Water	PPTL	150 mW 600 nm	5.6×10^{-7}	90

Gas Phase Determinations

NH_3	N_2	IN	250 W/cm² 9.6 μm	Sub ppb	135
SF_6	Air	IN	?	10 ppb	136
CH_3OH	Helium		10.6 μm	40 ppb	
Benzene	Air	PPTL	20 W 9.639 μm	500 ppb	148
NO_2	Air	PPTL	700 mW 488 nm	5 ppb	127
NO_2	Air	PPTL	40 μJ 420 nm	800 ppb	73
MeOH	Air	PPTL	7 W 9.67 μm	12 ppb	92
CCl_2F_2	Argon	PPTL	100 mJ 10 μm	10 ppb	70
C_2H_4	N_2	IN	250 W/cm² 9—10 μm	0.6 ppb	139
$CHClF_2$	Argon	TP	100 mJ	2 ppb	128
CCl_2F_2	Argon	TP	10 μm	1.3 ppb	
SO_2	Argon	TP		3 ppb	

Note: SBTL = Single beam thermal lens; PPTL = Pump-probe thermal lens; IC = intercavity thermal lens; TP = thermal prism; and IN = interferometric measurements.

Table 6
CHROMATOGRAPHY DETECTION: LONG PATH LENGTH TECHNIQUES

Analyte	Solvent	Type	Laser	Detection limit	Ref.
Nitroanalines	1:1 MeOH:water	SBTL	190 mW 458 nm	200 pg	108
Nitroanalines	7:3 MeOH:water	SBTL	90 mW 458 nm	50 pg	141
NBD	Acetonitrile	IN	60 mW 488 nm	200 ng	19
Nitroanalines	8:2 MeOH:water	PPTL	75 mW 458 nm	20 pg	149
Nitroanalines	8:2 MeOH:water	SBTL	80 mW 458 nm	1 ng	111
Nitroanalines	2:3 MeOH:water	SBTL	500 mW 458 nm	30 pg	150
Nitroanalines	8:2 MeOH:water	PPTL	75 mW 458 nm	1 ng	121
O-nitroanaline	8:2 MeOH:water	PPTL	7 mW	1 ng	151
Rug dye	65:35 MeOH:water	TP	1.2 W 488 nm	0.5 pg	152
SF_6	N_2	IF	250 W/cm^2	2 pg	144
C_2H_4			10.6 μm	8 pg	
Freons	Argon	PPTL	20 mJ 10.6 μm	7 ng	153

Note: SBTL = Single beam thermal lens; PPTL = Pump-probe thermal lens; IC = intercavity thermal lens; TP = thermal prism; and IN = interferometric measurements.

It is interesting to compare the two NO_2 determinations reported by Higashi et al. In the first paper, a pulsed nitrogen laser pumped dye laser and, in the second paper, a cw argon ion laser were employed as the excitation source.[73,127] Detection limits were about a factor of 150 better with the cw excitation source compared with the pulsed pump laser. The reason for the superior performance of the cw excitation source over the pulsed source is not clear. However, the good power stability of the cw argon ion laser compared with the pulsed dye laser should result in superior detection limits in a background limited experiment. On the other hand, Long and Bialkowski[115] have demonstrated excellent detection limits using a well-characterized pulsed CO_2 laser.

The long path length thermo-optical techniques have been employed for analysis of flowing samples in flow injection analysis and chromatographic detection. The mass detection limits for injected analyte are summarized in Table 6. Here, detection limits are determined not only by the sensitivity and background signal of the thermo-optical technique but also by the skill of the chromatographer to produce high-efficiency chromatograms.

Clearly, chromatographic detection utilizing the thermo-optical techniques is less well developed compared to bulk sample analysis; the chromatography reports primarily evaluate different thermo-optical configurations. Nitroanalines are the primary analyte considered. Detection limits fall in the 10-pg to 1-ng injected range. Since chromatographic detection limits depend upon both the chromatographic conditions and detector sensitivity, it is not easy to compare the detection limits produced by any particular thermo-optical technique. However, the pump-probe thermal lens configuration has been employed most often in chromatographic detection. Lock-in amplification of the thermal lens signal is particularly convenient for real-time chromatographic detection. The crossed-beam thermal lens is ideally suited to small-volume, low-dispersion chromatography and has begun to produce some very good detection limits.[163]

There have been two applications reported for single-beam thermal lens detection in flow injection analysis. The supercritical fluid work is particularly interesting in that it suggests future applications in supercritical chromatography detection. The primary difficulty in single-beam thermal lens detection in flow injection analysis or liquid chromatography is the need for rapid data analysis for real-time detection. Both of these flow injection analysis reports used a modified regression analysis technique to demodulate the signal.

IV. THERMO-OPTICS FOR SMALL VOLUME SAMPLES

A. Introduction

Several thermo-optical techniques have been developed for small-volume, short path length analysis. These techniques utilize a crossed-beam geometry wherein the probed volume is defined by the intersection region of the beams. Since laser beams may be focused to a very small spot-size, very small probed volumes may be produced. Furthermore, the signal is integrated over the pump beam diameter and independent of cuvette length. This independence of path length suggests that these techniques measure not absorbance but instead the concentration-absorptivity product.

In conventional transmission measurements, the analytical signal is the decrease in intensity of the light beam traversing the sample. Beer's law presents a relation between the transmission of the sample and the analyte concentration. For an inhomogeneous sample, Beer's law may be written

$$I/I_0 = T = 10^{-A} = 10^{-\int \epsilon C \, d\text{path}} \tag{68}$$

where I is the incident laser intensity, I_0 is the transmitted intensity, T is transmission, and the integral is over the optical path. This relationship shows two difficulties of Beer's law measurements in thin, inhomogeneous samples. In the first, the sensitivity of a concentration measurement goes to zero as path length goes to zero. Only a high-concentration, high-absorptivity analyte may be determined in thin samples by a transmission measurement. Also no information is provided on the distribution of analyte in inhomogeneous samples; that is, conventional Beer's law measurements integrate sample absorbance over the optical path.

Crossed-beam thermo-optical measurements provide excellent spatial resolution. For two beams crossed at right angles, the probed or intersection volume may be approximated by a cylinder whose radius equals the spot-size of the smaller beam and whose height equals twice the spot-size of the larger beam.[9] In the case that the two beams have the same spot-size, the probed volume is approximately given by $2\pi\omega^3$. As an example, the intersection volume of two 10-μm spot-size laser beams is only 6 pℓ, whereas the intersection volume of two 1-μm spot-size laser beams is 6 fℓ. These extremely small probed-volume measurements will be of value in chromatographic, electrophoretic, and microscopic imaging and detection.

The best developed crossed-beam thermo-optical measurement technique is the crossed-beam thermal lens. Here, a pump laser beam forms a cylinder of heated material. The heated region is crossed at right angles by a coplanar probe beam. The heated region acts as a thermal cylindrical lens to defocus the probe beam about the plane containing the pump and probe beams. Applications include liquid chromatographic detection and scanning laser microscopy.

A crossed-beam thermal prism instrument may be constructed by crossing the pump and probe beams at right angles but offset so that the probe beam passes through the maximum in the gradient of the temperature distribution. As in the long path length techniques, the thermal prism instrument utilizes position-sensitive detectors. The prism technique is primarily sensitive to spatial noise, whereas the thermal lens is primarily sensitive to intensity noise.

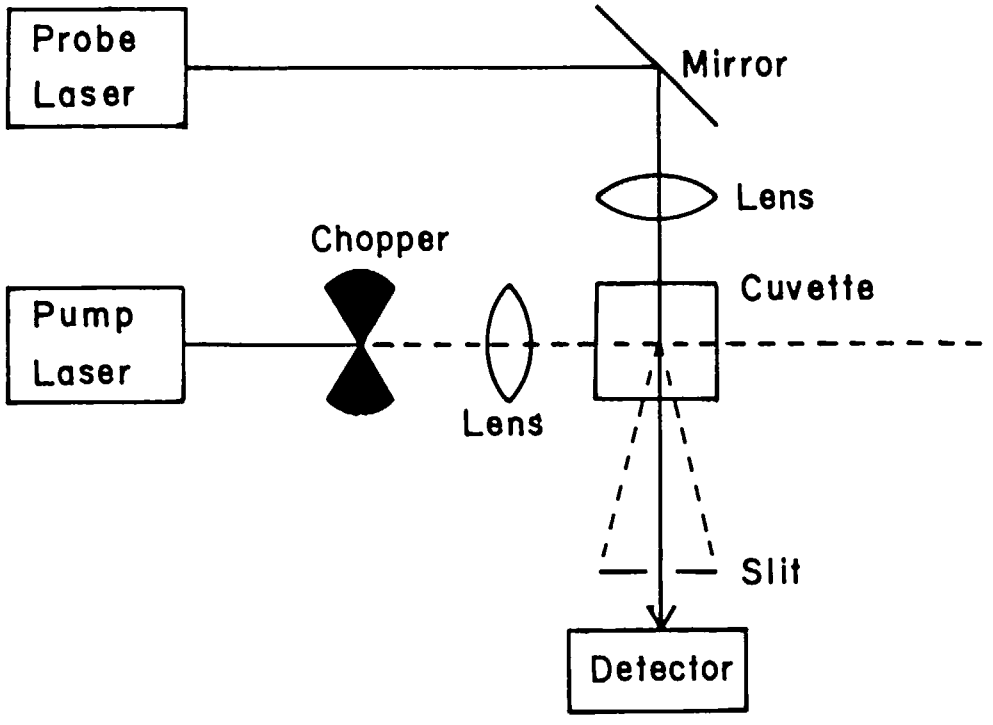

FIGURE 26. The crossed-beam thermal lens. The modulated pump beam produces a cylindrical temperature rise within the sample. The coplanar probe beam is crossed at right angles to the heated region and defocused out of the plane containing the two beams. A slit in the plane of the two beams isolates the probe beam center intensity.

One crossed-beam interferometric instrument has been reported using a Jamin interferometer. Unfortunately, the instrumentation for interferometric measurements is more complicated than either the crossed-beam thermal lens or prism.

Last, a four-beam thermo-optical technique has been developed based upon the thermal grating. Here, interference between two mutually coherent laser beams forms a sinusoidal intensity profile in the absorbing sample. The resulting temperature rise and refractive index profile acts like a grating to diffract a third probe beam to produce a fourth, spatially isolated, signal beam. The number of optical components, the stringent alignment constraints, relatively large probed volume, and the nonlinear calibration curve suggest difficulties applying the thermal grating to many analytical problems.

B. Crossed-Beam Thermal Lens

The crossed-beam thermal lens is based upon the interaction of a modulated pump beam and a coplanar probe beam, crossed at right angles, Figure 26.[14,28] As discussed in Section II of this paper, the heated sample acts to defocus the probe beam about the plane containing the two beams. Defocusing is detected as a change in the far-field probe beam center intensity. Since the probe beam is defocused in one dimension, a slit may be used to isolate the beam center intensity in the plane containing the two beams. The slit helps minimize noise by averaging spatial variations in the probe beam intensity over the slit area. The relative change in probe beam far-field intensity may be modeled either with the diffraction integral or with the paraxial approximation. The paraxial approximation provides good qualitative agreement between theory and data. Here, the focal length of the cylindrical thermal lens is given by Equation 43 of Section II.E.2 where r is replaced with x.

$$1/f = \int \frac{d^2\Delta n(x,y,t)}{dx^2}\, dY \qquad (69)$$

Note that $d^2\Delta n/dx^2$ is integrated over the probe beam path. The signal is insensitive to variations in the pump beam profile along the direction of the probe beam path.[155]

For the homogeneous sample illuminated by a pulsed Gaussian pump laser, the time-dependent inverse focal length evaluated at the beam center is given by

$$1/f = \frac{4.606E\epsilon C\, dn/dT}{\sqrt{2\pi}\omega k t_c (1 + 2t/t_c)^{3/2}} \tag{70}$$

where the terms have been defined in Section II. It is interesting to note that the signal is independent of sample length and inversely proportional to the cube of the pump beam spot-size; note that $t_c = \omega^2/4D$ where D is the thermal diffusivity of the sample. Unlike conventional Beer's law measurements (or coaxial thermo-optical techniques) which show a decrease in sensitivity with path length, the crossed-beam thermal lens measurement is independent of path length. More importantly, if the sample path length is identified with the pump beam spot-size, then the absorbance sensitivity of the crossed-beam measurement actually increases as the path length decreases and spatial resolution of the measurement improves.

A cylindrical lens acts to defocus a Gaussian beam in only one direction, whereas a conventional lens defocuses the beam in a radially symmetric fashion. The probe beam intensity at the far-field detector is given by

$$I = \frac{2P}{\pi\omega_x\omega_y} \tag{71}$$

where ω_x and ω_y are the spot-sizes aligned parallel and perpendicular to the plane containing the pump and probe beams. Since the cylindrical optical element defocuses the beam only in the plane containing the two beams, the cylindrical lens converts the probe beam from circular symmetry to elliptical symmetry. The change in the probe beam center intensity is given by

$$I(t) = I(0)[1 - 2z_1/f + (z_c^2 - z_1^2)/f^2]^{-1/2} \tag{72}$$

where Z1 is the distance from the probe beam waist to the sample.[14] The binomial distribution may be used to simplify this equation to yield the relative far-field beam-center intensity change

$$\Delta I = z_1/f \tag{73}$$

It is interesting to compare the magnitude of the coaxial thermal lens and the crossed-beam thermal lens signal. Under the assumptions of the paraxial approximation, the ratio of the probe beam-center intensity is given by

$$\frac{\Delta I_{coaxial}}{\Delta I_{crossed}} = \frac{\mathscr{L}}{\omega_{pump}} (2/\pi)^{1/2}(1 + 2t/t_c)^{-1/2} \tag{74}$$

It appears that the sensitivity of the coaxial thermal lens will be larger than the sensitivity of the crossed-beam instrument whenever the sample has a path length several times larger than the pump beam spot-size.

Of course, a discussion of sensitivity is meaningless without a discussion of noise. For example, detection limits in a proportional noise-limited experiment are not determined by

sensitivity but rather by pump laser stability. In long path length thermal lens determinations utilizing pump laser powers greater than about 100 mW, the detection limits appear to be determined by noise proportional to the blank signal. The best absorbance detection limits for coaxial techniques fall in the range $A = 10^{-6}$ to 10^{-7}/cm, at least for samples 1 cm or longer.

The best detection limit for the crossed-beam thermal lens is $\epsilon C = 10^{-5}$ cm^{-1} using a mixed water-methanol solvent and a 100-mW pump beam.[8] Similar detection limits have been obtained for chromatographic detection. The very tightly focused pump beam, $\omega_{pump} = 1.3$ μm, suggests that a very short path length measurement could be performed. The absorbance across the 200-μm cuvette was $A = 2 \times 10^{-7}$, whereas the absorbance across twice the pump beam spot-size was only $A = 3 \times 10^{-9}$! Recall that these detection limits are obtained with a relatively poor thermo-optical solvent, whereas the best detection limits produced by the long path length techniques have been obtained in very good solvents like CCl_4 and supercritical CO_2.

The crossed-beam thermal lens and the coaxial thermal lens should produce similar detection limits for samples in the 100-μm to 1-mm path length range. This observation appears to be at odds with the sensitivity comparison of Equation 74, which suggests that the sensitivity should be similar for samples of a few micrometers path length. This discrepancy is removed when it is realized that the coaxial, long path length measurement is background limited for path length longer than a few hundred micrometers, whereas the crossed-beam measurement is not background limited at much shorter path lengths.

A source of background signal in the long path length techniques is generated by absorbance within components used in the optical train. An inspection of all long path length thermo-optical measurements reveals that the pump and probe beams intersect several common optical components. If nothing else, the cuvette windows are illuminated by both beams, whereas most designs utilize beam splitters, lenses, filters, or choppers which are illuminated by both beams. Any optical element illuminated by both the pump and probe beams is a source of some background signal. The background signal generated due to these optical elements becomes proportionally larger as path length decreases for the long path length techniques.

On the other hand, the crossed-beam thermal lens utilizes *no* optical components common to both the pump and probe optical train. Since there are no optical components in common, background signals generated outside of the sample probe volume are eliminated. The reduction in background signal produced by the crossed-beam instrument must account for some of the improved performance of the crossed-beam technique.

Both lock-in detection and signal averaging followed by regression analysis have been performed for the crossed-beam thermal lens. At similar pump laser power, the detection limits produced by the two demodulation techniques are identical. The time-resolved data allow easier comparison with theory for a number of parameters. For example, the signal amplitude is inversely proportional to pump laser spot-size, even for small spot-size beams.[43] In the experiment, the pump beam spot-size was 12 μm and the probe beam spot-size was about 40 μm. Although the paraxial approximation demands the pump beam spot-size be much larger than the probe beam spot-size, it would appear that the crossed-beam instrument is well modeled by the paraxial approximation even when the pump beam spot-size is much smaller than the probe beam spot-size.

The crossed-beam thermal lens signal is proportional to Z1, the distance from the probe beam waist to the sample, over a distance given by several times the probe beam confocal distance.[28,43] It is interesting to note that the crossed-beam thermal lens signal changes sign as the probe beam waist crosses the interaction region. By placing a reference and sample cuvette equal distances from the probe beam waist and by using equal intensity pump beams,

it should be possible to construct a differential crossed-beam thermal lens instrument similar to the differential thermal lens instrument.

The amplitude of the crossed-beam instrument has been considered as a function of both frequency and time. The frequency response of the crossed-beam thermal lens is similar to the conventional thermal lens; both techniques demonstrate a 20 dB/decade decrease in signal for modulation frequencies much greater than the reduced modulation frequency.[14] The agreement between the time-resolved data and theory depends upon the sophistication of the theory. For a pump beam modulated with a mechanical chopper, it is necessary to consider the finite time for the chopper blade to cross the beam. Very good agreement has been reported between the theory based upon a trapezoidal excitation function and data.[43]

The crossed-beam thermal lens has been considered for flowing samples.[44] The time-resolved signal may be used to obtain the flow velocity at the intersection region of the pump and probe laser beams. The crossed-beam thermal lens technique provides a nonintrusive measure of flow velocity and has been used to map the flow profile within a 1-mm square flow chamber. The data were similar to the expected Laminar flow profile.

Flow acts to remove heat from the intersection of the pump and probe laser beams. This decrease in heat results in decreased magnitude for the cw laser-excited crossed-beam thermal lens. However, the probe beam may be offset downstream by a small distance to maximize the crossed-beam signal. The signal-to-noise ratio is similar for both the coplanar crossed-beam experiment in static samples and the offset crossed-beam experiment in flowing samples.[45]

C. Crossed-Beam Thermal Prism

Analogous to the long path length variant of the thermal prism, a crossed-beam design may be employed to produce spatially resolved absorbance measurements, Figure 27. Here, the cylindrical lens formed by absorbance of a Gaussian pump beam is probed at right angles with a tightly focused probe beam. However, the pump and probe beam axes are offset so that the probe beam passes through the maximum gradient in refractive index. The probe beam is deflected by the heated region through an angle θ given by the gradient of the refractive index profile

$$\theta = \frac{0.56E\epsilon C\, dn/dT}{kt_c(1 + 2t/t_c)} \tag{75}$$

where E is the energy of the pulsed pump laser.[44] Note that the deflection angle is independent of the path length but is dependent upon the square of the pump beam spot-size contained in the t_c term. Since the impulse response crossed-beam thermal lens instrument is dependent upon the cube of the pump beam spot-size, the thermal lens measurement may prove more useful for small volume applications.

Unfortunately, there is very little information concerning the analytical utility of the crossed-beam thermal prism. In one paper, the crossed-beam instrument for measurement of Beer's law loss due to absorbance of the pump beam between the cuvette window and the probed volume has been considered, but little experimental detail was provided.[156] This instrument employed a chopped argon ion excitation source and lock-in detection.

The effect of the displacement between the pump and probe beams has been considered.[157] As expected, the amplitude maximized when the probe beam passed through the inflection point in the temperature distribution.

A number of studies have been published for study of flowing, gas phase samples.[44,59-63,158] These studies verify that thermal prism measurements based upon the time-resolved deflection signal may be applied to flow velocity measurements.

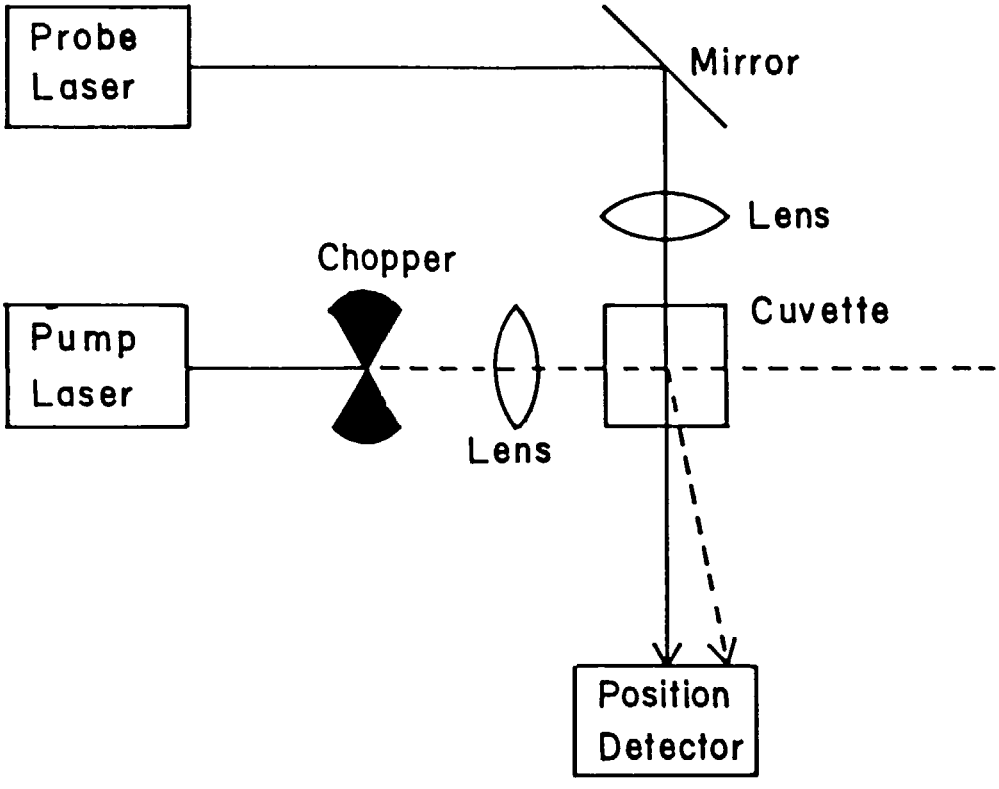

FIGURE 27. The crossed-beam thermal prism. The probe beam is aligned off axis from the pump beam. Deflection of the probe beam is monitored with a position-sensitive detector.

D. Crossed-Beam Interferometery

There appears to be only one crossed-beam thermo-optical measurement of sample absorbance using an interferometer.[159] In this experiment, a Jamin interferometer was constructed with the sample cell in one beam. A argon ion pump beam was focused into the cuvette at right angles to the probe beam. The probe and reference beams were recombined and sent to a photodiode detector. Interference between the two beams generated an intensity shift at the detector synchronous with the chopped argon ion beam; the signal was proportional to the phase shift in the probe beam arm of the interferometer.

The phase shift, $\Delta\phi$, induced by absorbance of a focused Gaussian beam in a homogeneous sample is given by the integral of Equation 14 over the probe beam optical path. The phase shift induced along the center of the pump beam is given by

$$\Delta\phi = \frac{2\pi\ dn/dT}{\lambda}\int \Delta T\ dpath = \frac{2.303\sqrt{2\pi}\ dn/dT\ E\epsilon C}{2\lambda k t_c \omega (1 + 2t/t_c)^{1/2}} \cdot W \qquad (76)$$

where λ is the wavelength of the probe laser. The change in intensity generated within the interferometer is proportional to $\Delta\phi$ for small phase shifts.

E. Thermal Grating

A thermal grating is formed from the absorbance of two intersecting, mutually coherent

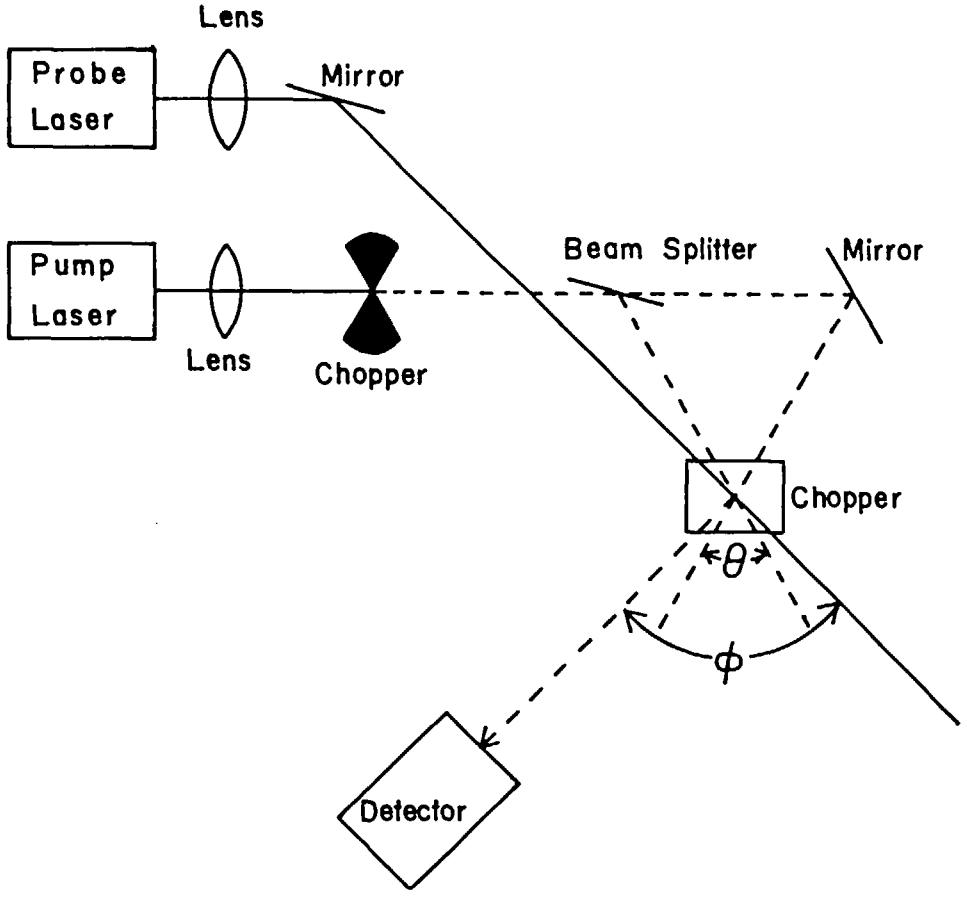

FIGURE 28. The thermal grating. The pump beam is split into two equal intensity beams which are crossed within the sample. The beams undergo interference, thereby generating a set of intensity fringes within the sample. The resulting heating of the sample generates a periodic (in space) refractive index perturbation which acts as a phase grating. The phase grating diffracts light from a probe beam aligned at Bragg's angle. The diffracted or signal beam is monitored with a high-sensitivity photodetector.

laser beams, Figure 28.[16,160-162] The two beams interfere, generating a set of light and dark intensity fringes within the sample. The spacing between the fringes, Ω, is given by

$$\Omega = \frac{\lambda}{2 \sin \theta} \tag{77}$$

where θ is the intersection angle between the two beams. If the laser beam spot-size at the intersection region is ω, then the number of fringes across the intersection region is approximately given by ω/Ω. The intersection volume is given by

$$\text{Volume} = \frac{8\pi\omega^3}{3 \sin \theta} \tag{78}$$

assuming that the pump beam spot-sizes are identical and equal to ω.

Absorbance of the intensity fringes produces a periodic temperature and refractive index

perturbation within the sample. The refractive index perturbation at the center of the fringe region is given by

$$\Delta n_{max} = \frac{9.2E_{pump}\epsilon C}{\pi\rho C_p\omega^2} \tag{79}$$

where E_{pump} is the total energy contained in both pump laser beams. Maximum fringe contrast is produced when the intensity of the two pump beams is equal.

The thermal relaxation time for the grating is given by

$$t_c = \frac{\rho C_p\Omega^2}{4\pi^2 k} \tag{80}$$

Note that the time constant is proportional to the square of the fringe spacing.

The grating may be probed in several ways. Most commonly, a probe beam intersects the grating at Bragg's angle

$$\theta = 2\sin^{-1}(\lambda_{probe}/2\Omega) \tag{81}$$

where θ is the angle between the incident and diffracted beam.

The diffraction efficiency is given by

$$\frac{I_+}{I_0} = \frac{8\pi}{\sqrt{3}}\left[\frac{2.303\ E_{pump}\ dn/dT\ \epsilon C}{\rho C_p\omega_{pump}\lambda_{probe}\sin(2\theta)}\right]^2 \tag{82}$$

where I_+ is the diffracted intensity and I_0 is the incident probe intensity.

Several important properties of the thermal grating have been pointed out.[16,160,161] The signal is quadratically dependent upon both analyte concentration and pump laser energy. Very high sensitivity may be obtained using high-energy pulsed pump lasers.[161] Unfortunately, background absorbance ultimately limits the highest useful pump laser energy.

The quadratic dependence of the signal upon analyte concentration is a nuisance at best, requiring many calibration points. Furthermore, if the pump energy is not sufficient to produce an appreciable background signal, then the quadratic concentration dependence implies that the concentration sensitivity goes to zero at low concentrations.

The signal is independent of path length, as are the other crossed-beam techniques. However, Pelletier and Harris[161] have shown that an appreciable number of fringes are required to produce a significant signal. The diffraction intensity drops well below the theoretical value of Equation 82 for less than 10 to 20 fringes. This fringe number requirement suggests that the minimum probed volume in the grating experiment will be relatively large compared to the other crossed-beam instruments.

A major limitation of this instrument is the severe alignment constraints.[161] Angular misalignments of the beams by 0.03 to 0.001° can produce significant deterioration in the signal amplitude. The thermal grating instrument is not robust with respect to alignment.

Detection limits using a pulsed pump laser were $\epsilon C = 6 \times 10^{-4}\ cm^{-1}$ using an aqueous sample.[16] Detection limits of $\epsilon C = 7 \times 10^{-4}\ cm^{-1}$ were reported using a chopped argon ion pump laser beam and carbon tetrachloride solvent.[161]

The thermal grating has been used to measure two-photon absorbance.[162] Since the two-photon absorbance cross section is proportional to the square of the pump laser intensity, there is a diffraction signal generated corresponding to one half the fringe spacing; two-photon absorbance generates a diffraction signal at twice the Bragg angle. The placement

Table 7
SMALL VOLUME ANALYSIS

Liquid Phase Determination

Analyte	Solvent	Type	Laser	Detection probe limit (*M*)	Probe volume	Detection limit-probe volume product	Ref.
Iron 1,10-phenanthroline	1:1 MeOH:water	XBTL	100 mW 514 nm	9×10^{-10}	0.2 pℓ	120 atoms	8

Liquid Chromatography Detection

Analyte	Solvent	Type	Laser	Detection limit	Ref.
DABSLY-amino acids	3:2 MeOH:water	XBTL	100 mW 488 nm	0.4—45 pg	163

Note: XBTL = crossed-beam thermal lens.

of one detector at the diffraction angle for one-photon absorbance and a second detector at the diffraction angle for two-photon absorbance allows the simultaneous measurement of both one- and two-photon absorbance. Two-photon absorbances corresponding to $\epsilon C = 1 \times 10^{-3}$ were reported using a pulsed pump laser.

F. Applications

Only a few analytical applications have been reported for crossed-beam thermo-optical techniques.[8,155] Iron was determined with 1,10-phenanthroline in a mixed 1:1 water-methanol solvent mixture and a 100-mW pump beam at 514.5 nm, Table 7. Detection limits were 9×10^{-10} *M* iron. Although the concentration detection limit is not particularly small, the determination was performed with an extremely small probed volume, 200 fL. The concentration-probed volume product corresponds to 120 iron atoms present at the detection limit. It should be noted that this instrument was *not* background limited. The solvent background was only a factor of five greater than the detection limit. At least another order of magnitude improvement in detection limit should be possible with higher pump laser power.

Detection limits of 6.7×10^{-4} *M* amaranth in methanol have been reported using 0.38-mJ pulsed pump laser in the crossed-beam thermal lens.[155] Unfortunately, an estimate of the probed volume in this experiment was not reported.

The crossed-beam thermal lens has also been applied to liquid chromatographic detection of (dimethylamino)azobenzenesulfonyl (DABSYL) derivatives of six amino acids.[163] A 3:2 methanol-water solvent was employed with a reversed-phase, 1-mm I.D. chromatographic column. Detection limits ranged from 5 fmol of glycene to 300 fmol of methionine injected onto the column. Recently, the technique has been applied to packed capillary column liquid chromatography, 250-μm I.D. columns, 75-cm long, of DABSYL amino acids and dinitrophenylhydrozone derivaties of ketons. Detection limits fell in the low femtomole-to-high attomole range.

The small probed volume of the crossed-beam thermal lens suggests a potential application for scanning laser microscopy. Here, the crossed-beam thermal lens signal is recorded as

the sample is translated through the intersection region of the pump and probe laser beams.[164] Both geological and biological tissue samples have been studied. In addition to absorbance information from the amplitude of the lock-in amplifier, the phase may be employed to generate information on the thermal properties of the sample. For example, the geological sample studied, the mineral sphalerite, ZnS, is somewhat unusual in that dn/dT is positive, whereas most substances have negative dn/dT. Small fluid inclusions trapped within the matrix generate a signal of opposite sign from the ZnS matrix.

V. THERMO-OPTICS FOR SURFACE ANALYSIS

A. Introduction

Several thermo-optical techniques have been developed for the measurement of absorbance at a surface. In all of the techniques, a modulated pump beam is directed at a right angle to the surface. The heated sample both deforms and heats the surrounding atmosphere. The heated atmosphere surrounding the illuminated sample will act to deflect a probe beam directed parallel to the surface through the heated region. This beam deflection is the basis of the mirage effect, the best developed of these surface thermo-optical techniques. By translating the sample through the intersection region of the pump and probe beams, images of surface absorbance may be constructed on a point-by-point basis.

Another thermo-optical technique has been considered for surfaces where a probe beam is reflected from the surface region illuminated by the modulated pump beam. Thermal expansion of the surface defocuses the reflected probe beam. Since the thermal defocusing produced by the surface deformation does not require interaction with the surrounding atmosphere, the surface deformation technique may be performed in a vacuum.

Thermo-optical techniques developed for surface analysis are not well suited for highly absorbing samples. Thermal saturation occurs when most of the pump beam energy is converted into heating the sample; the dynamic range of the measurement will not allow determination of small spatial changes in absorbance.

B. Mirage Effect

The mirage effect is based upon deflection of a probe beam near a surface heated by absorption of a pump beam and is named after the commonly observed mirage formed over a heated surface. Several investigators independently described or proposed the effect.[165-167] In a typical experiment, Figure 29, a modulated pump laser beam is focused onto the interface between a solid and a surrounding gas or liquid. The heated surface produces a temperature rise in the nearby gas or liquid. The heated gas or liquid forms a thermo-optical element which acts as a prism to deflect a probe beam directed parallel to the surface through the heated region.

As discussed in Section III.D, several types of position-sensitive detectors may be employed to measure the probe beam deflection, including a small photodiode located at the inflection point of the probe beam profile, a bicell, a lateral cell, or a photodiode array. The dominant noise sources in the mirage experiments appear to be vibration of optical components[165] and drift of the laser beam position.

Several analytically important parameters have been considered for the mirage effect.[168,169] The signal-to-noise ratio maximizes when the probe beam is closest to the absorbing surface and decreases steadily with distance away from the surface. The signal-to-noise ratio also increases with pump laser power until proportional noise becomes significant. The signal decreases with modulation frequency at about 20 dB/decade, as in other thermo-optical effects.

The signal decreases with the probe beam offset from the surface. This decrease should be minimal when the probe beam is within one thermal diffusion length of the surface, defined by

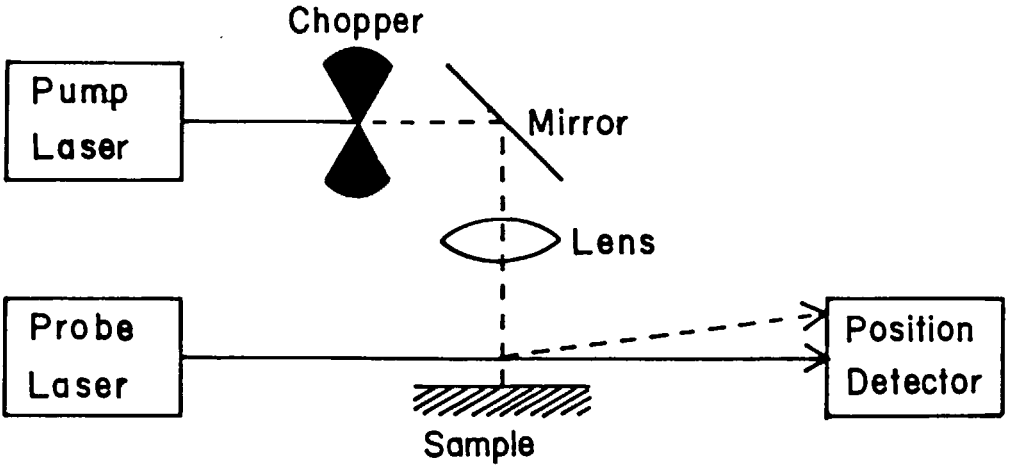

FIGURE 29. The mirage. A modulated pump beam is focused onto an absorbing surface. The heated surface heats the surrounding atmosphere which deflects a probe beam aligned parallel to the surface. Deflection of the probe beam is monitored with a position-sensitive detector.

$$\text{Thermal diffusion distance} = (D/\nu)^{1/2} \tag{83}$$

where D is the thermal diffusion constant and ν is the modulation frequency. For typical liquids, D falls near 1×10^{-3} sec^{-1} cm^2; at a modulation frequency of 10 Hz, the probe beam should be within 0.01 mm of the surface.

The frequency behavior of the signal is determined by two components. The first is due to thermal diffusion away from the surface to the probe beam, described above. The other is radial diffusion of heat away from the pump beam axis. This radial decay of heat will be dominated by thermal diffusion within the transparent gas or liquid surrounding the surface. A time constant can be estimated for the radial thermal diffusion by

$$t_c = \omega^2/4D \tag{84}$$

where ω is the pump beam spot-size and D is the thermal diffusivity of the transparent medium. To achieve high modulation rates, it is necessary to utilize a tightly focused pump laser beam.

An intercavity detector for the mirage effect has been reported.[98] A 100-mW krypton ion laser produced the pump beam at 351 to 356 nm. The pump beam was focused onto a solid sample located within a slightly detuned argon ion laser cavity, just below the intercavity beam path. The argon ion probe laser intensity would decrease when the sample was illuminated by the pump beam. The intercavity detector produces a factor of 16 improvement in signal-to-noise ratio compared with an extracavity conventional mirage instrument.

A Fourier transform spectrometer has been used to produce a modulated pump beam in the mirage experiments.[170] A reference beam was used to compensate for environmental disturbances in the probe beam path. Spectra were obtained from a number of organic and inorganic solids.

Instead of deflection by the thermo-optical element at the surface, a phase modulation can be induced by scattering from the sound waves propagating away from the surface.[171] The measurement requires a very high-frequency modulated pump beam, 1 GHz, and a heterodyne detection scheme to demodulate the signal. The primary advantage of this sound

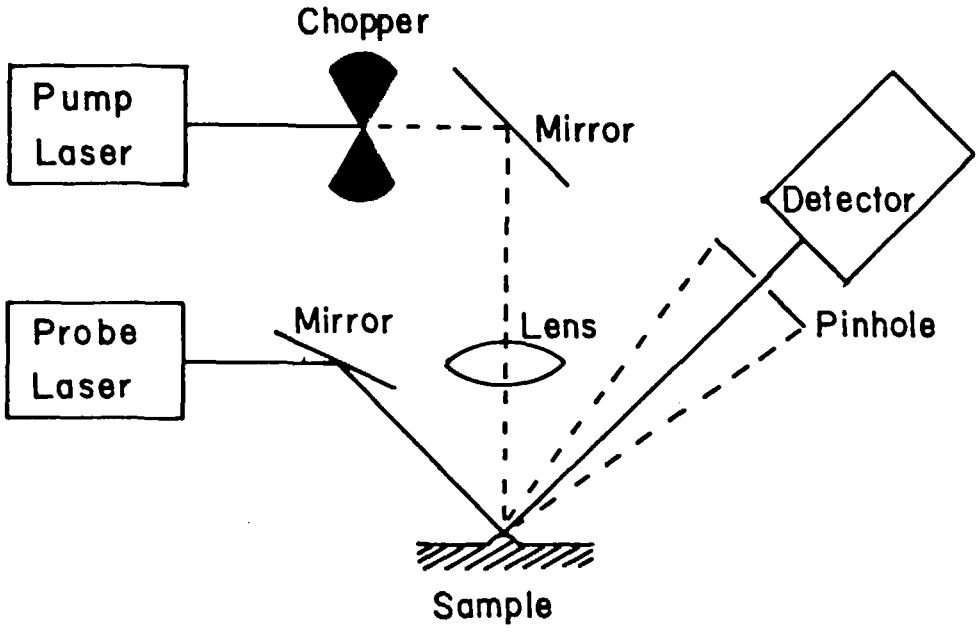

FIGURE 30. Thermal deformation. A pump laser illuminates a surface. Thermal expansion produces a convex surface which acts to defocus a probe beam illuminating the heated surface. If the surface is a liquid, thermally induced changes in surface tension produce a concave surface to focus the probe beam. The pump and probe beams may be coaxial, and the reflected beam may be used to isolate the signal in an epi-illumination configuration.

wave scattering technique is very high spatial resolution. Since the signal is modulated at very high frequencies, thermal diffusion does not govern the spatial resolution; instead, the pump beam spot-size limits the spatial resolution.

C. Surface Deformation

The mirage effect can only be applied to surfaces immersed in a liquid or gas; the measurement cannot be used in a vacuum. A related thermo-optical technique has been developed which measures the deformation of the surface induced by the temperature rise, Figure 30.[17,172,173] A modulated pump beam produces a time-varying temperature rise in the absorbing surface. Thermal expansion in solids and thermally driven capillary action in liquids acts to produce either a small hill or dimple on the surface. A cw probe laser beam is reflected from the deformation, and a time-dependent intensity change is observed in the far field. In essence, the deformed surface acts as a curved mirror to focus or defocus the probe beam.

A 100-mW argon ion laser beam is modulated at high frequencies, up to 10 MHz, to produce the surface deformation in the sample. A cw helium-neon probe beam is reflected from the sample. Microscope objectives may be employed to probe very small samples.

The surface deformation differs from other thermo-optical elements considered in this manuscript. The phase shift induced in the probe beam is not produced by a change in the refractive index of the medium but instead is due to a physical change in the path length due to the surface deformation. The thermal expansion is the primary characteristic of the sample which is probed, not the change in the refractive index with temperature.

Table 8
THIN-LAYER CHROMATOGRAPHY

Analyte	Pump laser	Detection limits	Ref.
1,2-Napthoquinone	20 mW	2.3 ng	175
Phenanthrenequinone	488 nm	31 ng	
Alpha-ionone		7.5 pg	
1,2-Napthoquinone	20 mW	25 pg	168
Phenanthrenequinone	457.9 nm	1.3 ng	
Alpha-ionone		6.2 pg	
Congo red	100 mW	0.5 ng	169
trans-Azobenzene	350—356 nm	0.9 ng	
trans-Azobenzene	21 mW 457.9 nm	1.3 ng	98

D. Thermally Induced Reflectance Changes

Another potential thermo-optical technique for the study of surface absorbance can be considered. It is known that the reflectivity of certain thin films, such as gold, is a function of temperature.[174] Reflectance changes of about 0.1% per degree temperature rise have been noted. It should be possible to produce a time-varying reflectance change in the film with a modulated pump beam and to monitor the reflectance change with a second probe laser.

E. Applications

There have been several applications of the mirage effect for analytical chemistry, particularly as a detector in thin-layer chromatography (TLC), Table 8. Detection limits fall in the low nanogram range and appear to be determined by both the background signal originating in the chromatographic plate and the skill of the chromatographer to produce low-dispersion spots. The area of thermo-optical densitometry as applied to TLC and two-dimensional electrophoresis appears to be fertile for future application.

The mirage effect also has been applied to a study of metal corrosion.[176] Slow temporal resolution appears to have resulted from the use of an unfocused pump laser beam. Quantitative detection limits have been determined for several substances using the intercavity beam deflection instrument.[177] Detection limits for copper of about 100 μg were shown. The mirage effect has also been applied to detection of absorbing species formed electrochemically in solids.[178]

The mirage effect has been used for scanning laser microscopy of solid surfaces. Several studies of subsurface flaws within solids have been reported.[179-189]

REFERENCES

1. **Alkemade, C. Th. J.,** Single atom detection, *Appl. Spectrosc.*, 35, 1, 1981.
2. **Greenlees, G. W., Clark, D. L., Kaufman, S. L., Lewis, D. A., Tonn, J. F., and Broadhurst, J. H.,** High resolution laser spectroscopy with minute samples, *Opt. Commun.*, 23, 236, 1977.
3. **Miller, C. M. and Nogar, N. S.,** Continuous wave lasers for resonance ionization mass spectrometry, *Anal. Chem.*, 55, 1606, 1983.
4. **Alfano, A. J., Fong, F. K., and Lylte, F. E.,** High repetition rate subnanosecond gated photon counting, *Rev. Sci. Instrum.*, 54, 967, 1983.
5. **Haugen, G. R. and Lytle, F. E.,** Quantitation of fluorophores in solution by pulsed laser excitation and time-filter detection, *Anal. Chem.*, 53, 1554, 1981.
6. **Betteridge, D. and Meylor, P. J.,** Analytical aspects of photoacoustic spectroscopy, *CRC Crit. Rev. Anal. Chem.*, 14, 267, 1984.
7. **Hirschfeld, T.,** Optical microscopic observation of single small molecules, *Appl. Opt.*, 15, 2965, 1976.
8. **Nolan, T. G. and Dovichi, N. J.,** Ultrasensitive analysis with the crossed-beam thermal lens, *IEEE Circuits Devices Mag.*, 2, 54, 1986.
9. **Dovichi, N. J., Martin, J. C., Jett, J. H., Trkula, M., and Keller, R. A.,** Laser-induced fluorescence of flowing samples as an approach to single-molecule detection in liquids, *Anal. Chem.*, 56, 348, 1984.
10. **Dovichi, N. J. and Harris, J. M.,** Time resolved thermal lens calorimetry, *Anal. Chem.*, 53, 106, 1981.
11. **Harris, J. M. and Dovichi, N. J.,** Thermal lens calorimetry, *Anal. Chem.*, 52, 695A, 1980.
12. **Whinnery, J. R.,** Laser measurement of optical absorption in liquids, *Acc. Chem. Res.*, 7, 225, 1974.
13. **Kliger, D. S.,** Thermal lensing: a new spectroscopic tool, *Acc. Chem. Res.*, 13, 129, 1980.
14. **Dovichi, N. J., Nolan, T. G., and Weimer, W. A.,** Theory for laser-induced photothermal refraction, *Anal. Chem.*, 56, 1700, 1984.
15. **Jackson, W. B., Amer, N. M., Boccara, A. C., and Fournier, D.,** Photothermal deflection spectroscopy and detection, *Appl. Opt.*, 20, 1333, 1981.
16. **Pelletier, M. J., Thorsheim, H. R., and Harris, J. M.,** Laser-induced thermal diffraction for calorimetric absorption measurements, *Anal. Chem.*, 54, 239, 1982.
17. **Da Costa, G.,** Real-time recording of light patterns in heavy hydrocarbons: a theoretical analysis, *Appl Opt.*, 20, 3523, 1980.
18. **Stone, J.,** Measurements of the absorption of light in low-loss liquids, *J. Opt. Soc. Am.*, 62, 327, 1972.
19. **Woodruff, S. D. and Yeung, E. S.,** Refractive index and absorption detector for liquid chromatography based on Fabrey-Perot interferometry, *Anal. Chem.*, 54, 1174, 1982.
20. **Long, M. E., Swofford, R. L., and Albrecht, A. C.,** Thermal lens technique: a new method of absorption spectroscopy, *Science*, 191, 183, 1976.
21. **Burberry, M. S., Morrell, J. A., Albrecht, A. C., and Swofford, R. L.,** Local mode overtone intensities of C–H stretching modes in alkanes and methyl substituted benzenes, *J. Chem. Phys.*, 70, 5522, 1979.
22. **Swofford, R. L., Burbery, M. S., Morrell, J. A., and Albrecht, A. C.,** C–H vibrational states of C_6D_5H and C_6F_5H in the visible region by thermal lensing spectroscopy. A test of the local mode model. *J. Chem. Phys.*, 66, 5245, 1977.
23. **Swofford, R. L., Long, M. E., Burberry, M. S., and Albrecht, A. C.,** "Free" O–H overtone absorption of methanols in the visible region by thermal lensing spectroscopy, *J. Chem. Phys.*, 66, 664, 1977.
24. **Parker, C. A.,** *Photoluminescence of Solutions*, Elsevier, New York, 1968.
25. **Matthews, T. G. and Lytle, F. E.,** Blank limitations in laser excited solution luminescence, *Anal. Chem.*, 51, 583, 1979.
26. **Tam, A. C. and Patel, C. K. N.,** Optical absorptions of light and heavy water by laser optoacoustic spectroscopy, *Appl. Opt.*, 18, 3348, 1979.
27. **Kondilenko, I. I., Korotkov, P. A., Klimenko, V. A., and Demyanenko, O. P.,** Transverse cross section of the Raman scattering of the ν_1 vibration of the water molecule in the liquid and gaseous states, *Appl. Spectrosc. (U.S.S.R.)*, 43, 384, 1977.
28. **Nolan, T. G., Weimer, W. A., and Dovichi, N. J.,** Laser induced photothermal refraction for small volume absorbance determination, *Anal. Chem.*, 56, 1704, 1984.
29. **Kolgenik, H. and Li, T.,** Laser beams and resonators, *Proc. IEEE*, 54, 97, 1966.
30. **Yariv, A.,** *Introduction to Optical Electronics*, 2nd ed., Holt, Rinehart & Winston, New York, 1976.
31. **Kushida, T. and Geusic, J. E.,** Optical refrigeration in Nd-doped yttrium aluminum garnet, *Phys. Rev. Lett.*, 21, 1172, 1968.
32. **Daree, K.,** Photochemical blooming of laser beams, *Opt. Commun.*, 4, 238, 1971.
33. **Brannon, J. H. and Magde, D. J.,** Absolute quantum yield determination by thermal blooming. Fluorescein, *Phys. Chem.*, 82, 705, 1978.
34. **Lesiecki, M. and Drake, J. M.,** Use of the thermal lens technique to measure the luminescent quantum yields of dyes in PMMA for luminescent solar concentrators, *Appl. Opt.*, 21, 557, 1982.

35. **Fuke, K., Hasegawa, A., Ueda, M., and Itoh, M.,** A thermal lensing study of a photolysis of di-*t*-butyl peroxide, *Chem. Phys. Lett.*, 84, 176, 1981.
36. **Carslaw, H. S. and Jaeger, J. C.,** *Operational Methods in Applied Mathematics*, 2nd ed., Oxford Press, London, 1949.
37. **Carslaw, H. S.,** *Introduction to the Mathematical Theory of the Conduction of Heat in Solids*, Dover, New York, 1945.
38. **Carslaw, H. S. and Jaeger, J. C.,** *Conduction of Heat in Solids*, 2nd ed., Oxford Press, London, 1959.
39. **Gordon, J. P., Leite, R. C. C., Moore, R. S., Porto, S. P. S., and Whinnery, J. R.,** Long-transient effects in lasers with inserted liquid samples, *J. Appl. Phys.*, 36, 3, 1965.
40. **Dabby, F. W., Boyko, R. W., Shank, C. V., and Whinnery, J. R.,** Short time-constant thermal self-defocusing of laser beams, *IEEE J. Quantum Electron.*, QE-5, 516, 1969.
41. **Hu, C. and Whinnery, J. R.,** New thermooptical measurement method and a comparison with other methods, *Appl. Opt.*, 12, 72, 1973.
42. **Twarowski, A. J. and Kliger, D. S.,** Multiphoton absorption spectra using thermal blooming, *Chem. Phys.*, 20, 253, 1977.
43. **Weimer, W. A. and Dovichi, N. J.,** Simple model for the time dependence of the periodically excited crossed-beam thermal lens, *J. Appl. Phys.*, 59, 225, 1986.
44. **Weimer, W. A. and Dovichi, N. J.,** Time-resolved crossed-beam thermal lens measurement as a non-intrusive probe of flow velocity, *Appl. Opt.*, 24, 2981, 1985.
45. **Weimer, W. A. and Dovichi, N. J.,** Optimization of photothermal refraction for flowing liquid samples, *Appl. Spectrosc.*, 39, 1009, 1985.
46. **Weimer, W. A. and Dovichi, N. J.,** Time-resolved thermal lens measurements in flowing samples, *Anal. Chem.*, 57, 2436, 1985.
47. **Swofford, R. L. and Morrell, J. A.,** Analysis of the repetitively pulsed dual-beam thermo-optical absorption spectrometer, *J. Appl. Phys.*, 49, 3667, 1978.
48. **Fang, H. L. and Swofford, R. L.,** Analysis of the thermal lensing effect for an optically thick sample — a revised model, *J. Appl. Phys.*, 50, 6609, 1979.
49. **Eichler, H. J.,** Lichtinduzierte, thermische phasengitter in absorbierenden flussigkeiten, *Z. Angew. Phys.*, 31, 1, 1971.
50. **Aamodt, L. C. and Murphy, J. C.,** Thermal effects in photothermal spectroscopy and photothermal imaging, *J. Appl. Phys.*, 54, 581, 1983.
51. **Grabiner, F. R., Siebert, D. R., and Flynn, G. W.,** Laser induced time-dependent thermal lensing studies of vibrational relaxation: translational cooling in CH_3F, *Chem. Phys. Lett.*, 17, 189, 1972.
52. **Bailey, R. T., Cruickshank, F. R., and Pugh, D.,** Pulsed source thermal lens. I. Theoretical analysis, *J. C. S. Faraday II*, 76, 633, 1980.
53. **Bailey, R. T., Cruickshank, F. R., Pugh, D., and Johnstone, W.,** Pulsed source thermal lens. II. Experimental test of the theory, *J. C. S. Faraday II*, 77, 1387, 1981.
54. **Barker, J. R. and Rothem, T.,** Theory of the time-dependent-thermal-lensing (TDTL) technique as used in energy-transfer experiments, *Chem. Phys.*, 68, 331, 1982.
55. **Bialkowski, S. E.,** The effect of mass diffusion in gas phase thermal lens experiments, *Chem. Phys. Lett.*, 104, 448, 1984.
56. **Schwartz, M.,** *Information, Modulation, and Noise*, 2nd ed., McGraw-Hill, New York, 1970, 84.
57. **Abromowitz, M. and Stegun, I. A.,** *Handbook of Mathematical Functions*, Dover, New York, 1965, chap. 5.
58. **Akhmanov, S. A., Krindach, D. P., Migulin, A. V., Sukhorukov, A. P., and Khokhlov, R. V.,** Thermal self-action of laser beams, *IEEE J. Quantum Electron.*, QE-4, 568, 1968.
59. **Gebhardt, F. G. and Smith, D. C.,** Effects of wind on thermal defocusing of CO_2 radiation, *Appl. Phys. Lett.*, 14, 52, 1969.
60. **Wagner, W. G. and Marburger, J. H.,** On laser induced turbulence, *Opt. Commun.*, 3, 19, 1971.
61. **Sell, J. A.,** Quantitative photothermal deflection spectroscopy in a flowing stream of gas, *Appl. Opt.*, 23, 1586, 1984.
62. **Sontag, H. and Tam, A. C.,** Time-resolved flow-velocity and concentration measurements using a traveling thermal lens, *Opt. Lett.*, 10, 436, 1985.
63. **Rose, A. and Gupta, R.,** Application of photothermal deflection technique to flow-velocity measurements in a flame, *Opt. Lett.*, 10, 532, 1985.
64. **Born, M. and Wolf, E.,** *Principles of Optics*, 5th ed., Pergamon Press, Elmsford, N.Y., 1975.
65. **Gaskill, J. D.,** *Linear Systems, Fourier Transforms, and Optics*, John Wiley & Sons, New York, 1978.
66. **Sheldon, S. J., Knight, L. V., and Thorne, J. M.,** Laser-induced thermal lens effect: a new theoretical model, *Appl. Opt.*, 21, 1663, 1982.
67. **Carter, C. A. and Harris, J. M.,** Comparison of models describing the thermal lens effect, *Appl. Opt.*, 23, 476, 1984.

68. **Bialkowski, S. J.,** Photothermal lens aberration effects in two laser thermal lens spectrophotometry, *Appl. Opt.*, 24, 2792, 1985.
69. **Le Berre, M., Ressayre, E., and Tallet, A.,** Self-focusing and spatial ringing of intense cw light propagating through a strongly absorbing medium, *Phys. Rev. A*, 25, 1604, 1982.
70. **Long, G. R. and Bialkowski, S. E.,** Pulsed infrared laser thermal lens spectrophotometric determination of trace-level gas-phase analytes: quantitation of parts per billion dichlorodifluoromethane, *Anal. Chem.*, 56, 2806, 1984.
71. **Carter, C. A. and Harris, J. M.,** Long path length samples in thermal lens calorimetry, *Appl. Spectrosc.*, 37, 166, 1983.
72. **Beysens, D. and Calmettes, P.,** Temperature dependence of the refractive indices of liquids: deviation from the Lorentz-Lorenz formula, *J. Chem. Phys.*, 66, 766, 1977.
73. **Mori, K., Imasaka, T., and Ishibashi, N.,** Determination of nitrogen dioxide by pulsed thermal lens spectrophotometry, *Anal. Chem.*, 55, 1075, 1983.
74. **Sparks, M.,** Optical distortion by heated windows in high-power laser systems, *J. Appl. Phys.*, 42, 5029, 1971.
75. **Abbate, G., Bernini, U., Ragozzino, E., and Somma, F.,** The temperature dependence of the refractive index of water, *J. Phys. D*, 11, 1167, 1978.
76. **Dovichi, N. J. and Harris, J. M.,** Laser induced thermal lens effect for calorimetric trace analysis, *Anal. Chem.*, 51, 728, 1979.
77. **Weast, R. C., Ed.,** *CRC Handbook of Chemistry and Physics*, 51st ed., CRC Press, Boca Raton, Fla., 1970.
78. **Leach, R. L. and Harris, J. M.,** Supercritical fluids as spectroscopic solvents for thermooptical absorption measurements, *Anal. Chem.*, 56, 1481, 1984.
79. **Timmermans, J.,** *Physico-Chemical Constants of Pure Organic Compounds*, Elsevier, New York, 1950.
80. **Timmermans, J.,** *Physico-Chemical Constants of Pure Organic Compounds*, Vol. 2, Elsevier, New York, 1965.
81. **Touloukian, Y. S., Liley, P. E., and Saxena, S. C.,** *Thermophysical Properties of Matter, Vol. 3, Thermal Conductivity of Nonmetallic Liquids and Gases*, Plenum Press, New York, 1970.
82. **Touloukian, Y. S. and Makita, T.,** *Thermophysical Properties of Matter, Vol. 6, Specific Heat of Nonmetallic Liquids and Gases*, Plenum Press, New York, 1970.
83. **Touloukian, Y. S. and Makita, T.,** *Thermophysical Properties of Matter, Suppl. to Vol. 6, Specific Heat of Nonmetallic Liquids and Gases*, Plenum Press, New York, 1970.
84. **Giglio, M. and Vendramini, A.,** Thermal lens effect in a binary liquid mixture: a new effect, *Appl. Phys. Lett.*, 25, 555, 1974.
85. **Carter, C. A. and Harris, J. M.,** Comparison of single- and dual-beam configurations for thermal lens spectroscopy, *Anal. Chem.*, 55, 1256, 1983.
86. **Fujiwara, K., Uchiki, H., Shimokoshi, F., Tsunoda, K. -I., Fuwa, K., and Kobayashi, T.,** Thermal lensing colorimetry of nitrite ion with single-laser system, *Appl. Spectrosc.*, 36, 157, 1982.
87. **Nakanishi, K., Imasaka, T., and Ishibashi, N.,** Thermal lens spectrophotometry of phosphorus using a near-infrared semiconductor laser, *Anal. Chem.*, 57, 1219, 1985.
88. **Pang, T.-K. J. and Morris, M. D.,** Differential thermal lens liquid chromatography detector, *Anal. Chem.*, 57, 2153, 1985.
89. **Mori, K., Imasaka, T., and Ishibashi, N.,** Thermal lens spectrophotometry based on pulsed laser excitation, *Anal. Chem.*, 54, 2034, 1982.
90. **Alfheim, J. A. and Langford, C. H.,** Determination of formaldehyde with the thermal lens effect, *Anal. Chem.*, 57, 861, 1985.
91. **Peck, K. and Morris, M. D.,** Sensitive photothermal densitometer for quantitation of Coomassie Brilliant Blue stained proteins in polyacrylamide gels, *Anal. Chem.*, 58, 506, 1968.
92. **Higashi, T., Imasaka, T., and Ishibashi, N.,** Thermal lens spectrophotometry of gaseous hydrocarbon molecules in the infrared region, *Anal. Chem.*, 56, 2010, 1984.
93. **Bialkowski, S.,** Pulsed laser thermal lens spectrophotometry of liquid samples using an optical fiber beam guide, *Anal. Chem.*, 58, 1706, 1986.
94. **Leite, R. C. C., Moore, R. S., and Whinnery, J. R.,** Low absorption measurements by means of the thermal lens effect using an He-Ne laser, *Appl. Phys. Lett.*, 5, 141, 1964.
95. **Solimini, D.,** Loss measurement of organic materials at 6328 A, *J. Appl. Phys.*, 37, 3314, 1966.
96. **Grishko, V. I., Yudelevich, I. G., and Grishko, V. P.,** A secondary laser cavity system for spectrophotometry of trace elements based on intercavity quenching and thermal lens effects, *Anal. Chim. Acta*, 160, 159, 1984.
97. **Cremers, D. A. and Keller, R. A.,** Thermally induced laser pulsing to measure weak optical absorptions, *Appl. Opt.*, 20, 3838, 1981.

98. **Masujima, T., Sharda, A. N., Lloyd, L. B., Harris, J. M., and Erying, E. M.,** Laser intercavity photothermal beam deflection spectrometer, *Anal. Chem.*, 56, 2975, 1984.
99. **Reddy, K. V.,** Intracavity dye-laser photothermal deflection spectroscopy, *Rev. Sci. Inst.*, 54, 422, 1983.
100. **Rieckhoff, K. E.,** Self-induced divergence of cw laser beams in liquids — a new nonlinear effect in the propagation of light, *Appl. Phys. Lett.*, 9, 87, 1966.
101. **Whinnery, J. R., Miller, D. T., and Dabby, F.,** Thermal convection and spherical aberration distortion of laser beams in low-loss liquids, *IEEE J. Quantum Electron.*, QE-3, 282, 1967.
102. **Dovichi, N. J. and Harris, J. M.,** Differential thermal lens calorimetry, *Anal. Chem.*, 52, 2338, 1980.
103. **Dovichi, N. J. and Harris, J. M.,** Background elimination thermal lens calorimetry, paper presented at 1979 ACS Anal. Summer Symp., Purdue University, June 27, 1979.
104. **Imasaka, T. and Ishibashi, N.,** Thermal lens spectrophotometry, *Trends Anal. Chem.*, 1, 273, 1982.
105. **Miyaishi, K., Imasaka, T., and Ishibashi, N.,** Thermal lens spectrophotometry based on image detection of a probe laser beam, *Anal. Chem.*, 54, 2039, 1982.
106. **Jansen, K. L. and Harris, J. M.,** Thermal lens measurements by optical computation of the laser beam spot size, *Anal. Chem.*, 57, 1698, 1985.
107. **Leach, R. A., Carter, C. A., and Harris, J. M.,** Least-squares polynomial filters for initial point and slope estimation, *Anal. Chem.*, 56, 2304, 1984.
108. **Leach, R. A. and Harris, J. M.,** Thermal lens calorimetry application to chromatographic detection, *J. Chromatogr.*, 218, 15, 1981.
109. **Leach, R. A. and Harris, J. M.,** Real-time thermal lens absorption measurements with application to flow-injection systems, *Anal. Chim. Acta*, 164, 91, 1984.
110. **Nickolaisen, S. L. and Bialkowski, S. E.,** A least squares digital filter for repetitive data acquisition, *J. Chem. Inf. Comput. Sci.*, 26, 57, 1986.
111. **Pang, T.-K. J. and Morris, M. D.,** Liquid chromatography detection at the second harmonic of the modulated thermal lens, *Anal. Chem.*, 56, 1467, 1984.
112. **Jansen, K. L. and Harris, J. M.,** Double-beam thermal lens spectrometry, *Anal. Chem.*, 57, 2434, 1985.
113. **Grabiner, F. R., Siebert, D. R., and Flynn, G. W.,** Laser induced time-dependent thermal lensing studies of vibrational relaxation: translational cooling in CH_3F, *Chem. Phys. Lett.*, 17, 189, 1972.
114. **Twarowski, A. J. and Kliger, D. S.,** Multiphoton absorption spectra using thermal blooming, *Chem. Phys.*, 20, 259, 1977.
115. **Long, G. R. and Bialkowski, S. E.,** Error reduction in pulsed laser photothermal deflection spectrometry, *Anal. Chem.*, 58, 80, 1985.
116. **Nickolaisen, S. L. and Bialkowski, S. E.,** Pulsed infrared laser thermal lens spectrophotometry of flowing gas samples, *Anal. Chem.*, 57, 758, 1985.
117. **Nickolaisen, S. L. and Bialkowski, S. E.,** Pulsed laser thermal lens spectrophotometry for flowing liquid detection, *Anal. Chem.*, 58, 215, 1986.
118. **Dovichi, N. J. and Harris, J. M.,** Thermal lens calorimetry for flowing samples, *Anal. Chem.*, 53, 689, 1981.
119. **Imasaka, T., Miyaishi, K., and Ishibashi, N.,** Application of the thermal lens effect for determination of iron(II) with 4,7-diphenyl-1,10-phenanthroline disulfonic acid, *Anal. Chim. Acta*, 115, 407, 1980.
120. **Haushalter, J. P. and Morris, M. D.,** Use of thermal blooming spectroscopy for enzymatic analyses, *Appl. Spectrosc.*, 34, 445, 1980.
121. **Pang, T.-K. J. and Morris, M. D.,** Pump/probe thermal lens spectroscopy with polarization-encoded laser beams, *Appl. Spectrosc.*, 39, 90, 1985.
122. **Yang, Y.,** Thermal lens spectrometry based on single-laser/dual-beam configuration, *Anal. Chem.*, 56, 2336, 1984.
123. **Yang, Y. and Hairrell, R. E.,** Single-laser/crossed-beam thermal lens detection for short path length samples and flow injection analyis, *Anal. Chem.*, 56, 3002, 1984.
124. **Oberhettinger, F.,** *Tabellen Zur Fourier Transformation*, Springer-Verlag, Berlin, 1957.
125. **Dovichi, N. J. and Harris, J. M.,** Frequency response of the thermal lens, *Proc. SPIE*, 288, 372, 1981.
126. **Berthoud, T., Delorme, N., and Mauchien, P.,** Beam geometry optimization in dual-beam thermal lensing spectrometry, *Anal. Chem.*, 57, 1216, 1985.
127. **Higashi, T., Imasaka, T., and Ishibashi, N.,** Thermal lens spectrophotometry with argon ion laser excitation source for nitrogen dioxide, *Anal. Chem.*, 55, 1907, 1983.
128. **Long, G. R. and Bialkowski, S. E.,** Saturation effects in gas-phase photothermal deflection spectrophotometry, *Anal. Chem.*, 57, 1079, 1985.
129. **Pawlizyn, J., Weber, M. F., and Dignam, M. J.,** Dual-beam laser deflection sensor, *Rev. Sci. Instrum.*, 56, 1740, 1985.
130. **Bertani, D., Cetica, M., Ciliberto, S., and Francini, F.,** High-resolution light spot localization with photodiode arrays, *Rev. Sci. Instrum.*, 55, 1270, 1984.
131. **Stone, J.,** Thermooptical technique for the measurement of absorption loss spectrum in liquids, *Appl. Opt.*, 12, 1828, 1973.

132. **Cremers, D. A. and Keller, R. A.,** Thermooptic-based differential measurements of weak solute absorptions with an interferometer, *Appl. Opt.*, 21, 1654, 1982.
133. **Gebhardt, F. G. and Smith, D. C.,** Kinetic cooling of a gas by absorption of CO_2 laser radiation, *Appl. Phys. Lett.*, 20, 129, 1972.
134. **Skolnik, L. H., Hordvik, A., and Kahan, A.,** Laser doppler interferometery for measuring small absorption coefficients, *Appl. Phys. Lett.*, 23, 477, 1973.
135. **Campillo, A. J., Lin, H.-B., Dodge, C. J., and Davis, C. C.,** Stark-effect modulated phase-fluctuation optical heterodyne interferometer for trace-gas analysis, *Opt. Lett.*, 5, 424, 1980.
136. **Davis, C. C.,** Trace detection in gases using phase fluctuation optical heterodyne spectroscopy, *Appl. Phys. Lett.*, 36, 515, 1980.
137. **Davis, C. C. and Petuchowski, S. J.,** Phase fluctuation optical heterodyne spectroscopy of gases, *Appl. Opt.*, 20, 2539, 1981.
138. **Lin, H.-B., Gaffney, J. S., and Campillo, A. J.,** Phase-fluctuation optical heterodyne spectrometer as a non-destructive detector for gas chromatography, *J. Chromatogr.*, 206, 205, 1981.
139. **Lin, H.-B. and Campillo, A. J.,** Photothermal aerosol absorption spectroscopy, *Appl. Opt.*, 24, 422, 1985.
140. **Leach, R. A. and Harris, J. M.,** Thermal lens absorption measurements by flow injection into supercritical fluid solvents, *Anal. Chem.*, 56, 2801, 1984.
141. **Buffett, C. E. and Morris, M. D.,** Thermal lens detection for liquid chromatography, *Anal. Chem.*, 54, 1824, 1982.
142. **Boccara, A. C., Fournier, D., Jackson, W., and Amer, N. M.,** Sensitive photothermal deflection technique for measuring absorption in optically thin media, *Opt. Lett.*, 5, 377, 1980.
143. **Dovichi, N. J. and Harris, J. M.,** unpublished data.
144. **Miyaishi, K., Imasaka, T., and Ishibashi, N.,** Thermal lensing spectrophotometric analysis with ion-pair extraction, *Anal. Chim. Acta.*, 124, 381, 1981.
145. **Fujiwara, K., Lei, W., Shimokoshi, F., Fuwa, K., and Kobayashi, T.,** Determination of phosphorus at the parts per trillion level by laser-induced thermal lensing colorimetry., *Anal. Chem.*, 54, 2026, 1982.
146. **Carter, C. A., Brady, J. M., and Harris, J. M.,** Infrared laser-induced thermal lens calorimetry, *Appl. Spectrosc.*, 36, 309, 1982.
147. **Deng, Y., Sheng, R., and Wang, M.,** Laser thermal lens effect and its application to trace solutes determination, *J. Phys. (Paris)*, C6, 565, 1983.
148. **Higashi, T., Imasaka, T., and Ishibashi, N.,** Trace analysis of benzene in air by carbon dioxide laser-induced thermal lens spectrophotometry, *Bunseki Kagaku*, 31, 680, 1982.
149. **Buffett, C. E. and Morris, M. D.,** Microcell thermal lens detector for liquid chromatography, *Anal. Chem.*, 55, 376, 1983.
150. **Sepaniak, M. J., Vargo, J. D., Kettler, C. N., and Maskarinec, M. P.,** Open tubular liquid chromatography with thermal lens detection, *Anal. Chem.*, 56, 1252, 1984.
151. **Yang, Y., Hall, S. C., and De La Crus, M. S.,** Pump/probe thermal lens spectrometry with oppositely propagating beams for liquid chromatography, *Anal. Chem.*, 58, 758, 1986.
152. **Collette, T. W., Parekh, N. J., Griffin, J. H., Carreira, L. A., and Rogers, L. B.,** Sensitive photothermal deflection detector for microbore liquid chromatography, *Appl. Spectrosc.*, 40, 164, 1986.
153. **Nickolaisen, S. L. and Bialkowski, S. E.,** Species selective detection in gas chromatography through photothermal deflection spectroscopy, *J. Chromatogr.*, submitted.
154. **Carter, C. A. and Harris, J. M.,** Thermal lens absorption measurements on small volume samples, *Anal. Chem.*, 56, 922, 1984.
155. **Teramae, N., Voigtman, E., Lanauze, J., and Winefordner, J. D.,** Pulsed photothermal refraction spectrometry using eliptic Gaussian excitation beam, *Anal. Chem.*, 58, 761, 1986.
156. **Wetsel, G. C. and Stotts, S. A.,** Absolute measurement of optical attenuation, *Appl. Phys. Lett.*, 42, 931, 1983.
157. **Tam, A. C., Sontag, H., and Hess, P.,** Photothermal probe beam deflection monitoring of photochemical particulate production, *Chem. Phys. Lett.*, 120, 280, 1985.
158. **Tam, A. C. and Sontag, H.,** Optical monitoring of photothermal transients in flowing media for velocity and concentration measurements, *Can. J. Phys.*, in press.
159. **Lee, W.-K., Gungor, A., Ho, P.-T., and Davis, C. C.,** Direct measurement of dilute dye solution quantum yield by photothermal laser heterodyne interferometry, *Appl. Phys. Lett.*, 47, 916, 1985.
160. **Eichler, H. J.,** Laser-induced grating phenomina, *Opt. Acta*, 24, 631, 1977.
161. **Pelletier, M. J. and Harris, J. M.,** Pulsed laser induced thermal diffraction for absorption measurements in small volumes, *Anal. Chem.*, 55, 1537, 1983.
162. **McGraw, D. J. and Harris, J. M.,** Diffraction from two-photon-excited thermal index gratings, *Opt. Lett.*, 10, 140, 1985.
163. **Nolan, T. G., Hart, B. K., and Dovichi, N. J.,** Photothermal refraction as a microbore liquid chromatography detector in femtomole amino acid determination, *Anal. Chem.*, 57, 2703, 1985.

164. **Burgi, D. S., Nolan, T. G., Risfelt, J. A., and Dovichi, N. J.,** Photothermal refraction for scanning laser microscopy, *Opt. Eng.*, 23, 756, 1984.
165. **Boccara, A. C., Fournier, D., and Badoz, J.,** Thermo-optical spectroscopy: detection by the mirage effect, *Appl. Phys. Lett.*, 36, 136, 1980.
166. **Murphy, J. C. and Aamodt, L. C.,** Photothermal spectroscopy using optical beam probing mirage effect, *J. Appl. Phys.*, 51, 4580, 1980.
167. **Dovichi, N. J.,** private communication dated August 23, 1978.
168. **Chen, T. I. and Morris, M. D.,** Effect of laser beam shape parameters on photothermal deflection densitometers, *Anal. Chem.*, 56, 1674, 1984.
169. **Peck, K., Fotiou, F. K., and Morris, M. D.,** Characterization of the photothermal deflection densitometer, *Anal. Chem.*, 57, 1359, 1985.
170. **Low, M. J. D., Lacroix, M., and Morterra, C.,** Infrared photothermal beam deflection Fourier transform spectroscopy of solids, *Appl. Spectrosc.*, 36, 582, 1982.
171. **Williams, C. C.,** High-resolution photothermal laser probe, *IEEE Trans. Sonics Ultrasonics*, SU-32, 365, 1985.
172. **Da Costa, G. and Calatroni, J.,** Transient deformation of liquid surfaces by laser-induced thermocapillarity, *Appl. Opt.*, 18, 233, 1979.
173. **Opsal, J., Rosencwaig, A., and Willenborg, D. L.,** Thermal-wave detection and thin-film thickness measurements with laser beam deflection, *Appl. Opt.*, 22, 3169, 1983.
174. **Yen, Y. C. and Stafsudd, O. M.,** Power dependence of reflectivity of metallic films, *Appl. Opt.*, 15, 127, 1976.
175. **Chen, T. I. and Morris, M. D.,** Photothermal deflection densitometer for thin-layer chromatography, *Anal. Chem.*, 56, 19, 1984.
176. **Masujima, T., Lloyd, L. B., and Eyring, E. M.,** Photothermal beam deflection study of titanium metal corrosion by a hot lubricant, *Appl. Spectrosc.*, 38, 804, 1984.
177. **Field, R. S., Leyden, D. E., Masujima, T., and Eyring, E. M.,** Quantitative applications of photothermal beam deflection photoacoustic spectrometry, *Appl. Spectrosc.*, 39, 753, 1985.
178. **Tamor, M. A. and Hetrick, R. E.,** Photothermal deflection spectroscopy of a powder-layer photoelectrochemical structure, *Appl. Phys. Lett.*, 46, 460, 1985.
179. **Murphy, J. C. and Aamodt, L. C.,** Signal enhancement in photothermal imaging produced by three-dimensional heat flow, *Appl. Phys. Lett.*, 39, 519, 1981.
180. **Grice, K. R., Inglehart, L. J., Favro, L. D., Kuo, P. K., and Thomas, R. L.,** Thermal wave imaging of closed cracks in solids, *J. Appl. Phys.*, 54, 6245, 1983.
181. **Lepoutre, F., Fournier, D., and Boccara, A. C.,** Nondestructive control of weldings using the mirage detection, *J. Appl. Phys.*, 57, 1009, 1985.
182. **Busse, G.,** Imaging with optically generated thermal waves, *IEEE Trans. Sonics Ultrasonics*, SU-32, 355, 1985.
183. **Aamodt, L. C. and Murphy, L. C.,** Thermal effects in photothermal spectroscopy and photothermal imaging, *J. Appl. Phys.*, 54, 581, 1983.
184. **Amer, N. M.,** New approaches to photothermal spectroscopy, *J. Phys. (Paris)*, C6, 105, 1983.
185. **Rosencwaig, A., Opsal, J., and Willenborg, D. L.,** Thin film thickness measurements with thermal waves, *J. Phys. (Paris)*, C-6, 483, 1983.
186. **Wetsel, G. C., Stotts, S. A., and Clark, C. G.,** Photothermal excitation of elastic waves by 10 ns laser pulses and detection by photoelastic laser-beam deflection, *J. Phys. (Paris)*, C6, 67, 1983.
187. **Murphy, J. C. and Aamodt, L. C.,** Reflective photothermal imaging, *J. Phys. (Paris)*, C6, 513, 1983.
188. **Jaarinen, J. P., Rajala, R. Y., Tiusanen, T. P., and Luukkala, M.,** Use of thermal waves for microscopic NDT purposes, *IEEE Trans. Sonics Ultrasonics*, SU-32, 375, 1985.
189. **Mandelis, A.,** Absolute optical absorption coefficient measurements using transverse photothermal deflection spectroscopy, *J. Appl. Phys.*, 54, 3404, 1983.